Vol.1, No.3, June-2023

APPLIED SCIENCES RESEARCH PERIODICALS

TABLE OF CONTENTS

EDITORIAL BOARD

DISCLAIMER

All the manuscripts are published in good faith and intentions to promote and encourage research around the globe. The contributions are property of their respective authors/owners and Applied Sciences Research Periodicals (ASRP) is not responsible for any content that hurts someone's views or feelings. Authors are responsible for if any plagiarism is found in published material.

Applied Sciences Research Periodicals
June 2023, Vol. 1, No. 3, pp. 01-17

Health Needs in Italy, Between Medical Desertification and the National Recovery and Resilience Plan. Province Where You Go, Shortage of Health Personnel That You Find

Mariano Votta, Maria Vitale, Bianca Ferraiolo, and Maria Eugenia Morreale

Abstract:
From the North (Bolzano) to the South (Caltanissetta) of the Country, health worker shortages run across Italy. Realized by the NGO Cittadinanzattiva an analysis on the phenomenon of "medical desertification" in Italy and the measures planned by the National Recovery and Resilience Plan. From the point of view of citizens and patients, this can only translate into a difficulty of access to care, an issue particularly close to Cittadinanzattiva's heart, which monitors it on a daily basis at national and local level thanks to the 250 sections of the Tribunal for Patients' Rights active across Italy. In particular, in Italy there are nine regions most affected by the above-mentioned phenomenon [1], which is not limited to the recent cases, however striking, of emergency room operators ignored in the budget law [2], and the growing voluntary post-pandemic resignation of nurses and social-health workers [3], but also concerns general practitioners, freely chosen paediatricians and many other specialists working in the National Health Service [4]. An initial civic mapping of the phenomenon of "medical desertification", combined with a detailed analysis of the actions planned on the territory under the measure of the NRRP Mission 6 Health - component C1: Proximity networks, facilities and telemedicine for territorial health care (all merged in the Operational Plans of the CIS-Contratti Istituzionali di Sviluppo [5] for the execution and implementation of direct investments, signed by Italian Regions and Autonomous Provinces with the Ministry of Health in May 2022), has been carried out in Italy by Cittadinanzattiva, and the related public presentation at the national level was realized on 19 January 2023 in Rome in the presence of institutions and stakeholders [6]. As part of the European project AHEAD - Action for Health and Equity Addressing Medical Deserts [7], together with the other project partners, Cittadinanzattiva has also produced an online map [8] with information, for each province, on certain categories of health professionals working in public hospitals (hospital gynaecologist, hospital cardiologist and hospital pharmacist) rather than in primary care (general practitioner and paediatrician of free choice). [9]

Keywords: Medical desertification, NRRP-National Recovery and Resilience Plan, access to care, patients' rights, civic participation, AHEAD-Action for Health and Equity: Addressing Medical Deserts, EU4Health, Inner Areas, health inequalities.

INTRODUCTION

Health workers wanted throughout Italy: from the North to the South there is a shortage of doctors, both GPs and hospital doctors, as well as nurses and pediatricians. The so-called medical desertification is particularly evident in territories where people find it difficult to access care due to, for example, long waiting times, a shortage of health care workers or long distances from the point of care delivery.

Overcrowding in the offices of general practitioners and pediatricians is especially evident in the North of the country, while the shortage of hospital gynecologists affects not only Caltanissetta, where there is one hospital gynecologist for every 40565 women, but also Macerata, Viterbo, La Spezia and three provinces in Calabria (Reggio Calabria, Vibo Valentia and Cosenza).

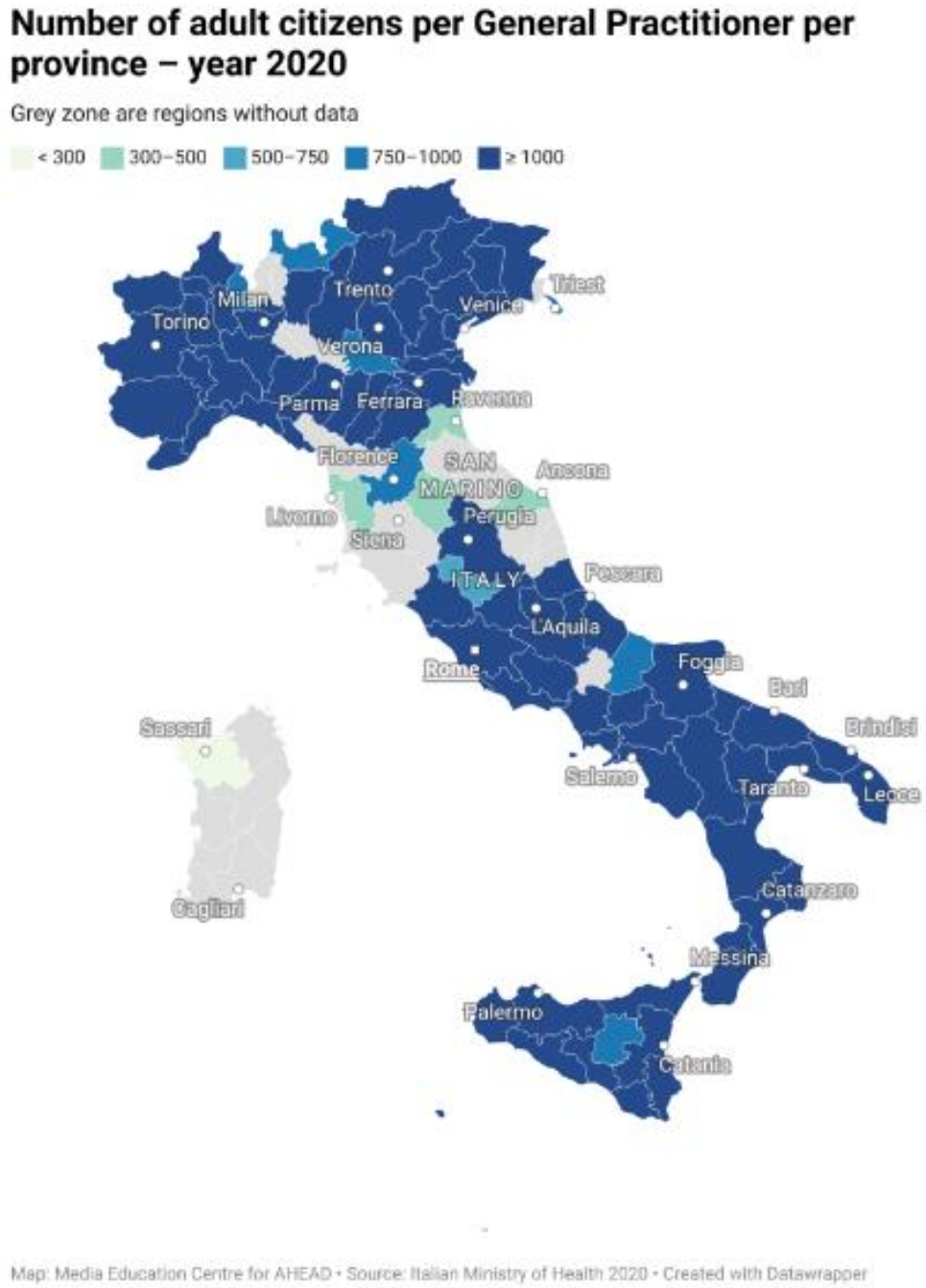

Fig. 1: Number of adult citizens per General Practitioner per province – year 2020. The map shows how many inhabitants in the 15 – 65+ age group there are – at the provincial level – for each General Practitioner (GP) in Italy. The colour code ranges from the lightest (the lowest number is 248) to the darkest (the highest number is 1539). The data refer to 2020 and the sources are the Italian Ministry of Health and Eurostat. https://ahead.health/number-of-adult-citizens-per-general-practitioner-per-province-year-2020/

Going into detail, Asti and its province have the fewest pediatricians per number of children (each professional cares for 1813 children between the ages of 0 and 15 years, the national average is 1/1061 and the regulations stipulate about 1 pediatrician per 800 children).

In the province of Bolzano, each general practitioner cares for an average of 1539 citizens aged 15 years and older (the national average is 1 doctor per 1245 patients, although the regulations set this ratio at 1/1500). In Caltanissetta and its province there is one hospital gynecologist for every 40565 women (the Italian average is 1/4132), the best figure is in Rome with a ratio of 1/2292: in other words, the situation in the province of Caltanissetta is 17 times worse than for those living in the province of Rome.

On the other hand, considering hospital cardiologists, the situation in the Autonomous Province of Bolzano is even 71 times worse than those living in the province of Pisa: in Bolzano there is one hospital cardiologist for every 224706 inhabitants (the average is 1/6741), the best rate in Pisa and province with 1/3147. Regarding hospital pharmacists, however, the worst ratio is reported in the province of Reggio Emilia where there is one professional for every 264805 inhabitants (the average is 1/26182), the best is in the province of Forlì-Cesena with 1/9982.

METHODOLOGY

The analysis conducted by Cittadinanzattiva used official data provided by the Ministry of Health related to 2020, regarding the following health care figures: pediatricians of free choice, general practitioners, gynecologists, cardiologists and pharmacists (the latter three hospital-based) for each Italian province. The choice of the five occupational categories may appear arbitrary but, in fact, it responds to a methodological decision shared in the context of the European AHEAD project to facilitate a comparison of data between all the countries involved in the project [10].

Moreover, a crucial and critical aspect of data collection in Italy concerned the unavailability and/or absence of this type of information. In fact, in most cases, these data were not publicly accessible and had to be requested expressly from the competent interlocutors (Ministry of Health, Federfarma, etc.).

The biggest obstacle was the total lack of these data for some other important professional categories. Finally, it was not possible to receive information at a higher level of accuracy (i.e., at municipal level) because it does not exist.

The full Report, which also contains specific regional focuses, can be downloaded at the official website of Cittadinanzattiva [11].

RESULTS

The following tables show the ten Italian provinces with the most marked disproportions in the ratio of people to health personnel.

Paediatricians and General Practitioners

The highest number of children [12] per free-choice paediatrician is found in the following provinces:

Tab. 1: N° of minors per Paediatrician in Italy

Position in the ranking	Province	N° of minors per Paediatrician
1	Asti	1.813
2	Brescia	1.482
3	Novara	1.370
4	Vercelli	1.367
5	Bolzano	1.364
6	Cuneo	1.331
7	Torino	1.320
8	Perugia	1.252
9	Udine	1.237
10	Alessandria	1.236
National average		1.061

Source: Elaboration Cittadinanzattiva on Ministry of Health data, 2020

Table almost hegemonised by Piemonte, and negative primacy for the northern provinces, a primacy that is also confirmed with regard to the family doctor. In fact, the data on the number of citizens [13] per General Practitioner (GP) tell us that the provinces in which the doctor has to divide himself among several people are as follows:

Tab. 2: N° of persons per General Practitioner in Italy

Position in the ranking	Province	N° of persons per General Practitioner
1	Bolzano	1.539
2	Bergamo	1.517
3	Brescia	1.516
4	Treviso	1.445
5	Trento	1.403
6	Pordenone	1.397
7	Verona	1.395
8	Imperia	1.392
9	Milano	1.392
10	Parma	1.391
National average		1.245

Source: Elaboration Cittadinanzattiva on Ministry of Health data, 2020

Hospital-Based Professionals

On the other hand, with regard to data on the female population [14] per hospitalgynaecologist, the provinces with the most complex situation are as follows:

Tab. 3: N° of women per hospital-based Gynaecologist in Italy

Position in theranking	Province	N° of women per hospital-based Gynaecologist
1	Caltanissetta	40.565
2	Macerata	18.460
3	Reggio Calabria	9.992
4	Viterbo	9.163
5	La Spezia	8.061
6	Vibo Valentia	8.002
7	Venezia	7.647
8	Lodi	7.528
9	Savona	7.370
10	Cosenza	7.229
National average		4.132

Source: Elaboration Cittadinanzattiva on Ministry of Health data, 2020

As can easily be seen, there is a worrying 'off the charts' situation in the province of Caltanissetta. The number of persons [15] per hospital-based cardiologist is particularly high in the following provinces:

Tab. 4: N° of persons per hospital-based Cardiologist in Italy

Position in theranking	Province	N° of persons per Hospital-based Cardiologist
1	Bolzano	224.706
2	Potenza	105.789
3	Crotone	72.172
4	Caltanissetta	36.941
5	Viterbo	34.137
6	Cosenza	21.584
7	Como	19.953
8	Reggio Calabria	15.278
9	Macerata	13.602
10	Brindisi	12.074
National average		6.741

Source: Elaboration Cittadinanzattiva on Ministry of Health data, 2020

In Bolzano, hospital-based cardiologists seem to be hiding among the population like a needle in a haystack! Certainly, the figures are far above any other province.

The last data collected concerns hospital-based pharmacists who present the highest imbalances in the ratio to the population [16] in the following provinces:

Tab. 5: N° of persons per hospital-based Pharmacist in Italy

Position in the ranking	Province	N° of persons per hospital-based Pharmacist
1	Reggio Emilia	264.805
2	Campobasso	108.681
3	Reggio Calabria	75.852
4	Piacenza	71.608
5	Lecco	55.827
6	Alessandria	52.161
7	Latina	46.883
8	Trieste	46.289
9	Como	45.972
10	Gorizia	45.932
National average		26.182

Source: Elaboration Cittadinanzattiva on Ministry of Health data, 2020

Again, the figures for the first two provinces in the ranking, Reggio Emilia and Campobasso, appear to be decidedly 'out of the league' because they are very far from the orders of magnitude found in the other Italian provinces.

Comments

In summary, from the analysis of official sources (Eurostat 2020 for population, Ministry of Health 2020 for number of professionals) and with reference to the top ten provinces - for each of the five professional figures mentioned - it emerges that in at least 39 provinces - and thus abundantly one third of the Italian provinces - a marked imbalance is evident, with two provinces (Bolzano and Reggio Calabria, at the extremes of the country, almost as if to underline how the phenomenon of medical deserts crosses the whole of Italy) that simultaneously reveal three shortages, and a further seven provinces (Alessandria, Brescia, Caltanissetta, Como, Cosenza, Macerata, Viterbo) that reveal two shortages. Specifically:

- Hospital-based pharmacists: the greatest imbalance between the number of professionals and the target audience is registered in the provinces of Reggio Emilia (1 in every 264805 people), Campobasso (1 for every 108681) and Reggio Calabria (1 for every 75852), while the best ratio at national level (1 for every 9883) is recorded in the province of Forlì-Cesena.
- Hospital-based cardiologists: the greatest imbalance between the number of professionals and the target group is registered in the provinces of Bolzano (1 per 224706 people), Potenza (1 in every 105789) and Crotone (1 in every 72172), while the best ratio at national level (1 in every 3147) is recorded in the province of Pisa.
- Hospital-based gynaecologists: the greatest imbalance between the number of professionals and target is recorded in the provinces of Caltanissetta (1 for every 40565 women), Macerata (1 for every 18460) and Reggio Calabria (1 for every 9992), while the best ratio at national level (1 for every 2292 women) is recorded in the province of Rome.

- There are clear territorial health inequalities, not necessarily between North and South, but also between provinces in the same region: in terms of hospital-based pharmacists, the situation in the province of Reggio Emilia is respectively 20 and 26 times worse than in the neighbouring provinces of Modena and Forlì-Cesena.
- Speaking of hospital-based gynaecologists, the situation in the province of Caltanissetta is 17 times worse than in the province of Rome. Considering instead hospital-based cardiologists, the situation in the Autonomous Province of Bolzano is even 71 times worse than in the province of Pisa!
- Keeping in mind the 39 provinces where the imbalances, between number of professionals and citizens, are most marked, nine are the most affected regions: Lombardia (Bergamo, Brescia, Como, Lecco, Lodi, Milano) and Piemonte (Alessandria, Asti, Cuneo, Novara, Torino, Vercelli) excel with six provinces, followed by Friuli Venezia Giulia (Gorizia, Pordenone, Udine, Trieste) and Calabria (Cosenza, Crotone, Reggio Calabria, Vibo Valentia) with four provinces. They are followed by Veneto (Treviso, Venezia, Verona), Liguria (Imperia, La Spezia, Savona) and Emilia Romagna (Parma, Piacenza, Reggio Emilia) with three provinces each, Trentino Alto Adige (both autonomous provinces of Bolzano and Trento) and Lazio (Latina and Viterbo) with two provinces.

Community homes and hospitals: what (and where) the NRRP foresees, between health desertification & proximity health services With the publication in the Official Gazette of the Regulation for the definition of models and standards for the development of territorial care within the National Health Service (Ministerial Decree N°77) and the signing of the CIS-Contratti Istituzionali di Sviluppo (Institutional Development Contracts) between the Ministry of Health and each Region and Autonomous Province, two important goals envisaged in Mission 6 Health of the National Recovery and Resilience Plan (NRRP) have been achieved to make the National Health System increasingly effective, with the aim of guaranteeing equal access to care, and strengthening prevention and services in the territory [17].

The NRRP provides funding for investments and only a small part for personnel-related management costs. But in order to make the new community health services work, it will be necessary to recruit staff and finance their costs [18]. Without an adequate link between structures and personnel - who will be called upon to work in those structures - as well as a careful analysis of the needs of the communities, the risk is that we will move towards a lack of effectiveness of the interventions. Hence Cittadinanzattiva's interest in monitoring both the state of progress of the NRRP with the presence and dislocation of Community Homes (CH) and Community Hospitals (HH), and the presence and dislocation of healthcare personnel, trying to match the data.

Thus, for example, the 39 provinces with the highest person/healthcare staff ratio (highlighted in pink in the following tables) do not correspond with the provinces receiving the highest number of Community Homes & Hospitals.

Fig. 2: Rome, 19 January 2023, European Commission Representation in Italy. The co-authors Mariano Votta and Bianca Ferraiolo together with Margherita Riccitelli from Cittadinanzattiva Piedimonte Matese at the conference "Health needs in inner areas, between medical desertification and NRRP".

Tab. 6: What the NRRP provides for the Community Houses in Italy

What the NRRP provides for	Community Houses (CH)		
	Total. CH	CH in Inner Areas [19]	
		(D)	(E-F)
Roma	**91**	13	5
Napoli	**88**	2	3
Milano	**55**	0	0
Torino	**42**	4	0
Palermo	**37**	9	16
Bari	**36**	7	1
Salerno	**33**	3	7
Brescia	**30**	7	10
Caserta	**30**	6	4
Catania	**29**	8	16
Foggia	**26**	12	10
Lecce	**24**	6	8
Cosenza	**22**	8	6
Bergamo	**21**	1	3
Messina	**21**	5	10
Agrigento	**21**	6	8
Varese	**20**	2	0
Padova	**20**	0	0
Bologna	**20**	5	2
Firenze	**20**	3	2
Sassari	**19**	6	7
Genova	**17**	2	0
Monza e Brianza	**17**	0	0

Vicenza	**17**	0	1
Treviso	**17**	0	0
Frosinone	**17**	5	1
Taranto	**17**	5	4
Reggio Calabria	**17**	9	2
Verona	**16**	0	0
Venezia	**16**	3	0
Latina	**15**	3	1
Chieti	**15**	2	9
Modena	**13**	3	6
Potenza	**13**	2	9
Trapani	**13**	2	3
Como	**12**	3	4
Pisa	**12**	0	1
Perugia	**12**	2	4
Siracusa	**12**	7	2
Sud Sardegna	**12**	2	4
Pavia	**11**	2	0
Udine	**11**	5	1
L'Aquila	**11**	3	3
Benevento	**11**	5	1
Catanzaro	**11**	4	2
Cuneo	**10**	1	0
PA Bolzano	**10**	2	4
PA Trento	**10**	3	3
Reggio Emilia	**10**	4	3
Avellino	**10**	3	2
Mantova	**9**	5	0
Parma	**9**	1	1
Campobasso	**9**	1	6
Brindisi	**9**	6	0
Barletta-Andria Trani	**9**	0	1
Caltanissetta	**9**	3	4
Ragusa	**9**	6	0
Alessandria	**8**	1	0
Lecco	**8**	0	0
Ravenna	**8**	0	0
Forlì-Cesena	**8**	1	0
Livorno	**8**	1	2
Ancona	**8**	0	1
Macerata	**8**	3	0
Teramo	**8**	2	0
Novara	**7**	2	0
Sondrio	**7**	2	3
Arezzo	**7**	5	0
Viterbo	**7**	0	0
Nuoro	**7**	2	5
Cagliari	**7**	1	0
Savona	**6**	1	0
Piacenza	**6**	0	0

Ferrara	**6**	4	1
Siena	**6**	1	2
Grosseto	**6**	2	2
Pescara	**6**	1	0
Matera	**6**	0	6
Crotone	**6**	2	1
Asti	**5**	1	0
Imperia	**5**	1	0
La Spezia	**5**	0	0
Lodi	**5**	0	0
Rovigo	**5**	3	1
Pordenone	**5**	1	0
Rimini	**5**	0	1
Lucca	**5**	1	0
Pistoia	**5**	1	0
Terni	**5**	0	0
Ascoli Piceno	**5**	1	0
Rieti	**5**	2	0
Vibo Valentia	**5**	2	1
Enna	**5**	2	3
Oristano	**5**	3	0
Aosta	**4**	1	0
Cremona	**4**	0	0
Belluno	**4**	2	0
Gorizia	**4**	0	0
Massa-Carrara	**4**	1	0
Prato	**4**	1	1
Pesaro e Urbino	**4**	1	0
Fermo	**4**	0	0
Isernia	**4**	2	2
Vercelli	**4**	0	1
Biella	**3**	1	0
Verbano-Cusio-Ossola	**3**	0	0
Trieste	**3**	0	0

Source: Elaboration of Cittadinanzattiva-Civic Evaluation Agency on data:
CIS-Contratti Istituzionali di Sviluppo [20], 2022 and ISTAT- La geografia delle aree interne nel 2020 [21]

Tab. 7: What the NRRP provides for the Community Hospitals in Italy

What the NRRP provides for	**Community Hospitals (HH)**		
	Tot. HH	**HH in Inner Areas**	
		(D)	**(E-F)**
Napoli	**23**	2	3
Roma	**22**	4	0
Milano	**19**	0	0
Torino	**15**	1	0
Palermo	**10**	1	3
Catania	**10**	2	7
Bari	**9**	2	1
Cosenza	**9**	2	4
Brescia	**8**	3	3

Verona	**8**	3	0
Caserta	**8**	2	2
Salerno	**8**	0	4
Vicenza	**7**	0	1
Foggia	**7**	2	4
Genova	**6**	2	0
Bergamo	**6**	2	0
Treviso	**6**	0	0
Bologna	**6**	3	1
Frosinone	**6**	1	0
Brindisi	**6**	2	1
Lecce	**6**	2	1
Barletta-Andria Trani	**6**	1	1
Messina	**6**	2	1
Sassari	**6**	1	2
Como	**5**	1	1
Mantova	**5**	4	0
Firenze	**5**	0	1
Benevento	**5**	3	1
Varese	**4**	2	0
Lecco	**4**	0	0
Pavia	**4**	1	0
Venezia	**4**	1	0
Padova	**4**	0	0
Modena	**4**	1	1
Livorno	**4**	2	0
Latina	**4**	1	0
Avellino	**4**	1	0
Taranto	**4**	2	0
Catanzaro	**4**	3	1
Reggio Calabria	**4**	0	3
Siracusa	**4**	2	1
Cuneo	**3**	0	0
Alessandria	**3**	0	0
Sondrio	**3**	2	1
Cremona	**3**	0	0
Monza e Brianza	**3**	0	0
PA Bolzano	**3**	1	0
PA Trento	**3**	0	0
Belluno	**3**	1	1
Rovigo	**3**	1	0
Udine	**3**	1	0
Parma	**3**	1	0
Reggio Emilia	**3**	1	1
Rimini	**3**	0	1
Lucca	**3**	0	1
Arezzo	**3**	1	1
Perugia	**3**	1	0
Ancona	**3**	0	0
L'Aquila	**3**	0	0

Pescara	**3**	2	0
Chieti	**3**	0	2
Potenza	**3**	0	3
Trapani	**3**	1	0
Agrigento	**3**	0	2
Ragusa	**3**	1	0
Novara	**2**	1	0
Savona	**2**	1	0
La Spezia	**2**	1	0
Lodi	**2**	0	0
Pordenone	**2**	1	0
Gorizia	**2**	0	0
Piacenza	**2**	0	0
Ferrara	**2**	0	1
Ravenna	**2**	0	0
Forlì-Cesena	**2**	0	0
Pistoia	**2**	0	0
Prato	**2**	0	0
Grosseto	**2**	0	1
Terni	**2**	0	0
Pesaro e Urbino	**2**	1	0
Macerata	**2**	0	0
Ascoli Piceno	**2**	0	0
Viterbo	**2**	0	0
Rieti	**2**	1	1
Teramo	**2**	1	0
Matera	**2**	0	2
Vibo Valentia	**2**	1	0
Caltanissetta	**2**	0	1
Enna	**2**	0	2
Nuoro	**2**	0	2
Cagliari	**2**	0	0
Oristano	**2**	1	1
Vercelli	**1**	1	0
Biella	**1**	0	0
Verbano-Cusio-Ossola	**1**	0	0
Asti	**1**	0	0
Aosta	**1**	0	0
Imperia	**1**	0	0
Massa-Carrara	**1**	0	0
Pisa	**1**	0	0
Siena	**1**	0	0
Isernia	**1**	1	0
Campobasso	**1**	0	1
Crotone	**1**	0	1
Sud Sardegna	**1**	0	0
Trieste	**0**	0	0
Fermo	**0**	0	0

Source: Elaboration of Cittadinanzattiva-Civic Evaluation Agency on data:
CIS -Contratti Istituzionali di Sviluppo, 2022 and ISTAT- La geografia delle aree interne nel 2020

The same is true for 9 regions (highlighted in pink in the following tables) most affected by the phenomenon of "medical deserts": the correlation with the number of Community Homes & Community Hospitals envisaged by the NRRP is not particularly strong.

Tab. 8: What the NRRP provides for the Community Houses in each Italian Region

What the NRRP provides for	
Regions	**N° Community Houses**
Lombardia	199
Campania	172
Sicilia	156
Lazio	135
Puglia	121
Veneto	95
Emilia Romagna	85
Piemonte	82
Toscana	77
Calabria	61
Sardegna	50
Abruzzo	40
Liguria	33
Marche	29
Friuli Venezia Giulia	23
Basilicata	19
Umbria	17
Molise	13
PA Bolzano	10
PA Trento	10
Valle d'Aosta	4

Source: Cittadinanzattiva Civic Evaluation Agency on official data
CIS/Contratti Istituzionali di Sviluppo, 2022

Tab. 9: What the NRRP provides for the Community Hospitals in each Italian Region

What the NRRP provides for	
Regions	**N° Community Hospitals**
Lombardia	66
Campania	48
Sicilia	43
Puglia	38
Lazio	36
Veneto	35
Piemonte	27
Emilia Romagna	27
Toscana	24
Calabria	20
Sardegna	13
Liguria	11
Abruzzo	11
Marche	9
Friuli Venezia Giulia	7

Umbria	5
Basilicata	5
PA Bolzano	3
PA Trento	3
Molise	2
Valle d'Aosta	1

Source: Cittadinanzattiva Civic Evaluation Agency on official data:
CIS/Contratti Istituzionali di Sviluppo, 2022

CONCLUSIONS

Many countries in the European region struggle with severe shortages of health personnel and an ageing and burned-out health workforce. This is leading to a lack of access to healthcare for many European citizens. Several countries, such as Italy, Romania, Serbia and Moldova, also face the challenge of so-called "medical deserts". These are areas with limited health services, resulting in unmet health needs of the population. They can exacerbate health inequalities, mostly affecting vulnerable groups.

Medical deserts and the lack of access to care for European citizens are therefore an increasingly urgent joint public health concern in Europe. This EU-wide problem needs EU-wide collaboration to come up with an EU-level sustainable solution, to ensure that European citizens receive optimal access to skilled and motivated health workers. Europe cannot wait – it is time to act now! For this reason, on 27 April 2023, a policy dialogue event, hosted by the Italian Member of the European Parliament Beatrice Covassi, was organised at the European Parliament in Brussels, in the presence of Members of European Parliament, the European Commission (DG Santè and DG Agri), the WHO, the President of the Italian National Institute of Health, civic organizations, patient's advocacy groups and other relevant stakeholders. Experts debated and agreed about the following four pillars and recommendations:

- European Institutions should prioritise the problem of medical deserts on the political agenda throughout the next European Commission's mandate – and beyond.
- The national governments of European Member States should improve the quality, systematic collection and analysis of data related to the health workforce, health services, and related indicators to medical deserts.
- Health professionals' associations should advocate the right to health for all, especially people in areas with limited or difficult access to health services, both in rural and remote areas, as in urban areas.
- Citizens should call for multi-dimensional actions by duty-bearers to improve their health and well-being, especially for the most vulnerable.

Fig. 3: Brussels, 27 April 2023, European Parliament. Beatrice Covassi, Member of the European Parliament - Group of the Progressive Alliance of Socialists and Democrats (S&D) together with Anna Lisa Mandorino, Secretary General at Cittadinanzattiva at the conference "Addressing medical desertification in Europe: a call to action".

DECLARATIONS

Each of the authors confirms that this manuscript has not been previously published by another international peer-review journal and is not under consideration by any other journal. Additionally, all of the authors have approved the contents of this paper and have agreed to the submission policies of the journal.

ACKNOWLEDGEMENTS

The analysis conducted by Cittadinanzattiva is part of the European project AHEAD "Action for Health and Equity: Addressing Medical Deserts" (funded by EU4Health, the European Union's fourth program dedicated to health in effect for the period 2021-2027), which aims to analyze the phenomenon of so-called "medical deserts" at the European level.

REFERENCES

[1] The term "medical desert" is used to refer to various situations or areas where people have difficulty accessing care due to, for example, long waiting times, a shortage of health personnel or long distances from the point of care. See: www.agenas.gov.it/oases-promoting-evidence-based-reforms

[2] The EUR 200 million increase in the allowance for emergency medical workers, which had been promised by the government, found no place in the budget law. The reason for the allocation was explained by the Italian Minister Schillaci himself. Those who work in emergency departments do not do private work, and therefore have lower incomes than many colleagues. The aim would be 'to make these specialities more attractive', the

health minister had explained. See: www.open.online/2022/12/28/legge-di-bilancio-sanita-fondi-tumori-pronto-soccorso/

[3] www.insalutenews.it/in-salute/oltre-2mila-tra-infermieri-e-oss-hanno-dato-le-dimissioni-dal-ssn-nel-2021-nursing-up-dati-allarmanti/

[4] www.sanita24.ilsole24ore.com/art/aziende-e-regioni/2022-11-10/fiaso-grandi-dimissioni-sanita-2021-via-servizio-national-health-3 thousand-medics-155536.php?uuid=AESsHuFC&refresh_ce=1

[5] Institutional Development Contracts

[6] More info here: www.activecitizenship.net/insights/1070-shortage-of-doctors-and-medical-desert-nine-italian-regions-with-the-smallest-workforce.html

[7] https://ahead.health/

[8] Available at https://ahead.health/italy/

[9] The paediatrician of free-choice is the doctor who assists children from 0 to 14 years of age, affiliated with the National Health Service. In a nutshell, he is the equivalent of the general practitioner in paediatrics, i.e. a doctor who offers his services free of charge on behalf of the SSN.The paediatrician of free-choice is mandatory for all children up to the age of 6, in order to access all services and benefits guaranteed by the public health service, including the Essential Levels of Care (LEA). After the age of 6, the parent is free to decide whether to keep the paediatrician or to rely on their general practitioner.
www.salute.gov.it/portale/lea/dettaglioContenutiLea.jsp?area=Lea&id=4697&lingua=italiano&menu=distrettuale

[10] Italy, Moldova, the Netherlands, Romania and Serbia. See: https://ahead.health.

[11] The Report was presented by Cittadinanzattiva on occasion of the **event** "Health needs in inner areas, between medical desertification and NRRP"**,** held in Rome at the European Commission Representation in Italy on January 19, 2023. The Report was edited by Mariano Votta, Head of European Policies of Cittadinanzattiva, in collaboration with his colleagues Maria Vitale, Senior Project Manager, and Bianca Ferraiolo, Head of Cittadinanzattiva's representativeoffice at the European Institutions and Head of the AHEAD Project. Data processing was carried out by Cittadinanzattiva's Civic Evaluation Agency in the persons of Maria Eugenia Morreale and Maria. Vitale. Claudia Ciriello,Cittadinanzattiva Project Manager, also collaborated in the data collection. The Report, which also contains specific regional focuses, can be downloaded at this webpage: www.activecitizenship.net/insights/1070-shortage-of-doctors-and-medical-desert-nine-italian-regions-with-the-smallest-workforce.html.html

[12] AHEAD project target population: children and adolescents from 0 to 15 years of age.

[13] AHEAD project target population: people aged 15 and over.

[14] AHEAD project target population: female population aged 10 and over.

[15] AHEAD project target population: people aged 15 and over.

[16] Target population from AHEAD project: total population.

[17] www.agenas.gov.it/comunicazione/primo-piano/2099-missione-6-salute-pnrr-in-gazzetta-il-dm-77-siglati-i-contratti-institutional-development

[18] www.luoghicura.it/sistema/finanziamento-e-spesa/2021/06/i-finanziamenti-per-la-missione-salute-del-pnrr-opportunities-and-risks/

[19] Italian municipalities are classified between centres and inner areas. Centres are classified as follows: (A): Polo (Polo); (B): Polo intercomunale (Inter-municipal pole); (C): Cintura (Belt). Inner areas are classified as follows: (D): Intermedio (Intermediate); (E): Periferico (Peripheral); (F): Ultraperiferico (Ultraperipheral).

[20] PNRR- Contratti Istituzionali di Sviluppo tra il Ministero della Salute e le Regioni e Province Autonome Anno 2022, cfr: www.salute.gov.it/portale/documentazione/p6_2_2_1.jsp?lingua=italiano&id=3240

[21] Cfr: www.istat.it/it/archivio/273176

Applied Sciences Research Periodicals
June 2023, Vol. 1, No. 3, pp. 18-20

The Now and the Universe

Berov G. Lyubomir

1. Independent Innovative Ideas Researcher, Smolyan 4700, Bulgaria

Abstract:
The present, at any particular moment, is the realization of one of the many intentions of the All-creating Intellect. Here "realization" specifically means the materialization or the appearance of an object in the material world, which had not existed until now. This newly born material object exists only for the duration of the moment of "now". This moment is infinitely short, or, if we use a concept from calculus, it is infinitesimal in duration. In my hypothesis, this new object is a product of a specific energy field of the All-creating Intellect. We call this particular energy field Time.

Keywords: Time, Dark Energy, Infinitesimal, All-creating Intellect, Universe

Dear reader, in my article "Time. Philosophy of Science" I presented Time as a powerful energy field created by the intellectual field of the dark energy.

Here, I will try to describe some of the characteristics of the energy field of Time, which, according to my hypothesis, explain its interaction with both the energy field of the All-creating Intellect and the material world.

Let us first recall certain elements of my article "Time. Philosophy of Science": We can trace the search for an answer to the question "What is Time?", as far back as the era of St. Augustine. He believed that Time exists only in our consciousness and depends only on how we interpret it. The ancient philosopher explained that people can say that something lasts long or short, but there is no real way to objectively measure the lengthen of Time. So, St. Augustine reached the logical conclusion that the concept of Time exists exclusively in our minds. Well, we all understand this to some degree, don't we? Remarkably, an answer to the question about the essence of Time has been offered by all of the great philosophers, physicists and psychologists in human history, from ancient times to the present. And there has never been a single answer.

Time is both subjective and objective. There may be time, but there may not be. The concept that Time is a physical quantity where material changes occur is often replaced by a more convenient one, where Time is simply the order of changes in the material world.

Let's look at things in greater detail. According to Sir Isaak Newton, time is absolute, independent, and moves at a constant speed. However, since Newton, the interpretation of Time has been constantly changing. The most significant changes occurred with the development of Einstein's General Theory of Relativity (GTR).

Generally, Einstein's interpretation of Time is: "Time has no independent existence except in the order of events by which we measure it. Time is a sequence of events - that is my conclusion."."

The view that time is a sequence of events is shared by most scientists in the modern world. But can time be both a physical quantity and the order in which changes occur in the material world? According to my hypothesis presented here, this is entirely possible.

And now more specifically. First, let's clarify the concepts of Future, Present, and Past.

The Future for me are the goals of the All-creating Intellect, expressed more specifically in its intentions. These goals are not yet material objects. By the way, we, humans, apply the same process when setting up goals and intentions before creating something new - at the beginning, those goals and intensions are only in our minds.

However, there is a significant difference when it comes to the material objects that our goals and intentions eventually create vs. the goals and intentions of the All-creating Intellect. And the difference is that what we create is simply reshaping or recombining already existing objects while the All-creating Intellect creates, and constantly changes, the material world itself. Also, another difference is the feedback loop where the material world created by The All-creating Intellect, in some way, affects the intentions of the Intellect itself (I think this is likely related to preserving the stability of our material world).

The next stop of our journey from the Future to the Past is the Present. So, how is the material world created and continues to be created?

The Present is the realization, at a particular moment of Time, of one of the many intentions of the All-creating Intellect. Here "realization" specifically means the materialization or the appearance of an object in the material world, which had not existed until now. Here is the essence of my hypothesis. Each material object, be it an atom, a planet, a star, etc. is a transformed part of a specific energy field of the All-creating Intellect. We call this particular energy field Time.

Each material object exists only for the duration of the moment of "now". This moment is infinitely short, or, if we use a concept from calculus, it is infinitesimal in duration. Then, for the next infinitesimal period of time, the material object transforms again into the energy field Time. And then the process of transformation from energy into matter and back repeats. This "pulsation" continues for as long as the material object exists as such.

Let's summarize: Time, in my opinion, is a type of energy field which is a specific form of the energy field of the All-creating Intellect. It deals only with the creation and management of the material world. The age of each object is determined by the number of these pulsations of the energy field Time that the All-creating Intellect memorize. And this applies to any object created by it.

Only a limited number of the created material objects to some extent carry the ability of the All-creating Intellect to create new "things", of course in accordance with its goals and intentions. This is a very important quality and maybe we humans have it too.

The pulsation process of the present is how our material world was born and continues to be born, consisting of material particles, and known and unknown types of energy fields.

And so, the new idea in my hypothesis, is that each element of the material world begins to exist from the moment of its first-Time pulsation and continues to exist in the moments of each subsequent Time pulsation, i.e., only in the Now. This is why I call this article "The Now and the Universe". For now, we have not recognized that Time as an energy field and we are not making any efforts in this direction because no one believes that it is possible for this to be the reality.

Dear reader, don't worry. Science has always started with a hypothesis, no matter if it were right or wrong. As for the All-creating Intellect and its variety Time, we are all certain that Time exists, but not as an energy field.

And now on to our last stop – the past.

In my opinion, the past does not really exist. The past of the material world exists only in the memory of the All-creating Intellect and partly in the memories of countless types of secondary intellects. Man is one of these secondary intellects. We humans also measure the age of everything in all sorts of ways, counting different types of recurring events. These events can be space cycles, the number of orbits of the Earth around the sun, the number of seconds measured by our clocks, and the most modern approach in recent times - the number of periods of radiation, corresponding to the transition between two ultrafine levels of the base state of the cesium 133 atom. These findings are the past and the history, and, as I have already mentioned, they are stored in our memory and do not really exist.

In our human memory, they are subjective and very inaccurate. I am convinced that the memory of the All-creating Intellect is nothing like the human memory. It is probably extremely accurate and endless in its longevity. Moreover, the events stored in its memory in some way also affect the intentions of the Intellect, i.e., there is feedback between the past and the future.

Dear reader, with this article I have tried to present a simpler and more comprehensible picture of our material world. I described it as a world of the continuous transformation of the energy field Time into Matter and of Matter into Time. I hope I have succeeded.

REFERENCES

Berov Lyubomir. A Time: Philosophy of Science. 2020

Rubin, Vera. Bright Galaxies, Dark Matter. 1997

Castaneda, Carlos. The Art of Dreaming. 1993

Stephen W. Hawking. A Brief History of Time. 1973

Applied Sciences Research Periodicals
June 2023, Vol. 1, No. 3, pp. 21-33

Development of a Cybernetics Phishing Detection Approach

Onyema Chinazo Juliet, Chidi Ukamaka Betrand, and Douglas Allswell Kelechi

1. Department of Computer Science, School of Information and Communication Technology, Federal University of Technology Owerri, Imo State

Abstract:
Phishing being one of the core problems encountered by online community has led to numerous financial losses, identity theft, kidnappings, deaths and lots more. Phishing detection and response software which is a cybersecurity tool that identifies and rectifies phishing threats before the phishing attack causes harm, is a part of the broader threat detection and online security response. The phishing detection system employed in this study is a one-page web application model aimed at solving phishing problems, with high-rate detection accuracy, low-rate false alarm and consistent database updates. Machine Learning technology was used by the detection system in extracting and analyzing different features of malicious and phishing URLs. Extreme Gradient Booster (XGBoost), Decision trees, Multilayer Perceptron and Random Forest models were compared in detecting phishing websites with the aid of Python, Science-kit learn (sklearn) and Flask. The Frontend of the one-page web application was done using HTML and CSS. The generated dataset from which the models were tested and trained were extracted from various open-source platforms which provided some phishing URLs in various formats like JSON and CSV with hourly updates. Up to 2000 random phishing URLs were collected from this dataset to train and test the Machine Learning models. Out of all these types, the benign URL dataset was considered for this paper. An accuracy of 86.6% with 13.34% false-positive rate was achieved in our proposed approach on our dataset, together with 13.6% false-positive rate and 86.4% accuracy on the benchmark dataset, which performs better than the existing baseline approaches.

Keywords: Machine Learning, Feature Selection, URL, Classification, XGBOOST, Detection, Phishing.

INTRODUCTION

The term Phishing is a cybercrime that involves a perpetrator sending a fraudulent or malicious mail in disguise, making it seem like it comes from a legitimate source thereby requesting for some particular and sensitive information like username, phone number, bank account details, and so forth [1].

Phishing attacks constitute a significant danger to online space along with IT companies that operate with highly sensitive data and this has been on the increase over the years surpassing every effort to curtail it.

As a result of over 33000 worldwide phishing assaults in 2012 a loss of $687 million was recorded likewise in 2004, when over 50 million phished emails caused a loss of $10 billion in financial institutions. According to the Anti-Phishing Working Group (APWG), the top targets in the second quarter are financial bodies (16%), web (15%), cloud storages (9%) and payment systems (45%) [2].

However, it is crucial for all internet and computer users to keep information secure and safe as to reduce the risk of fraud that may occur while accessing various websites by identifying phishing links and emails thus helping protect them against these attacks.

THE CONCEPT OF PHISHING ATTACKS

Phishing attacks generally fall in two classes; social engineering and malware-based attacks. Attackers in the social engineering phishing-base usually try to control the victims' accounts by sending them simulated emails with fake URLs that deliver to phishing websites. Social engineering-base attacks, also called deceptive phishing are further categorized into email-based and website-based phishing. Malware-based phishing on the other side uses a variety of malicious programs that run on the victims' machines. This type of phishing is further classified as; keyloggers/screen loggers, session hijacking, host file poisoning, content injection and DNS phishing [3].

According to Zhang et al. (2012), different regions may use different phishing techniques such as

- Spear Phishing
- Link Manipulation
- Vishing (Voice Phishing)
- Web-Based Delivery
- Smishing (SMS Phishing)
- Payment/delivery scam
- Downloads

According to Yasin et al. (2018), some address bar-based features on how to predict phishing websites include the followings:

The Use of Internet Protocol (IP) Address

Whenever a domain name is substituted with an IP address in the URL, it is certain that a perpetrator is attempting to gather some sensitive information. For instance, the following link illustrates a domain being replaced by an IP address and an IP address converted to hexadecimal code respectively: http://126.78.2.134./fake/html and
http://0x67.0xAA.0xDA.0x63/3/paypal.ca/index.html

Rule: IF (Domain part has an IP Address = phishing
Otherwise = Legitimate

Use of Long Universal Resource Locator (URL)

Phishers can conceal suspicious information using long URLs as illustrated: http://fedacadefifo.com.fr/4/ute/ab56e3e419e51502h318bde47b884e4a/cd=home&receive=
11004d58f5b74f8dc1e7c2e8dd4105e811004d58f5b74f8dc1e7c2e8dd4105e8@malicious.website.HTML

Guarantying the accuracy of the study, the length of the Universal Resource Locator in the dataset was calculated to produce a certain average length. This implies that when URL's length is equal or greater than 54 characters, the URL is suspected to be phishing. Reviewing the dataset, 1220 URL lengths were equal or greater than 54 constituting 48.8% size of the entire dataset.

Rule: IF {$URLlength$ < 54 → $feature$ = Legitimate
$elseif URLlength$ ≥ 54 and ≤ 75 → $feature$ = $Suspicious$
$otherwise$ → $feature$ = Phishing

This feature rule has been updated by using a method based on the frequency, hence improving its accuracy.

The Use of Sub Domain and Multi-Sub Domains

Considering this link: hhtp//www.hud.ac.ng/students/, the domain includes the country-code Top-Level Domain (ccTLD) which is 'ng' in our given link, 'ac' is shortened form of academics, and 'ac.ng' being a Second-Level Domain (SLD) with 'hud' the domain's real name. Creating a rule to extract this feature, the 'www.' in the Universal Resource Locator which is the subdomain must be removed, then the ccTLD deleted if it already exists. The left over dots are then added,if there are more than one dot and only a subdomain the URL is categorized as malicious. However, dots with multiple subdomains are classified as phising otherwise, it will assign 'Legitimate' to the feature.

Rule: IF {Dots in Domain Part = 1 =Legitimate
Dots in Domain Part = 2 = Suspicious
Otherwise →Phishing

The Use of Hypertext Transfer Protocol with Secure Sockets Layer (HTTPS)

Though using HTTPS is crucial in creating a legitimate website, it is deemed insufficient. Kazemian H. B. & Ahmed S. (2021) recommend verifying the HTTPS certificate's validity, the issuer's level of trust, and perhaps the certificates length of existence. Among the most reliable certified authorities are "GeoTrust, GoDaddy, Network Solutions, Thawte, Comodo, Doster, and VeriSign." Furthermore, it was discovered that the minimum age of a trustworthy certificate is two years by putting our datasets to the test.

Rule: IF {Using HTTPS with trusted Issuer and Certificate >=1year=Legitimate
Using HTTPS and Untrusted Issuer = Suspicious
Otherwise=Phishing

Favicon

This is visual representation (icon) connected to a certain website. However, Favion is shown in the address bar, including newsreaders and graphical browsers as visual reminder of the website identifier. If the favicon loads from a different domain than the one displayed in the URL bar, the webpage is probably a phishing attempt.

Rule: IF {Favicon Loads from External Domain → Phishing
Otherwise → Legitimate

Use of Non-Standard Port

This feature is useful for confirming if a particular service like the HTTP is available or not on a particular server. It is far preferable to only open the ports you need to do what you need to do to control intrusions. Many firewalls, proxy servers, and Network Address Translation (NAT) servers will by default block all or the majority of the ports and only open the ones that are chosen. User

information is at risk if all ports are open because phishers can operate almost any service they want.

The most important ports and their preferred status are shown in Table 1

Rule: IF {Port # is of the Preferred Status → Phishing
Otherwise → Legitimate

Table I: Important ports and their most preferred status

PORT	SERVICE	MEANING	PREFERRED STATUS
21	FTP	Transfer files from one host to another	Close
22	SSH	Secure File Transfer Protocol	Close
23	Telnet	Provides a bidirectional interactive text-oriented communication.	Close
80	HTTP	Hypertext transfer protocol	Open
443	HTTPS	Hypertext transfer protocol secured.	Open
445	SMB	Providing shared access to files, printers, serial ports	Close
1433	MSSQL	Store and retrieve data as requested by other software applications.	Close
1521	ORACLE	Access the Oracle database from the web.	Close
3306	MySQL	Access MySQL database from the web.	Close
3389	Remote Desktop	Allow remote access and remote collaboration	Close

The Existence of 'https' in the Domain of an URL.
Phishers may add the "HTTPS" token to the domain part of a URL to trick users. For example, http://https-www-paypal-it-webapps-mpp-home.soft-hair.com/.

Rule: IF {Using HTTP Token in Domain Part of The URL → Phishing
Otherwise → Legitimate

In the existing system, the detection processes include:

- The use of blacklist database which has all the phishing URLs.
- The use of IP address
- The use of mail/mail-to attributes

Meanwhile, that an address is on a blacklist does not mean it is malicious. Legitimate addresses can be blacklisted though this is not very flexible and can be time-consuming to maintain. However, an effective blacklist has to be kept up-to-date with new threats and this takes extra time and effort.

Thus, a real-time detection system is developed to help reduce the stress undergone in observing and analyzing the physical features of URLs alone in other to tell if it is phishing or not.

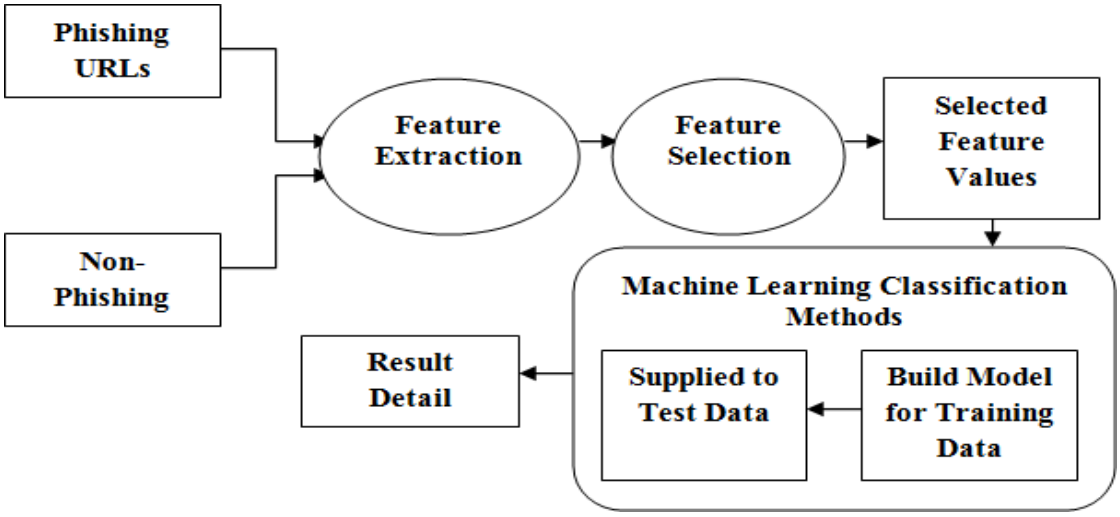

Figure I.: Architecture of Our Proposed System

Data Set Collection

The data that generated the datasets from which the models were trained and tested were extracted from various open-source platforms known as Phish Tank. These datasets comprise of both legitimate and phishing URLs in multiple formats like CSV, JSON, and so on that get updated hourly.

	A
1	http://1337x.to/torrent/1048648/American-Sniper-2014-MD-iTALiAN-DVDSCR-X264-BST-MT/
2	http://1337x.to/torrent/1110018/Blackhat-2015-RUSSIAN-720p-WEB-DL-DD5-1-H264-RUFGT/
3	http://1337x.to/torrent/1122940/Blackhat-2015-x264-1080p-WEB-DL-eng-nl-subs-sharky/
4	http://1337x.to/torrent/1124395/Fast-and-Furious-7-2015-HD-TS-XVID-AC3-HQ-Hive-CM8/
5	http://1337x.to/torrent/1145504/Avengers-Age-of-Ultron-2015-CAM-New-Audio-x264-CPG/
6	http://1337x.to/torrent/1160078/Avengers-age-of-Ultron-2015-HQ-CAM-H264-AC3-MURD3R/
7	http://1337x.to/torrent/294349/American-Idol-S11E04-Auditions-4-HDTV-XviD-FQM-ettv/
8	http://189.cn/dqmh/userCenter/myOrderInfoList.do?method=listMyOrderInfo_new&isVs=no
9	http://2gis.ru/moscow/search/%D0%9F%D0%BE%D0%B5%D1%81%D1%82%D1%8C/tab/firms/zoom/11
10	http://abc.go.com/shows/general-hospital/episode-guide/2015-05/08-friday-may-8-2015
11	http://abc.go.com/shows/the-muppets/video/new-abc-comedy-trailers?cid=abchp_muppets
12	http://abcnews.go.com/US/wireStory/regulators-delays-georgia-nuclear-plant-31020059
13	http://adultfriendfinder.com/css/live_cd/ffadult/english/0/font_face-1427390957.css
14	http://akhbarelyom.com/news/newdetails/410322/1/%D8%A8%D9%88%D8%B6%D9%88%D8%AD.html
15	http://allegro.pl/amadeus-quartet-haydn-string-quartets-collectors-i5207998383.html
16	http://allegro.pl/narzedzia-i-sprzet-warsztatowy-18554?ref=simplified-category-tree
17	http://allegro.pl/royal-string-quartet-music-for-string-quartet-cd-i5262876831.html
18	http://allegro.pl/sexy-g-string-stringi-z-koralikami-must-have-uni-i5039087215.html
19	http://allegro.pl/sporty-strzeleckie-i-myslistwo-13495?ref=simplified-category-tree
20	http://allegro.pl/sporty-towarzyskie-i-rekreacja-13408?ref=simplified-category-tree
21	http://allegro.pl/triumph-miss-sexy-allday-string-stringi-36-s-bez-i4855636396.html
22	http://allegro.pl/triumph-stringi-exquisite-essence-string-stal-38-i5073330901.html
23	http://allegro.pl/wyszczuplajace-body-string-pod-biust-jony-srebra-i5124700240.html

Benign_url_file

Figure II: Phishing URLs Dataset

	A	B	C	D	E	F	G	H	I	J
1	phish_id	url	phish_det	submissio	verified	verificatic	online	target		
2	6911546	https://ja	http://ww	2021-01-0	yes	2021-01-0	yes	Other		
3	6911545	http://po	http://ww	2021-01-0	yes	2021-01-0	yes	Other		
4	6911536	https://sp	http://ww	2021-01-0	yes	2021-01-0	yes	Other		
5	6911494	https://hy	http://ww	2021-01-0	yes	2021-01-0	yes	Other		
6	6911483	http://sto	http://ww	2021-01-0	yes	2021-01-0	yes	Other		
7	6911482	https://oc	http://ww	2021-01-0	yes	2021-01-0	yes	Other		
8	6911481	https://tr	http://ww	2021-01-0	yes	2021-01-0	yes	Other		
9	6911480	https://jo	http://ww	2021-01-0	yes	2021-01-0	yes	Other		
10	6911467	https://su	http://ww	2021-01-0	yes	2021-01-0	yes	Other		
11	6911466	https://cr	http://ww	2021-01-0	yes	2021-01-0	yes	Other		
12	6911465	http://est	http://ww	2021-01-0	yes	2021-01-0	yes	Other		
13	6911424	https://et	http://ww	2021-01-0	yes	2021-01-0	yes	eBay, Inc.		
14	6911414	https://is	http://ww	2021-01-0	yes	2021-01-0	yes	Development Bank of Singa		
15	6911408	http://wir	http://ww	2021-01-0	yes	2021-01-0	yes	Other		
16	6911403	http://ma	http://ww	2021-01-0	yes	2021-01-0	yes	ABSA Bank		
17	6911400	http://ww	http://ww	2021-01-0	yes	2021-01-0	yes	Other		
18	6911398	https://bi	http://ww	2021-01-0	yes	2021-01-0	yes	Other		
19	6911395	https://fg	http://ww	2021-01-0	yes	2021-01-0	yes	Other		
20	6911394	http://fgh	http://ww	2021-01-0	yes	2021-01-0	yes	Other		
21	6911389	https://wl	http://ww	2021-01-0	yes	2021-01-0	yes	Other		
22	6911388	https://wl	http://ww	2021-01-0	yes	2021-01-0	yes	Other		
23	6911382	http://clfi	http://ww	2021-01-0	yes	2021-01-0	yes	Other		

online-valid_ds

Figure III: Legitimate URL Dataset

REVIEW OF RELATED WORKS

Phishing attacks severely affect national security, intellectual properties and the economy at large in a negative way as online businesses, banks, Internet users and government are the primary target [4]. An algorithm that would generate random credit card numbers was developed in the early 1990s, in an attempt to create fake American Online service provider (AOL) accounts.

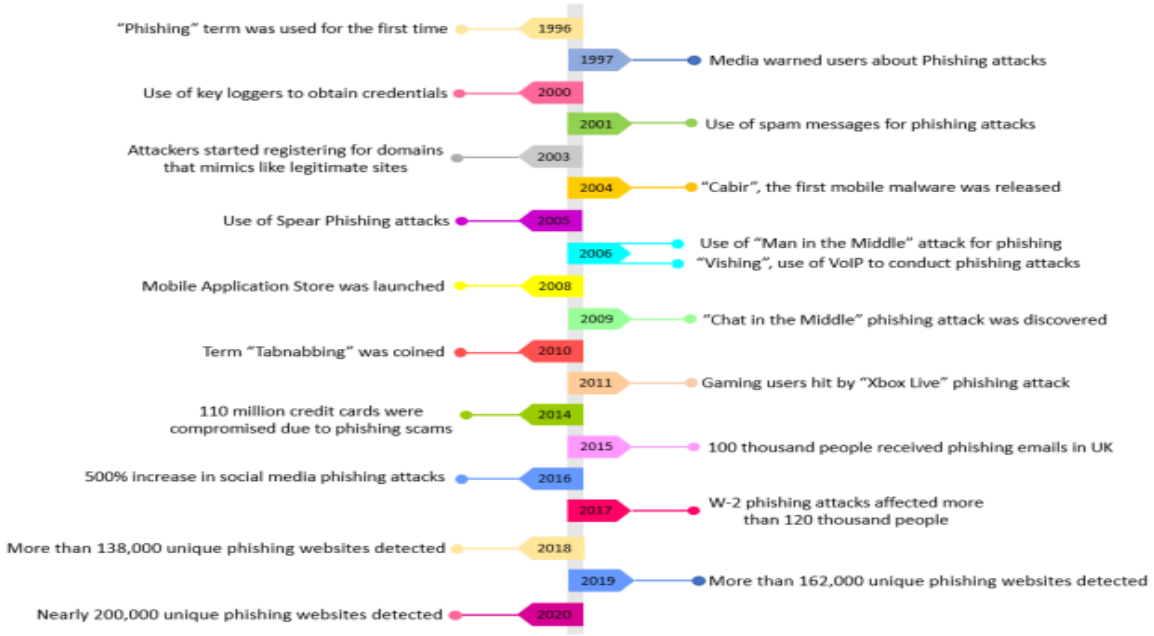

Figure IV: Evolution of phishing attacks

Phishing attack progression as shown in Figure 4[6] started in 1996 when the word "phishing" was first introduced in 1996, however, it spread via different information channels as time went on starting with spam messages, mobile malware to spear-phishing and so on. and This became an eye opener to researchers when a huge financial loss was made in 2014.

Due to the emergence of the Internet and its prevalence on media platforms, phishing has risen tremendously and has continued to rise [7] hence, becoming increasingly sophisticated, giving the phisher access to observe the activities of his victims while navigating the web, however, transversing any security boundaries with the victim. Phishing being a form of social engineering where attackers deceive their victims into installing malwares like ransomware thus revealing sensitive information can be averted when users protect themselves from phishing assaults using a variety of methods, such as the heuristic approach, rule-based approach, Visual Similarity-Based Phishing Detection Systems and a supervised machine learning (ML) approach [10].

Supervised Machine Learning algorithm is shown to be more extensively used for classification when compared to other ways of identifying phishing websites, hence giving a high accuracy in phishing detection and in a very short while.

Detection being a process of identifying an attempted computer intrusion is particularly based on the recurrence of the carrier signal, just like the radio broadcasting frequencies, but requires separating background noises from the weak signals just as in radio astronomy or constructing a hidden signal as seen in steganography.

Stegnographic analysis which refers to detection of concealed or hidden messages is in contrast to the detection of simply encrypted signals where the cipher text is usually identified even though it cannot be decoded. Steganalysis simply determines the probability of the existence of hidden messages making it an interesting distinction from other forms of detection.

In conclusion, the art of detection, also called 'following clues', is an attempt to reconstruct a sequence of events by identifying the relevant information concerning the situation.

Phishing Websites

A domain that duplicates an official website in appearance and name in other to deceive people into believing they are legitimate is referred to as phishing website [12].

Phishing had more changes in implementation in the early 2000s, in which the "love bug of 2000" is a typical example where victims were sent 'I LOVE YOU' email with an attachment that overwrites files on the victim's computer and copies itself to the user's contact list. That same year, different phishers began to register phishing websites.

In recent years, phishing websites appear frequently and poses as a new cyber security threat which has caused a great harm in data security and online financial services [13].

It has been assumed that the creation of most phishing websites is attributed to the vulnerability of most web servers, allowing phishers to host websites without the owner's knowledge or even host a new and independent web server just for phishing activities.

According to Shapiro (1992), the ability of the computer system to acquire knowledge and be able to use the acquired knowledge in self-improvement rather than being programmed with the knowledge is known as Machine Learning (ML) which is a branch of AI that enables machines to automatically gain knowledge and improve on the knowledge with minimal human intervention. Machine Learning also cuts across other scientific disciplines like cognitive science and statistics.

Machine Learning is vast following its production of basic statistical theories of learning processes, designed learning algorithms like speech recognition used in commercial systems [14].

EXPERIMENTAL RESULT AND ANALYSIS

Comparing the four leading ML models (Random Forest, Decision Tree, Multilayer Perceptrons and XGBOOST), XGBOOST shows to be more accurate as shown in Table II and figure V below.

Table II. Accuracy and Performance of the four leading Models

ML Model	Train Accuracy	Test Accuracy
XGBOOST	0.866	0.864
Multilayer Perceptrons	0.865	0.864
Decision Tree	0.814	0.812
Random Forest	0.818	0.811

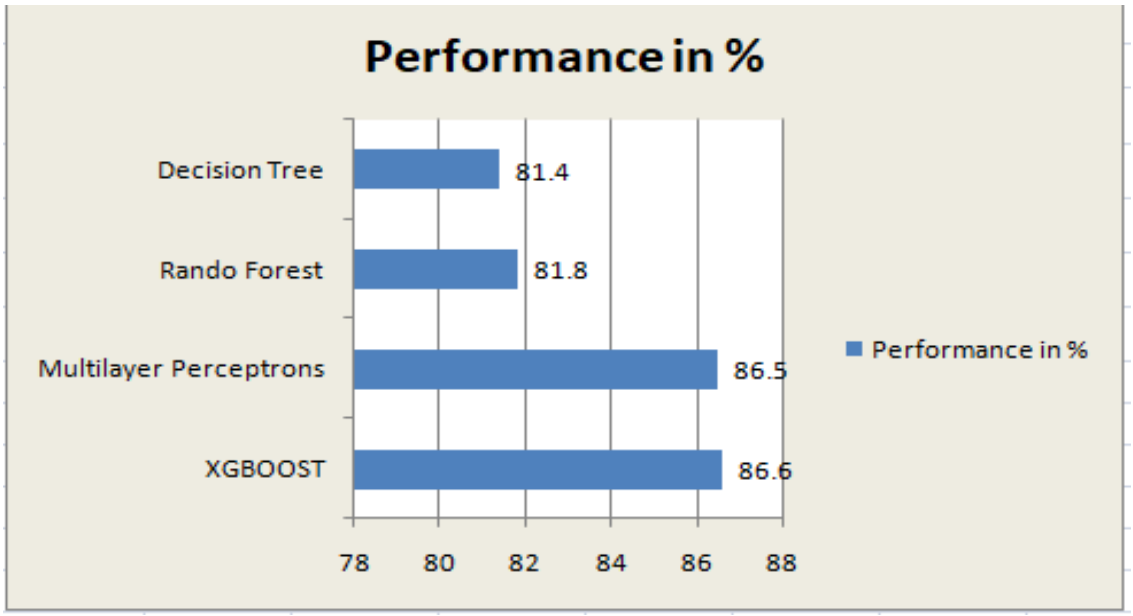

Figure V: Chart Accuracy Comparison of the Four Leading Models

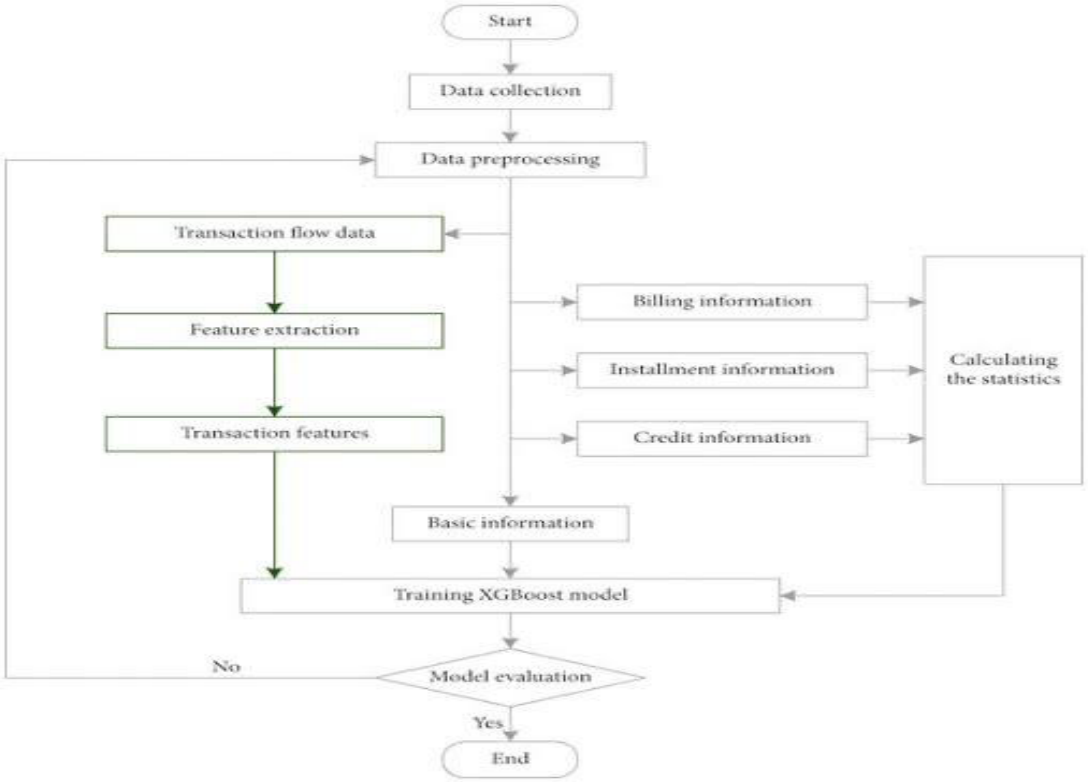

Figure VI: Visualization of XGBOOST Model

index.html

```
<!DOCTYPE html>
<html >
<head>
  <meta charset="UTF-8">
  <title>ML API</title>
  <link href='https://fonts.googleapis.com/css?family=Pacifico' rel='stylesheet' type='text/css'>
<link href='https://fonts.googleapis.com/css?family=Arimo' rel='stylesheet' type='text/css'>
<link href='https://fonts.googleapis.com/css?family=Hind:300' rel='stylesheet' type='text/css'>
<link href='https://fonts.googleapis.com/css?family=Open+Sans+Condensed:300' rel='stylesheet' type='text/css'>
<link rel="stylesheet" href="style.css">

</head>

<body>

 <div class="login">
  <h1>Detecting Phishing WebPage using XGBoost</h1>


    <!-- Main Input For Receiving Query to our ML -->
    <form action="{{ url_for('predict')}}" method="post" id="myform">
      <input type="text" name="URL" placeholder="URL" required="required" />

        <button type="submit" class="btn btn-primary btn-block btn-large">Detect</button>
  <br>
  Alert! Phishing Webpage Detected
  http://www.facebook.com/home/service
    </form>
  <br>
  <br>


 </div>


</body>
</html>

```

Figure VII: A HTML webpage application

```
index.html   style.css
style.css > ...
@import url(https://fonts.googleapis.com/css?family=Open+Sans);
.btn { display: inline-block; *display: inline; *zoom: 1; padding: 4px 10px 4px; margin-bottom: 0; font-size: 13px; line-height: 18px; color: #333333;
.btn:hover, .btn:active, .btn.active, .btn.disabled, .btn[disabled] { background-color: #e6e6e6; }
.btn-large { padding: 9px 14px; font-size: 15px; line-height: normal; -webkit-border-radius: 5px; -moz-border-radius: 5px; border-radius: 5px; }
.btn:hover { color: #333333; text-decoration: none; background-color: #e6e6e6; background-position: 0 -15px; -webkit-transition: background-position
.btn-primary, .btn-primary:hover { text-shadow: 0 -1px 0 rgba(0, 0, 0, 0.25); color: #ffffff; }
.btn-primary.active { color: rgba(255, 255, 255, 0.75); }
.btn-primary { background-color: #4a77d4; background-image: -moz-linear-gradient(top, #6eb6de, #4a77d4); background-image: -ms-linear-gradient(top,
.btn-primary:hover, .btn-primary:active, .btn-primary.active, .btn-primary.disabled, .btn-primary[disabled] { filter: none; background-color: #4a77d4;
.btn-block { width: 100%; display:block; }

* { -webkit-box-sizing:border-box; -moz-box-sizing:border-box; -ms-box-sizing:border-box; -o-box-sizing:border-box; box-sizing:border-box; }

html { width: 100%; height:100%; overflow:auto; }

body {
    width: 100%;
    height:100%;
    font-family: 'Open Sans', sans-serif;
    background: #092756;
    color: #fff;
    font-size: 18px;
    text-align:center;
    letter-spacing:1.2px;
    background: -moz-radial-gradient(0% 100%, ellipse cover, rgba(104,128,138,.4) 10%,rgba(138,114,76,0) 40%),-moz-linear-gradient(top,  rgba(57,17
    background: -webkit-radial-gradient(0% 100%, ellipse cover, rgba(104,128,138,.4) 10%,rgba(138,114,76,0) 40%), -webkit-linear-gradient(top,  rgb
    background: -o-radial-gradient(0% 100%, ellipse cover, rgba(104,128,138,.4) 10%,rgba(138,114,76,0) 40%), -o-linear-gradient(top,  rgba(57,173,2
    background: -ms-radial-gradient(0% 100%, ellipse cover, rgba(104,128,138,.4) 10%,rgba(138,114,76,0) 40%), -ms-linear-gradient(top,  rgba(57,173
    background: -webkit-radial-gradient(0% 100%, ellipse cover, rgba(104,128,138,.4) 10%,rgba(138,114,76,0) 40%), linear-gradient(to bottom,  rgba(
    filter: progid:DXImageTransform.Microsoft.gradient( startColorstr='#3E1D6D', endColorstr='#092756',GradientType=1 );

}
.login {
    position: absolute;
    top: 40%;
    left: 50%;
    margin: -150px 0 0 -150px;
    width:400px;
    height:400px;
}

.login h1 { color: #fff; text-shadow: 0 0 10px rgba(0,0,0,0.3); letter-spacing:1px; text-align:center; }

input {
    width: 100%;
    margin-bottom: 10px;
    background: rgba(0,0,0,0.3);
    border: none;
    outline: none;
    padding: 10px;
    font-size: 13px;
    color: #fff;
    text-shadow: 1px 1px 1px rgba(0,0,0,0.3);
    border: 1px solid rgba(0,0,0,0.3);
    border-radius: 4px;
    box-shadow: inset 0 -5px 45px rgba(100,100,100,0.2), 0 1px 1px rgba(255,255,255,0.2);
    -webkit-transition: box-shadow .5s ease;
    -moz-transition: box-shadow .5s ease;
    -o-transition: box-shadow .5s ease;
    -ms-transition: box-shadow .5s ease;
    transition: box-shadow .5s ease;
}
input:focus { box-shadow: inset 0 -5px 45px rgba(100,100,100,0.4), 0 1px 1px rgba(255,255,255,0.2); }
```


Figure VIII: A CSS webpage application

Figure X: XGBOOST Webpage design

As indicated in Fig.V, XGBOOST model leads in performance, hence used in our phishing detection web-page design as shown in Figure IX.

Using a web application that integrates the model with the highest accuracy based on the feature and algorithm used in distinguishing phishing URL from legitimate URL links, users can enter website URL links to determine whether they are legitimate or phishing.

CONCLUSION

From the above study, XGBOOST model shows more performance accuracy compared with Decision Tree, Random Forest and Multilayer Perceptrons. Hence, it is used in the design of a URL phishing detection webpage which detects if a URL link is authentic or not.

The Phishing detection approach implemented in this study is imperative in other to avoid and drastically reduce the chances of data theft and other cyber frauds achieved either through name or brand impersonation and subdomain attacks.

Required content-based features of both phishing and benign URLs of websites were extracted and phishing websites were easily predicted using trained machine learning models.

REFERENCES

[1] B. B. Gupta, A. Tewari, A. K. Jain, and D. P. Agrawal, "Fighting against phishing attacks: state of the art and future challenges," Neural Comput. Appl., vol. 28, no. 12, pp. 3629–3654, 2017, doi: 10.1007/s00521-016-2275-y.

[2] Anti-Phishing Working Group, "Phishing Activity Trends Report 3rd Quarter," no. November, pp. 1–9, 2021.

[3]. M. Jakobsson and S. Myers, "Phishing and Countermeasures: Understanding the Increasing Problem of Electronic Identity Theft," John Wiley Sons, 2006.

[4] Subasi, A., Molah, E., Almkallawi, F. and Chaudhery, T.J. (2017), *Intelligent phishing website detection using random Forest classifier*, International Conference on Electrical and ComputingTechnologies and Applications (ICECTA '17), IEEE, pp. 1-5.

[5] Kuyama, M., Kakizaki, Y., … Sasaki,R.(2016).*Method for detecting a malicious domain by using whois and dns features*, The Third International Conference on Digital Security and Forensics (DigitalSec2016).

[6] G. Diksha and J. A. Kumar, "Mobile phishing attacks and defence mechanisms: State of art andopen research challenges,"Comput. Secur., vol. 73, pp. 519–544, Mar. 2018, doi: 10.1016/j.cose.2017.12.006.

[7] Shrivas, A.K. and Suryawanshi, R. (2017). *Decision Tree Classifier for Classification of Phishing Website with Info Gain Feature.* Int. J. for Res. Appl. Sci. Eng. Technol.

[8] Verified Phishing URL, Available at: https://www.phishtank.com. Last accessed on September 22, 2017.

[9] Ankit,K.J and Gupta B.B. Phishing Detection: Analysis of Visual Similarity Based Approaches. National Institute of Technology, Kurukshetra, India, 10 January2017, ticle ID 5421046, 20 pages.

[10] Zhang L. and Zhan C. *Machine Learning in Rock Facies Classification: An Application of XGBOOST*. In International Geophysical Conference, Qingdao, China, 17-20 April 2017, pp. 1371-1374.

[11] Buber, E., Demir O., Sahingoz O. K. (2017). *Feature selections for the machine learning based detection of phishing websites*: International Artificial Intelligence and Data Processing Symposium (IDAP).

[12] Jain, A. (2016) *Complete Guide to Parameter Tuning in XGBOOST (with code in python)*: Complete guide to parameter tuning in XGBOOST (with code in Python).

[13] Kazemian,H. B. and Ahmed S. (2021)*Comparisons of machine learning techniques for detecting malicious webpages:*Expert Systems with Applications.

[14] Khonj M., Iraqi, Jones,A. (2013).*Phishing detection: a literature survey*. IEEEcommunications surveys & tutorials.

[15] Lord, N. (2018). *What is a Phishing Attack? Defining and Identifying Different Types of Phishing Attacks:*https://digitalguardian.com/blog/what-phishing-attack-defining-and-identifying-different-types-phishing-attacks.

[16] M. Jakobsson and S. Myers, "Phishing and Countermeasures: Understanding the Increasing Problem of Electronic Identity Theft," John Wiley Sons, 2006.

[17] Mustafa,A. and Nazife, B. (2015).Feature Extraction and Classification Phishing Websites Based on URL: IEEE.

[18] Pradeepthi, K.V. and Kannan, A. (2014). Performance Study of Classification Techniques for Phishing URL Detection: Sixth International Conference on Advanced Computing (ICoAC) IEEE.

[19] Rao,R. S. and Pais,A.R. (2018).*Detection of phishing websites using an efficient feature-based machine learning framework:*Neural Computing and Applications.

[20] Routhu S.R. and Alwyn, R.P. (2018). *Detection of phishing websites using an efficient feature-based machine learning framework*: In Springer.

[21] Sahoo D., Liu C. and Hoi S.C. (2017). *Malicious URL detection using machine learning: A survey*. arXiv:1701.07179.

[22] H. Zhang, G. Liu, T. W. S. Chow, and W. Liu, "Textual and visual content-based anti-phishing: a Bayesian approach," *IEEE Transactions on Neural Networks*, vol. 22, no. 10, pp. 1532–1546,2011

[23] S. Sheng, M. Holbrook, P. Kumaraguru, L. F. Cranor and J. Downs, "Who falls for phish?: a demographic analysis of phishing susceptibility and effectiveness of interventions", *Proceedings of the 28th international conference on Human factors in computing systems ser. CHI'10. New York NY USA:ACM*, pp. 373-382, 2010.

[24] C. H. Hsu, P. Wang, and S. Pu, "Identify fixed-path phishing attack by STC," in *Proceedings of the 8th Annual Collaboration, Electronic Messaging, Anti-Abuse and Spam Conference (CEAS '11)*, pp. 172–175, ACM, Perth, Australia, September 2011.

[25] Ahmad, A., Anazida, Z., … Oluwatobi, A. (2013). Feature Extraction Process: *A Phishing Detection Approach*: In IEEE communications and surveys.

[26] Anti-Phishing Working Group (APWG) (2019), *Phishing activity trends report, 1st quarter https://apwg.org/trendsreports_q3_2019*.

Applied Sciences Research Periodicals
June 2023, Vol. 1, No. 3, pp. 34-68.

A Mathematical Model for Accessing Liquid Accumulation in Production Tubing: Effect of Tubing Height

Ikputu, Woyengikuro Hilary., Dulu Appah., Emeka Okoro and Solomon Williams

1. Department of Petroleum and Gas Engineering Faculty of Engineering, University of Port Harcourt, Rivers State, Nigeria

Abstract:
Liquid-loading is challenging in mature gas-fields globally. It causes increasing reverse-pressure from increasing liquid-column, thereby significantly affecting production overtime. In this study, a new critical-velocity model was developed for predicting onset of liquid-loading in gas-wells. This was done following the reverse film concept, while incorporating separate pressure drops for both liquid and gaseous phases. Also, influence of production tubing length and liquid-film thickness was equally considered. A comparative analysis of prediction-accuracy of developed-model was also conducted alongside other critical velocity models like Turner et al. (1969), Coleman et al. (1991), Nossier et al. (2000), Li et al. (2001), and Pagou and Wu (2020) models using data from literature. The obtained field data was from 18 vertical gas-wells from Xinjiang North-West gas field in China. The prediction accuracies of critical-velocity models followed the order, Nossier et al. (2000), Turner et al. (1969), Coleman et al. (1991), Li et al. (2001), Pagou and Wu (2020), and developed-model. To increase the prediction accuracy of developed-model, model coefficient adjustments were done by percentage-reduction of developed model coefficient. In the end, the prediction-accuracy of developed-model was tremendously increased by reducing model coefficient.

Keywords: Liquid-loading critical-velocity model, gas-wells, reverse film concept, tubing length

INTRODUCTION

With time, gas-wells experience reduced production as reservoir-pressure depletes. Liquids can cause reduction in production even quicker. Liquid-loading is challenging in mature gas-fields. It comes as an increasing reverse pressure due to increasing liquid-column, which at first will reduce gas well production but overtime, causes a complete stoppage of production (Fan *et al.*, 2018). Therefore, in theory, all gas-wells will encounter liquid-loading at some point. Liquid-loading is liquid-accumulation in wells, causing reduction or in more severe cases, no production. Liquid-loading cause's inefficient recovery and also very expensive remedial solutions is often needed, particularly in wet/retrograde gas-wells (Pagou and Wu, 2020).

Liquid-loading occurs in vertical or deviated wells during production from natural gas reservoirs, and is independent of gas-composition, well temperature or pressure. This is typical in both offshore and onshore production systems and causing simultaneous gas, liquid-hydrocarbons and water flows (Shi *et al.*, 2016). The condensed water vapor is from the fractional water cut and its production is unavoidable. Any effort to prevent it could cause a drastic permeability reduction, which will in-turn cause severe damage to the formation (Belfroid *et al.*, 2008).

Production data analysis for gas wells often must contend with liquid-loading due to inability to concurrently expel produced liquids and gas (Wang *et al.*, 2018). The produced liquids gather to form a hydrostatic pressure in the well. This is very unfavorable to the formation pressure, which is depleting steadily as gas is produced, eventually reducing production to the point where artificial lift must be deployed to lift the liquid load from the well so as to begin gas production again (Guo *et al.*, 2005).

During transient operations, liquid rates can get higher, and will typically show nonlinear responses to the rate change, a phenomenon known as entrainment. Another major source of liquid is when water escapes into the wellbore through a path different from gas (Ardhi, 2016). The water could flow from: casing or parker leaks, behind pipes as a result of cement bond failure, fractures or faults between injectors and producers, natural fracture leading to an aquifer, unfractured wells with or without effective barrier to cross flow, cusping /conning etc (Shi *et al.*, 2016). In any of these cases, whether dry or wet gas-reservoir, is susceptible to early liquid-accumulation (Aboutaleb and Vahid, 2015).

Though liquid-loading is a natural phenomenon, early and massive liquid production could be aggravated by ineffective completion design and poor production practices. Water being the most abundant liquid on earth is very crucial especially when used to boost the reservoir pressure which enhances recovery of hydrocarbon fluids but could also pose technical difficulties when it negatively impacts productive performance and affects the overall operational economics of a field (Joseph and Ajienka, 2010). Unlike oil wells where a large aquifer is of a huge advantage to operators due to its ability to sustain reservoir-pressure, in gas-wells, it poses a very huge challenge to gas-well productivity (Ikoku, 1992).

This is because gas molecules are very light that they would flow without help even at low formation permeability but with water flowing simultaneously with it, the relative permeability is drastically reduced which significantly affects production (Ikoku, 1992). With time, liquid accumulation continues with more condensation from intermediate hydrocarbons and water vapor into production-tubing together with water that directly finds its path. This will cause back-pressure and afterwards kill wells if not properly managed (Nosseir *et al.*, 2000).

The commonest way of predicting onset of liquid-loading is determination of critical-gas velocity through some well-established models. Using this approach, many models have previously been developed (Riza *et al.*, 2016). These critical velocity models are based on continuous film, liquid droplet or reverse film theories of liquid-loading. Some models are quite popular since the parameters needed are readily obtained at the wellhead, which serves a great convenience for field operators (Luo *et al.*, 2014). However, in practice, the existing critical velocity models still fall short in accurately predicting onset of liquid-loading. Sometimes, a coefficient is usually needed to 'adjust' predicted critical-velocities to better fit the situation in fields. This scenario creates need for a better critical velocity model that better predicts liquid-loading.

Therefore, this study focuses on development of a new analytical critical velocity model for predicting liquid-loading.

Concepts of Liquid-Loading in Gas Wells

The first recognizable liquid-loading work was first done by Turner *et al.* (1969). In their study, they proposed two concepts reportedly responsible for liquid-loading. The proposed concepts were continuous-film and entrained liquid-droplet models.

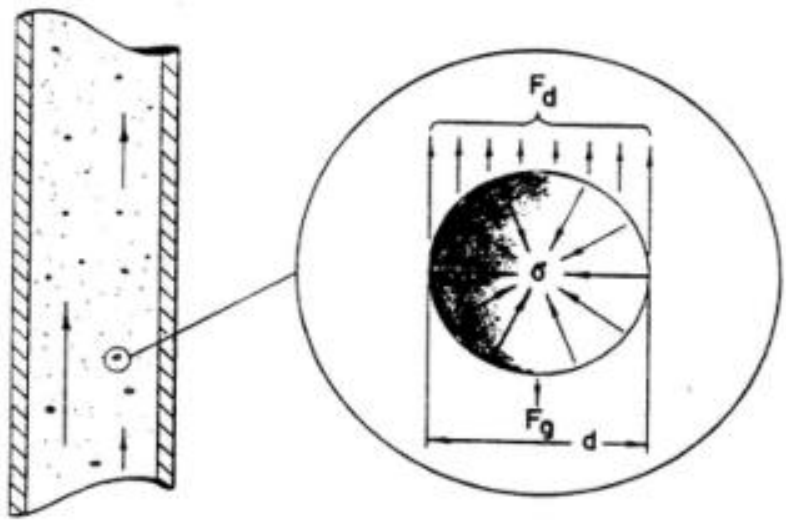

Figure .1 Entrained droplet movement (Turner *et al.*, 1969)

Another popular concept that gained traction later was the reverse film model popularized by Banea (1986). Reverse film model attributes liquid-loading to liquid-film reversal along pipe-walls when the prevalent gas velocity cannot sufficiently carry all liquid. In this concept, liquid-droplets tend to stick to pipe-walls on coming in contact with it. Then, overtime the droplets will coalesce into larger a droplet, which correspondingly increases their dimensions. This continues until droplets are large-enough to flow in a direction opposite the dominant flow direction under gravity. These droplets accumulate overtime at the wellbore causing liquid-loading.

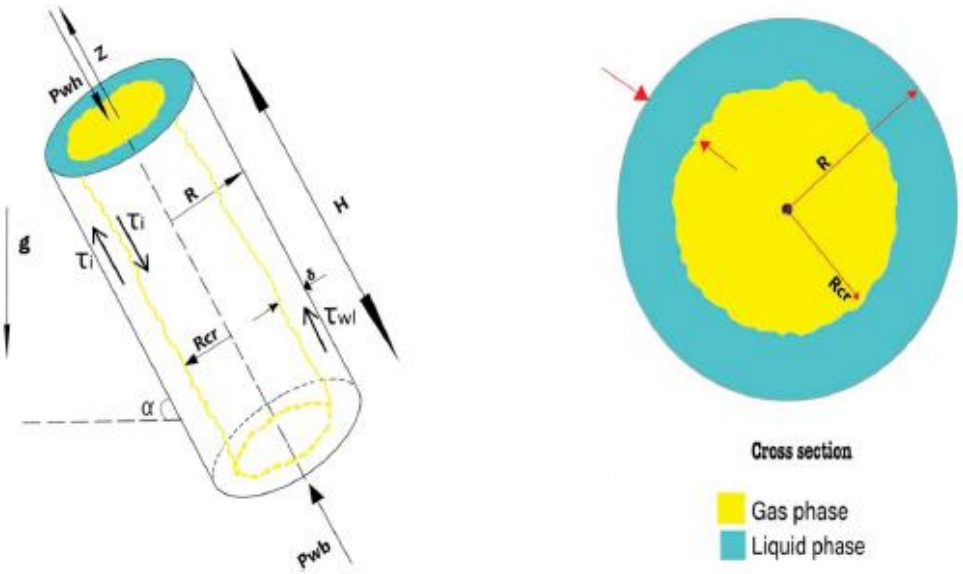

Figure 2 Reverse film flow in annular-flow in gas-wells (Pagou and Wu, 2020)

Following success of Turner *et al.* (1969) model, over time, several scientists have proposed modifications to this model considering various parameters. Pagou and Wu (2020) were able to relate critical-velocity to the liquid-phase viscosity and density, the gravitational forces, gas-liquid in tubing (gas void fraction), and gas-well geometry (tubing diameter, inclination-angle and circumferential angle). Unlike their predecessors, Li *et al.* (2001) supposed liquid-drops transported by gas stream under a high flow rate do have an ellipsoidal shape under the force of pressure difference and high flow-rate, and thereby established their correlation.

Subsequently, Guo *et al.* (2005) built a model dependent on influence of droplets' kinetic energy. Belfroid *et al.* (2008) considered the influence of inclination-angles on inclined gas-wells. Wang *et al.* (2015) considered effect of Weber number on liquid drop and established a new critical gas-velocity. Kumar *et al.* (2017) characterized loading phenomenon using void-fraction. Riza *et al.* (2016) developed a flow regime prediction model that locates loading-point across the pipe. Chen *et al.* (2016) established a model based on liquid-film and gas-core force balances. Okoro *et al.* (2019), while improving the liquid-film model of Chen *et al.* (2016), also considered the volumetric gas-concentration.

However, there appears no research on influence of parameters like height of tubing on liquid-loading. Recently, Wang *et al.* (2018) conducted numerous experiments and found that there is an interconnection between pressure-gradient and gravitational-force, which is partly responsible for the loading phenomenon. But these parameters are sometimes omitted or completely ignored in developing critical velocity models for mathematical convenience. Classical physics indicate that gravitational-force is directly-proportional to height, while pressure-drop in different forms generally accompanies fluid flow in conduits. It becomes imperative that these are incorporated to generate more robust models that truly explains the phenomenon of liquid-loading.

Liquid Unloading Options for Natural Gas Wells

Foaming Agents/Surfactants:

The use of foam produced by surfactants can be effective for gas wells that accumulate liquid at low rates. Foam reduces the density and surface tension of the fluid column, which reduces the critical gas velocity needed to lift fluids to surface and aids liquid removal from the well. Compared to other artificial lift methods, foaming agents are one of the least costly applications for unloading gas wells. Foaming agents work best if the fluid in the well is at least 50 percent water. Surfactants are not effective for natural gas liquids or liquid hydrocarbons.

Surfactants are delivered to the well as soap sticks or as a liquid injected directly into the casing-tubing annulus or down a capillary tubing string. For shallow wells, the surfactant delivery can be as simple as the operator periodically pouring surfactant down the annulus of the well through an open valve. For deep wells, a surfactant injection system requires the installation of surface equipment, as well as regular monitoring. The surface equipment includes a surfactant or 'soap' reservoir, an injection pump, a motor valve with a timer (depending on the installation design), and a power source for the pump. No equipment is required in the well, although foaming agents and velocity tubing may be more effective when used in combination (USEPA, 2011).

Electric pumps can be powered by AC power where available or by solar power to charge batteries. Other pump choices include mechanical pumps that are actuated by the movement of another piece of equipment or pneumatic pumps actuated by gas pressure. Different pump types

have different advantages with respect to reliability, precision, remote operation, simplicity, maintenance frequency, efficiency, and equipment compatibility (USEPA, 2011)

Velocity Tubing:

The velocity at which gas flows through pipe determines the capacity to lift liquids. When the gas flow velocity in a well is not sufficient to move reservoir fluids, the liquids will build up in the well tubing and eventually block gas flow from the reservoir. One option to overcome liquid loading is to install a smaller diameter production tubing or 'velocity tubing'. The cross-sectional area of the conduit through which gas is produced determines the velocity of flow and can be critical for controlling liquid loading. A velocity string reduces the cross-sectional area of flow and increases the flow velocity, achieving liquid removal while limiting blowdowns to the atmosphere (USEPA, 2011).

Usually, it is expected that gas velocity must be at least 5 to 10 ft/sec (300 to 600 ft/min) to effectively remove hydrocarbon liquids from a well, and at least 10 to 20 ft/ sec (600 to 1200 ft/min) to move produced water. Hence, as a rule of thumb, gas flow velocity of 1,000 feet per minute is needed to remove liquid. These figures assume used pipe in good condition with low relative roughness of the pipe wall. The installation of a velocity string is relatively simple and requires calculation of the proper tubing diameter to achieve the required velocity at the inlet and outlet pressures of the tubing. Velocity tubing to facilitate liquid removal can be successfully deployed in low volume gas wells upon initial completion or near the wells upon initial completion or near the end of their productive lives. Candidate wells include marginal gas wells producing less than 60 Mfcd. Installation of velocity tubing requires a well workover rig to remove the existing production tubing and place the smaller diameter tubing string in the well (USEPA, 2011). Coiled tubing may also be used, allowing for easier installation and the application of a greater range of tubing diameters as small as 0.25 inches. Coiled tubing can be applied in wells with lower velocity gas production due to better relative roughness characteristics of the tubing and the absence of pipe joint connections. Studies indicate that seamed coiled tubing provides better lift characteristics due to the elimination of turbulence in the flow stream because the seam acts as a straightening vane.

Plunger Lift with Smart Well Automation:

Plunger lifts are commonly used to lift fluids from gas wells. A plunger lift system is a form of intermittent gas lift that uses gas pressure buildup in the casing-tubing annulus to push a steel plunger and a column of fluid above the plunger up the well tubing to the surface. The operation of a plunger lift system relies on pressure build-up in a gas well during the time that the well is shut-in (not producing). The well shut-in pressure must significantly exceed the sales line pressure in order to lift the plunger and load of accumulated fluid to the surface against the sales line backpressure (USEPA, 2011).

Most plunger systems operate on a fixed time cycle or on a preset differential pressure. Regardless of activation system (manual, fixed time cycle, or preset pressure differential), a valve mechanism and controller at the surface cause gas volume and pressure to build up in the wellbore initiating the plunger release cycle. At this point, the surface valve closes and the plunger drops to the bottom of the well. Once adequate pressure is reached, the surface valve opens and the plunger rises to the surface with the liquid load. Insufficient reservoir energy, or too much fluid build-up can overload a plunger lift. When that occurs, venting the well to the atmosphere (well blowdown) instantaneously reduces the backpressure on the plunger and

usually allows the plunger to return to the surface. Automated control systems optimize plunger lift and well unloading operations to prevent overloading (plunger cannot overcome backpressure and rise to the surface) and underloading (plunger rises to the surface quickly, possibly damaging equipment), therefore reducing or eliminating well venting. Smart automated control systems combine customized control software with standard well control hardware such as remote terminal units (RTUs) and programmable logic controllers (PLCs) to cycle the plunger system and lift fluids out of the tubing. The artificial intelligence component of a smart automation system monitors the tubing and sales line pressures and allows the PLC to learn a well's performance characteristics (such as flow rate and plunger velocity) and to build an inflow performance relationship (IPR) curve for the well. The frequency and duration of the plunger cycle is then modified to optimize well performance. Data analysis combined with wellhead control technology is the key to an effective gas well smart automation system. A smart automation system stores historical well production data allowing the program to learn from experience by monitoring and analyzing wellhead instrument data. The control system relays wellhead instrument data to a central computer, tracks venting times, and reports well problems and high-venting wells, all of which allow custom management of field production (USEPA, 2011).

The components of a smart well automation system that must be installed on each gas well include: remote terminal unit with PLC, tubing and casing transmitters, gas measurement equipment, control valve, and plunger detector. Automated controllers at the wellhead monitor well parameters and adjust plunger cycling. These typically operate on low-voltage, solar batteries. A host system capable of retrieving and presenting data is also required for continuous data logging and remote data transition. Operators configure all controls and send them to the RTU from the host system. Engineering time is needed to customize the control software and optimize the system.

Rod Pumps and Pumping Units:

A downhole positive displacement, reciprocating rod pump with surface pump unit can be deployed in the later stages of a well's life to remove liquids from the wellbore and maximize production until the well is depleted. Pumping units can be installed when there is insufficient reservoir pressure to operate a plunger lift. The units can be manually controlled by the field pumper, or very low volume wells may be operated with a timer. Pumping units not only eliminate the need to vent the well to unload fluids but also extend the productive life of a well. Methane emissions can be further reduced by operating pumping units with electric motors, rather than natural gas-fueled engines. The annual fuel requirement for a typical pumping unit is approximately 1,500 Mcf per unit, of which 0.5 percent is emitted as unburned methane (8 Mcf per unit per year). A well workover rig is required to install the downhole rod pump, rods, and tubing in the well. Field personnel must be trained for rod pump operations and proper maintenance of the surface equipment. Excessive wear of the rods and tubing can be a major expense for rod pump applications where solids are produced or down hole corrosion is a problem. A common problem with reciprocating pumps in gas wells is gas locking of the rod pump valves, which prevents the pump from delivering fluid to the surface at the design rate. The presence of free gas in the subsurface sucker rod pump decreases the volumetric pump efficiency and can prevent the pump from lifting fluid. This is not a problem found in progressive cavity pumps as there are no valves to gas lock (USEPA, 2011).

However, Liquid loading has remained a big challenge and a fundamental issue in gas wells as all gas wells will undergo this phase in their productive life cycle. It is more obvious and severe in aging fields but can also occur in new wells having poor completion designs. When improperly managed or failure to predict its onset accurately, it could lead to not only a tremendous reduction in production but also pose a potential challenge of killing the well. Several studies have developed models to predict the onset of liquid loading. Some of the parameters identified that affect liquid loading include gas density, liquid density, friction factor etc. One of the potential factors that affect critical height is tubing height. However, tubing height has not been considered as a factor in previous studies

Moreso, Liquid loading poses development challenge for both high rate/high pressure gas wells as well as low rate/low pressure gas wells. And depending on tubing string size, surface pressure and density of liquid produced simultaneously with the gas, it could reduce the capacity of a gas well to produce at a required rate over a particular period of time. The implications of a liquid loaded gas well are seen first in reduced revenues due to reduced production rates. Overtime, reduced revenues gradually to zero revenue if the well is not unloaded. The developed model which incorporates tubing height as determining factor will substantially improve understanding of liquid loading in gas wells. This can drastically affect the economics of a given gas project given the effect of delayed profits in a capital-intensive industry like the exploration and production industry. Armed with a better critical velocity model, this problem can be better envisaged and the accompanying costs averted.

In general, loading gas-wells means backflow and liquid-accumulation in wellbores. Some have described this phenomenon (Veeken *et al.*, 2010) as liquid-film that is initially dragged to surface by the gas core along tubing-walls, and later falling and accumulating in wellbores. Some others (Turner *et al.*, 1969; Li *et al.*, 2001; Christiansen *et al.*, 2003; Belfroid *et al.*, 2008) describe it as the flow reversal of droplets initially drained by gas-stream. The flow reversal materializes once reservoir-pressure is insufficient to drain all entrained-liquid to wellhead. When a gas-well experiences loading the backpressure increases, while gas-production decreases; if the accumulation rate is too high, gas-production stops. In the worst-case scenario, operating-company must abandon the wells, and sustain significant economic damages. Therefore, predictions of critical gas-velocity and flow-rate must be made at loading-point to avoid such circumstances and benefit from a long-term, non-loading gas well. If gas-flow rate is smaller than critical-flow rate, the well loads; and, if greater, the well does not load.

Scientists have performed numerous investigations regarding the loading phenomenon, and this has resulted in a division of the scientific community over liquid-loading is explainable using two opposing models: liquid droplet and liquid-film models.

The Liquid Drop Models

The liquid drop model infers that the loading phenomenon originates from the flow reversal or the descent of droplets toward the wellbore. Many scientists have developed models to characterize it. The most widespread model by Turner *et al.* (1969), stipulates that the droplets entrained in high-speed gas stream are spherical. They adopted Hinze (1955) critical Weber-number ranges from 20 to 30 and considers drag-coefficients of 0.44 to be constant in Reynold's number, ranging from 104 to 105. Then, after applying Newton's first law to the ascendant drag force, the ascending buoyant force and the gravity force acting upon the motionless liquid drop, they established critical gas-velocity called Turner model.

Over time, several scientists have proposed modifications to this model. Coleman *et al.* (1991), guided by Turner *et al.* (1969) theory of liquid drop, investigated 56 low-pressure gas-wells and developed a new critical flow-velocity and flow rate correlation. While establishing their model, they validated Turner *et al.* (1969) model, using their field-data, and decried 20% coefficient increase by Turner *et al.* (1969) as unnecessary. Unlike their predecessors, Li *et al.* (2001) supposed that liquid drops transported by gas stream under a high flow rate do, under the force of pressure-difference and high gas-flowrate, have an ellipsoidal shape, and thereby established their correlation. Subsequently, Guo *et al.* (2005) built a model dependent on the influence of the droplets' kinetic energy. Belfroid *et al.* (2008) considered influence of inclination angles on inclined gas-wells, and established a model based on Turner *et al.* (1969) model and the angle correction term of Fiedler and Auracher (2004) which is designed for small diameter tubing. Zhou *et al.* (2010) identified influence of liquid drops amalgamation upon loading-loading and established a critical droplets concentration to determine critical gas-flowrate. Wang *et al.* (2015) considered effect of Weber number on the liquid drop and established a new critical gas-velocity. Li *et al.* (2016), based on Turner *et al.* (1969), developed one to compute critical gas-flowrate in gas-wells. Apart from size and deformation of liquid-drop, their model also accounts for liquid quantities. By authenticating their model with datasets of Turner *et al.* (1969) and Li *et al.* (2001), they found a good match of the computed predictions with the datasets investigated.

Subsequently, Zhang *et al.* (2018) developed dimensionless critical-gas mass-flowrate to identify loading along the entire wellbore. This correlation relies on force balance of liquid-drops in gas-streams. After analysis of the droplet size in the gas stream, they found that largest liquid-sizes rely on the liquid drop breakup in co-current annular-flow and the liquid drop drainage in churn-annular flow. Furthermore, they found that, as gas flow-rate increases and the tubing diameter decreases, dimensionless critical mass flow rate decreases, thus reducing loading. Additionally, they also found that loading could be prevented by lowering surface-tension.

Although liquid-droplet model is recognized and appreciated by the scientific community for its simple design, some scientists have failed to find visual proof, in experiments or gas-wells, that corroborates the conception of liquid-droplets as causing liquid-loading. Therefore, Alamu *et al.* (2012) conducted some experiments and proved that the proportion of entrained-droplets is fewer than that liquid-film during change in flow regime (annular to churn flow regime). Wang (2014) conducted some experiments on two-phase flow-regimes (gas-liquid) in the deviated and horizontal tubes. They discovered liquid-drop flows to a certain point and then arrive at tubing-wall to amalgamate into liquid-films.

The Liquid Film Models

Unlike the liquid drop model, liquid-film model infers that the liquid film must flow primarily upward along tubing-wall. The moment it starts to flow downward is the loading point. Several scientists established models to determine initial loading point based on liquid film reversal theory. Wallis (1969) established a model to compute sufficient gas velocity needed to entrain all the liquid to wellhead. Barnea *et al.* (1982), after multiple investigations, found down flow of liquids occurs at a gas void fraction equal to 0.65. Later, a model based on change of flow regime proposed by Barnea (1986) showed unsteadiness of liquid-film and the blockage of gas-core generates the annular to slug/churn flow regime conversion. He developed his model based on the film-thickness is uniform inside the inclined pipe, and neglected occurrence of droplets in gas-stream. Usui and Sato (1989), Jiang and Rezkallah (1993), and Kumar *et al.* (2017) characterized the loading phenomenon according to void-fraction. Through multiple

experiments, they found that loading manifests when gas void-fraction ranges from 0.8 to 0.9. Based on those experiments, they established correlations to compute gas void-fraction.

Later, Godbole (2009) and Bhagwat (2011) followed their example and used gas void-fraction to predict loading. After performing several experiments, they determined that the gas void fraction ranges from 0.7 to 1 at the loading onset, and then established their correlations. Van't Westende *et al.* (2007), after conducting air-water flow measurement experimentations on liquid-drop size and velocity in a 12 m long tubing, with a 0.05 m inner diameter, concluded loading starts when film and gas flow are moving in directions that are counter-current. Veeken *et al.* (2010) confirmed those observations while modeling loading via transient-multiphase flow-simulator "OLGA". Later, Van't Westende (2008), Guner (2012), Alsaadi (2013), and Li *et al.* (2014), on the basis of the Barnea (1986, 1987) model, established a mechanistic-model to forecast loading in inclined wells.

After conducting numerous experiments, they found that from 0° (corresponding to horizontal) to 60°, film thickness increases gradually, until reaching its maximum value at nearly 60°, as does critical-gas flowrate; then, from 60° to 90°, film-thickness at lower section of pipe reduces rapidly, as does critical-gas flowrate. Thus, they established correlations characterizing the non-uniform film-thickness on the basis of the inclination angle and the position of the pipe circumference. Additionally, Li *et al.* (2014); Luo *et al.* (2014); Fan *et al.* (2018) through several experiments, identified an interdependency between film-gravity and the pressure gradient that has a significant influence on loading. After numerous experimentations on liquid-film reversal, Waltrich *et al.* (2015) concluded that Wallis (1969) model is accurate enough to predict loading.

Chen *et al.* (2015) investigated the inclined pipe dynamic wave characteristics before the liquid reversal happens and flow-regime transition when it happens by using the computational fluid dynamic (CFD) method. The validation of their model shows their results agree well with the laboratory dataset collected. Their results show smaller surface tension will shred the interfacial waves into minuscule droplets, which will expand into the mist flow. Further analysis showed increase of liquid viscosity would cause denser liquid film holdup which would be more favourable to develop a slug flow.

Riza *et al.* (2016), after assuming loading initiates when annular-flow changes to a slug flow regime, developed a flow regime prediction model that locates loading-point across the pipe. They found loading occurs at wellbore, rather than at top. Chen *et al.* (2016) established a model based on liquid-film and gas-core force balances. Final model combined Turner et al. model and a correction term for every inclination-angle.

Pagan and Waltrich (2016) gave a model for initiation of loading in transient flows. Their model is based on nodal-analysis technique. Rather than implementing the usual critical-velocity or minimum-pressure notion, they modified tubing-performance-relationship. This modification facilitated the simple implementation of nodal analysis to forecast liquid-loading inception and time frame necessary for production to stop after the beginning of loading. After validating their model with field-dataset, they found that their prediction-results matched well with field-data.

Joseph and Hicks (2018) proposed a dynamic-simulation method to investigate liquid-loading in gas-wells experiencing mist-flow. They considered the two-component gas-liquid two-phase flow. Then, they implemented the coupled hydrodynamic and thermodynamic model, with

constitutive-equations that integrate Peng-Robinson EoS and convex-hull algorithm. They obtained a correlation that assesses loading by determining liquid-density distribution in the pipe via flow-variables. They validated their model by comparing phase densities they computed to results from NIST RefProp, which showed good-match between the two results.

Tang *et al.* (2018) gave a fully-implicit coupled wellbore/reservoir model to delineate the transitional flow in horizontal gas-wells experiencing loading. Relying on control-volume finite-difference method, they completely coupled a wellbore model with simulator designed by themselves. They proposed an adjusted drift-flux model, which can predict variation in flow-regime in horizontal and vertical gas wells. Then, they integrated this latter to coupled wellbore/reservoir simulator to illustrate two-phase flow in horizontal-wellbores. After validation of their model, they noted amended drift-flux correlation, aside from matching the production prediction and wellbore pressure of commercial simulator, also forecasts the inconstant liquid production generated by flow-regime changes.

Moreover, a parametric analysis showed that increase in inflow zones decreases flow-regime's variation time. Further analysis demonstrated that simultaneously increasing the tubing-head pressure and reducing the reservoir depth led to an increase in flow-regime transition time. Additionally, while implementing their model at an artificial field scale, their model was able to predict 23 more days of gas-production than a commercial-simulator. Later, Wang *et al.* (2018) conducted numerous experiments and found an interconnection between pressure-gradient and gravitational-force, which is partly responsible for loading phenomenon. Given those findings and after investigating the film thickness at the lower end, and liquid-gas interfacial friction-factor, they developed a loading mechanism for all pipes.

Based on film force balance at bottom of deviated and vertical tubing, they established an analytical model to evaluate loading, which considers influences of variations in fluids properties. Liu *et al.* (2018), after several investigations, also found loading was firmly related to film-gravity. They assumed film-thickness to be uniform at any inclination angle (0^{o}–90^{o} corresponding to vertical well), and then by implementing Navier-Stokes liquid-film equations only, derived a critical gas velocity correlation.

Then, they associated their critical velocity expression with the Fiedler and Auracher (2004) well inclination angle model to predict loading in inclined wells. It is noteworthy that the Liu *et al.* (2018) correlation is exclusively a function of film parameters, tubing-diameter, and inclination-angle.

Tang *et al.* (2019) also developed a fully-implicitly coupled wellbore/reservoir model based on both the momentum and mass balances. The developed model investigates influences of liquid-loading on horizontal-wells in low-permeability gas-reservoirs. Furthermore, it also studies reservoir dynamics and wellbore after the occurrence of loading. After validation of their model, they found that horizontal gas-wells in low-permeability reservoirs could endure natural cyclic-production after the occurrence of loading. To mitigate this latter, they suggested the implementation of both uniform-stimulation and hydraulic-fracturing method. Choosing between the two methods is because they will lower the initial pressure-difference between near-wellbore and wellbore reservoir when the loading phenomenon takes place.

Later, Adaze *et al.* (2019) performed a CFD-simulation to the falling film phenomenon in annular-flow in a vertical-pipe of 76.2 mm by performing 2D axisymmetric numerical-simulations via ANSYS. Water and air were the working-fluids, and the tubing was 3 m long. After authentication with dataset from literature, results from their model match well the laboratory results. Moreover, a considerable fluctuation of the shear stress due to viscous sub-layer was observed at proximity of tubing-wall where liquid is more significant, then reduced progressively towards tubing center. Additionally, they also concluded that transfer of mass at the gas-liquid boundary might also have impact on shear stress and its time-space fluctuations. Afterwards, Okoro *et al.* (2019) developed model to predict loading by modifying the Chen *et al.* (2016) model accounting for non-uniform film-thickness and integrating a new interfacial friction-factor more representative of large film-thickness. Upon validation with a deviated gas field dataset, their model obtained better prediction accuracy than the Chen *et al.* (2016) model.

Finally, Rastogi *et al.* (2019), through laboratory experimentations, demonstrated liquid-film reversal causes loading. Therefore, they proposed a model based on mechanism triggering liquid-film reversal. Moreover, they developed a model to compute film-thickness around tubing-wall. They obtained a model that reflects well influences of liquid flow-rate, densities and viscosities, inclination-angle and tubing-diameter on critical-gas flowrate. The authentication of their model shows it outperforms all others. Throughout gas-production, gas-stream is driving-force while draining the liquids.

Several scientists showed that gradual decrease of gas-flowrate in annular-flow changes into an annular wavy, with uniform film-thickness in vertical-wells (Wallis, 1969; Barnea, 1986, 1987; Guner *et al.*, 2015; Liu *et al.*, 2018) and non-uniform film-thickness in inclined wells (Guner, 2012; Alsaadi, 2013; Li *et al.*, 2014; Luo *et al.*, 2014; Shekhar *et al.*, 2017). Ultimately, as superficial gas-velocity continues to decrease, wave height continues to increase until they form a gas-core blockage, thereby initiating the loading phenomenon.

Pagou and Wu (2020) also developed a new model for liquid-loading. From their review of literature, they found liquid-flowrate is often far smaller than gas-flow rate. So, they reasoned it more logical to relate critical-gas flowrate model to flowing gas-rate rather than to film-flow rate. Furthermore, they also thought it more reasonable to relate it to uniform film-thickness (for vertical wells), non-uniform film-thickness (inclined wells), pressure-gradient, and gas-phase viscosity and density.

Additionally, they were able to relate critical-velocity to the liquid-phase viscosity and density, the gravitational forces, gas-liquid in the tubing (gas void fraction), and gas-well geometry (tubing diameter, inclination angle and circumferential angle). They developed their model, which predicts and identifies liquid-loading in gas wells through two steps. The first step consisted of establishing the correlation that quantifies the gas-liquid amount in gas-well (gas void fraction) through modification of Barnea (1986) model, thereby predicting the loading and unloading flow regime. Then, they developed the Hagen-Poiseuille equations, with gravity being considered for the gas-phase and liquid-phase. Then, they associated flowrate correlation to the Luo *et al.* (2014) circumferential angle to consider non-uniform film-thickness in inclined gas wells. Consequently, their new model related loading directly to liquid-film, flowing gas-core influential parameters, the gas-liquid amount (gas void fraction), the tubing inner diameter, inclination-angle, and circumferential-angle. Moreover, it also related the loading phenomenon to the flowing gas rate, pressure-gradient, gravitational-forces, uniform film-thickness (for

vertical wells), the non-uniform film thickness (for inclined wells only), and changes in both fluids' properties (densities and viscosities). They collected field data from vertical wells like the Xinjiang North-West gas field, Turner *et al.* (1969) dataset, and Coleman *et al.* (1991) data set and inclined gas wells data set like the Chuanxi and Daniudi gas field published by Gao (2012) and Veeken *et al.* (2010) data set to authenticate their proposed model.

Vieira *et al.* (2021) introduced a new model for predicting liquid loading onset, based on the reversal of a non-uniform liquid film. The momentum balance equation for annular flow in the proposed model was expressed as a function of liquid holdup instead of liquid thickness. The model employs auxiliary correlations to obtain liquid holdup and an interfacial friction factor, developed from literature data. The accuracy of their proposed model was quantified by comparing laboratory data from their work and field datasets from previous studies, with the predictions of existing models.

The proposed model was able to successfully reproduce the experimental data and field data, and gives the highest prediction accuracy and the lowest average error when compared with existing models. The applicability of the auxiliary correlations shows that their model is restricted to upward pipe inclinations of 30°–90° from the horizontal, liquid viscosities of 1.1 cP and 0.018 cP, and superficial velocities of gas of 3–60 m/s and of liquid of 0.01–0.2 m/s. Their results also showed that the model exhibits poor performance when applied to pipe inclinations lower than 30◦ from the horizontal.

Prediction Models for Critical Velocity

Turner's Model:

Turner *et al.* (1969) proposed two physical models for the removal of gas well liquids. The models are based on: (1) the liquid film movement along the walls of the pipe and (2) the liquid droplets entrained in the high velocity gas core. They used field data to validate each of the models and concluded that the entrained droplet model could better predict the minimum rate required to lift liquids from gas wells.

This is because the film model does not provide a clear definition between adequate and inadequate rates as satisfied by the entrained droplet model when it is compared with field data. A flow rate is determined adequate if the observed rate is higher than what the model predicts and inadequate if otherwise. Again, the film model indicates that the minimum lift velocity depends upon the gas-liquid ratio while no such dependence exists in the range of liquid production associated with field data from most of the gas wells (1 - 130 bbl/MMSCF). The theoretical equation for critical velocity V_t to lift a liquid drop is given below in field units and in terms of pressure.

$$V_{c,w} = \frac{5.304\,(67-0.0031P)^{1/4}}{\sqrt{0.0031P}} \qquad (1)$$

Where

$V_{c,w}$ = critical velocity (ft/s)

P = pressure (psia)

Coleman's Model:

Using the Turner model but validating with field data of lower reservoir and wellhead flowing pressures all below approximately 500 psia, Coleman *et al.* (1991) was convinced that a better prediction could be achieved without a 20% upward adjustment to fit field data with the following expressions in field units and in terms of pressure:

$$V_{c,w} = \frac{4.434\,(67-0.0031P)^{1/4}}{\sqrt{0.0031P}} \quad (2)$$

Where

$V_{c,w}$ = critical velocity (ft/s)

P = pressure (psia)

Li's Model:

Li *et al.* (2001) in their research posited that Turner and Coleman's models did not consider deformation of the free-falling liquid droplet in a gas medium. They contended that as a liquid droplet is entrained in a high- velocity gas stream, a pressure difference exists between the fore and aft portions of the droplet. The droplet is deformed under the applied force and its shape changes from spherical to a convex bean with unequal sides (flat). They therefore, proposed the following model represented here in S.I. units:

$$V_{c,w} = \frac{2.5\,\sigma^{1/4}(\rho_l-\rho_g)^{1/4}}{\sqrt{\rho_g}} \quad (3)$$

Where

$V_{c,w}$ = critical velocity (m/s)

σ = interfacial tension (N/m)

ρ_g = natural gas density (Kg/m^3)

ρ_l = liquid density (Kg/m^3)

Nossier's Model:

Nosseir *et al.* (2000) focused their studies on the impact of flow regimes and changes in flow conditions on gas well loading. They followed the path of Turner droplet model but, they made a difference from Turner model by considering the impact of flow regimes on the drag coefficient (C). Turner model takes the value of C_d to be 0.44 under laminar, transition and turbulent flow regimes, which in turn determine the expression of the drag force and hence critical velocity equations. On comparing Nossier observed that Turner model values were not matching with the real data for highly turbulent flow regime. Dealing with this deviation, Nossier found out the reason to be the change in value of C_d for this regime from 0.44 to 0.2. For

$$V_{c,w} = \frac{14.6\,\sigma^{0.35}(\rho_l-\rho_g)^{0.21}}{\mu_g^{0.134}\rho_g^{0.426}} \quad (4)$$

Where

$V_{c,w}$ = critical velocity (ft/s)

σ = interfacial tension (lbf/ft)

ρ_g = natural gas density (Kg/m^3)

ρ_l = liquid density (Kg/m^3)

μ_g = viscosity (cP)

Nossier derived the critical flow equations by assuming C_d value of 0.44 for Reynolds number (R_e) 2×10^5 to 10^6 and for Re value greater than 10^6 he took the C_d value to be 0.2. Again, the critical velocity equation for highly turbulent flow regime is given in field units as:

$$V_{c,w} = \frac{21.3\,\sigma^{0.25}(\rho_l-\rho_g)^{0.25}}{\rho_g^{0.5}} \quad (5)$$

Where
$V_{c,w}$ = critical velocity (ft/s)
σ = interfacial tension (lbf/ft)
ρ_g = natural gas density (Kg/m^3)
ρ_l = liquid density (Kg/m^3)

Coefficient of Drag

Multiphase flow involving suspensions of liquid droplets or gas bubbles are frequently encountered in many industrial processes including oil and gas production. The ability of fluids in horizontal motion to suspend the droplets depends mainly on the balance of two actions: gravity, which causes the droplets to fall or settle in the fluid, and an upward diffusion, caused by a concentration gradient which in turn is created by gravity. The droplet movement thus, depends on their properties such as solids density, particle size and particle shape. The gravitational force causing the particle to rise or fall can be defined as (Govier and Aziz, 1972):

$$F_G = \frac{\pi}{6} d^3 g\left(\rho_l - \rho_g\right) \quad (6)$$

The rise or fall of the droplet in the fluid results in a lift and drag force where this force may be expressed as:

$$D = \frac{\pi}{8} d^2 \rho_g C_d u^2 \quad (7)$$

Where ρ_l is the liquid density, ρ_g is the gas density, d is the diameter, m, g is the acceleration due to gravity, C_d is the drag coefficient and v is the rise or fall velocity. The drag force arises from pressure and viscous stresses applied to the particle surface and resist the relative fluid velocity v. The magnitude of drag is primarily dictated by the particle's Reynolds number, R_e, defined as:

$$R_e = 1488\,\frac{\rho u d}{\mu} \quad (8)$$

Where u is the fluid velocity (ft/s), d is the particle diameter (ft), ρ is fluid density (lbm/ft^3) and μ is the fluid viscosity (cp). The drag coefficient is a very important hydrodynamic parameter involved in the modelling and design of multiphase processes, especially when entrained with droplets.

The definition of the drag force on a droplet in a fluid flow generally involves the understanding of the relationship between the drag coefficient C_d and particle's Reynolds number, R_e. The drag coefficient represents the fraction of the kinetic energy of the settling velocity that is used to overcome the drag force on the droplet, while the Reynolds number is a ratio between the inertial and viscous forces of a fluid. As the droplet size or flow velocity increases for a given kinematic viscosity, so does the Reynolds number, and the character of flow changes. For very small

Reynolds numbers, Stokes proposed an analytical solution of drag coefficient by solving the general differential equation of Navier–Stokes (Bello and Idigbe, 2015).

$$C_d = \frac{24}{R_e} \tag{9}$$

An analytical attempt to extend the range of approximation for the drag coefficient beyond Stokes flow was proposed by some authors by including the inertia terms in the solution of Navier–Stokes. Several correlations for drag coefficient have been proposed over a wide range of Reynolds number in the literature. A number of empirical and semi empirical C_d–$R_e$relationships have been proposed.

Cheng (2009) proposed a drag coefficient model which has greater applicability when compared with other models evaluated. These other models can only be used for limited Reynolds numbers and even those applicable for wider range of R_e, may involve tedious application procedure. The model proposed by Cheng given below, despite its simple form, gives the best approximation of experimental data for R_e, from Stoke's regime to about 2×10^5 (Bello and Idigbe, 2015).

$$C_d = \frac{24}{R_e}(1 + 0.27R_e)^{0.43} + 0.47[1 - exp(-0.04R_e^{0.38})] \tag{10}$$

This drag coefficient C_d is predicted from two terms. The first term on the RHS can be considered as an extended Stokes' law, applicable approximately for $R_e < 100$; and the second term is an exponential function accounting for slight deviations from the Newton's law for high R_e. The sum of the two terms is used to predict drag coefficient for any R_e over the entire regime.

Ruiquing and Huiqun (2017) also proposed a cubic equation representing the relationship between drag coefficient and Reynolds number for both transition and turbulence flow regimes.As known by the standard experimental drag curve, drag coefficient fluctuates heavily under the condition of transition flow and turbulence flow ($2\times10^5 \leq R_e \leq 10^6$). It is obviously unreasonable to take drag coefficient as a fixed value. Thus, they used SPSS to conduct nonlinear fitting of the experimental data in transition flow and turbulence flow (Ruiquing and Huiqun, 2017).

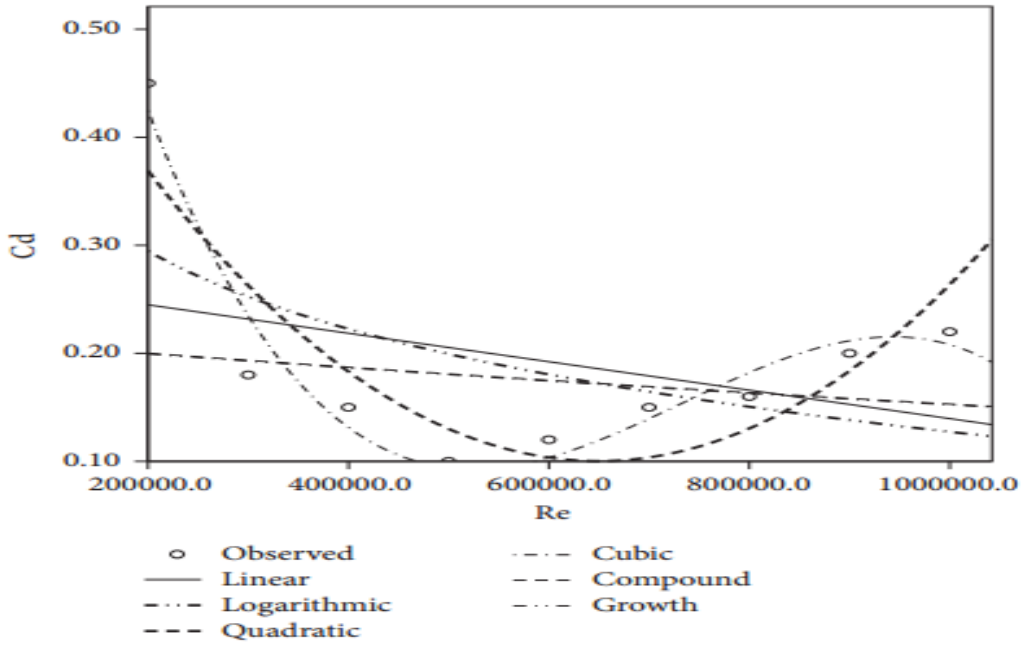

Figure 3: Showing non-linear fitting of experimental data of drag coefficient and Reynold's number for transition and turbulence flow regimes (Ruiquing and Huiqun, 2017)

As can be seen from Figure 2.1, which shows that the cubic fitting of this model is better than others, indicating that regression model fitting results are good. Therefore, the cubic model in transition flow and turbulence flow was taken as presented below:

$$C_d = -3.3316 \times 10^{-18} R_e^3 + 7.3 \times 10^{-12} R_e^2 - 4.918 \times 10^{-6} R_e + 1.143 \quad (11)$$

Gas Well Deliquefaction Techniques

There is no one size fits all solution for wells with liquid loading. The optimal solution depends on the particular conditions of the well. Methods like downsizing of production tubing inner diameter (ID), reduction of the density of the production liquids, cyclic shut-in control, and plunger lift rely on the internal energy of the well. On the other hand, the applications of artificial lift methods such as gas lift and production pumps rely on the introduction of external energy. Contrary to some other studies, the current study does not recognize compression as a liquid lifting technique. Compression is considered a must-have in gas wells (in late-life) and thus thought to be indispensable.

When the produced gas is directed to the suction of the compressor, gas pressure is increased as much as the compression ratio before the gas is injected into the pipeline. This allows lowering of the WHP much below the pipeline pressure. Lowering the WHP (and accordingly BHP) causes considerable increments in drawdown pressure, hence in gas flow rate. Increased rate (gas velocity) helps unload the wellbore much easier. In addition, when the abandonment pressure of the well is reduced, ultimate recovery is increased considerably. Contrary to their relatively high initial investment requirement, compressors are almost always necessary to get the most out of gas wells and they can be used in several wells within their economic life.

Deliquification (dewatering) is also a necessity in most unconventional gas wells to initiate production. With the growth of unconventional plays, the topic of deliquification will continue to be of great importance. For example, in coalbed methane (CBM) wells, initially water is produced

to reduce reservoir pressure and leads to gas desorption from the organic matter, which flows into the wellbore. Likewise, methane hydrate (gas hydrate) formations need pressure reduction, which can be provided by the production of free formation water. Production of this free water breaks the hydrate equilibrium condition (hydrate cage structure) and methane is produced. Most shale gas wells suffer from liquid loading during the initial flow-back phase (producing the fracturing fluid) and sometimes during the production phase (according to formation characteristics).

Several authors have extensively reviewed deliquification methodologies and provided screening criteria or decision-making tools. The parameters which determine the deliquification method selection criteria are very easy-to-monitor production parameters such as liquid rate, liquid type, WHP, and GLR. Other well/wellbore design parameters such as well inclination, tubing ID/uniformity, well/perforation depth and other bottom hole equipment (subsurface safety valves (SSSV), mandrels) also have bearing on the chosen deliquification method.

When screening the unloading techniques, both technical and economic feasibility should be considered

MATERIALS AND METHODS

Research Design

a) The first step taken in carrying out this research was to conduct extensive review of literature to identify existing gaps.
b) Following the identified gaps, a new analytical critical-velocity model was developed based on reverse film concept.
c) Meanwhile, the evaluation of the model accuracy was done using 18 gas wells data acquired from North-West Xinjiang gas-field as gotten from Pagou and Wu (2020).
d) Furthermore, comparisons of the accuracy results were carried against critical-velocities obtained using Turner *et al.* (1969), Coleman *et al.* (1991), Nossier *et al.* (2000), Li *et al.* (2001), and Pagou and Wu (2020) models.

Model Development

The configuration of the annular flow locates the liquid between the inner tubing wall and the gas stream. The model developed is founded on fluid-film reversal. It is assumed that the change of flow-regime from annular (gas core surrounded by liquid-film) to churn or slug generates loading. For ensuing treatment, following assumptions were made:

a) Flow of liquid-film is gravity-driven
b) Liquid-film flow is steady and considered fully developed laminar
c) Liquids are Newtonian and incompressible
d) Film-thickness is uniform all-around circumference zone

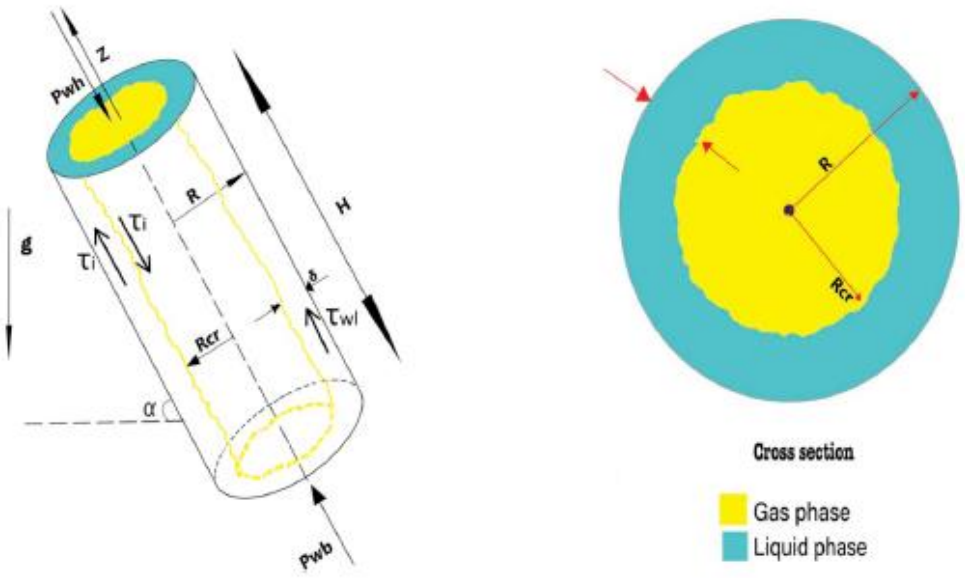

Figure 4 Reverse film flow in annular flow in gas wells (Pagou and Wu, 2020)

Occurrence of Bubbles is Negligible

Carrying out a force-balance on gas-core and surrounding liquid moving in production tubing in Figure 3.1 experiencing annular flow (Barnea, 1986),

$$-V_c\left(\frac{dP}{dL}\right)_c - \tau_i S_i - V_c\frac{\rho_g g}{g_c} = 0 \tag{12}$$

$$-V_f\left(\frac{dP}{dL}\right)_f + \tau_i S_i - \tau_{wi} S_l - V_f\frac{\rho_l g}{g_c} = 0 \tag{13}$$

Where

V_c = gas core volume (ft³)

$\left(\frac{dP}{dL}\right)_c$ = gas core pressure drop (psf)

S_i = gas core surface area (ft²)

ρ_g = gas density (lbm/ft³)

V_f =liquid film volume (ft³)

$\left(\frac{dP}{dL}\right)_f$ =liquid film pressure drop (psf)

S_l =liquid film surface area (ft²)

ρ_l =liquid film density (lbm/ft³)

τ_i = interfacial shear-stress (lbf/ft²)

τ_{wi} = liquid film wall shear-stress (lbf/ft²)

g = acceleration due to gravity (32.17 ft/s²)

g_c =conversion factor (32.17 lbm-ft/lbf-s²)

Subtracting Equ. (1.2) from Equ. (13),

$$-V_c\left(\frac{dP}{dL}\right)_c - \left\{-V_f\left(\frac{dP}{dL}\right)_f\right\} - \tau_i S_i - \tau_i S_i - (-\tau_{wi} S_l) - V_c\frac{\rho_g g}{g_c} - \left\{-V_f\frac{\rho_l g}{g_c}\right\} = 0 \tag{14}$$

Simplifying,

$$-V_c\left(\frac{dP}{dL}\right)_c + V_f\left(\frac{dP}{dL}\right)_f - 2\tau_i S_i + \tau_{wi} S_l - V_c\frac{\rho_g g}{g_c} + V_f\frac{\rho_l g}{g_c} = 0 \quad (15)$$

Rearranging,

$$V_f\left(\frac{dP}{dL}\right)_f - V_c\left(\frac{dP}{dL}\right)_c - 2\tau_i S_i + \tau_{wi} S_l + V_f\frac{\rho_l g}{g_c} - V_c\frac{\rho_g g}{g_c} \quad (16)$$

But,

$$V_f = (1-\epsilon)\frac{\pi D^2}{4}L \quad (17)$$

$$V_c = \epsilon\frac{\pi D^2}{4}L \quad (18)$$

Where

$\epsilon =$ volumetric gas concentration (-)

$D =$ tubing diameter (ft)

$L =$ tubing length (ft)

Substituting Equ. (16) and Equ. (17) into Equ. (15), we have

$$(1-\epsilon)\frac{\pi D^2}{4}L\left(\frac{dP}{dL}\right)_f - \epsilon\frac{\pi D^2}{4}L\left(\frac{dP}{dL}\right)_c - 2\tau_i S_i + \tau_{wi} S_l + (1-\epsilon)\frac{\pi D^2}{4}L\frac{\rho_l g}{g_c} - \epsilon\frac{\pi D^2}{4}L\frac{\rho_g g}{g_c} \quad (19)$$

When fluid-film obstructs gas-stream, gas-core energy is less than liquid-film gravity-force. At that moment, not only does frictional pressure gradient becomes negligible compared to film gravity force, but also liquid-film wall shear stress vanishes. Here, pressure-drop is expressed as (Pagou and Wu, 2020):

$$\left(\frac{dP}{dL}\right)_c = \frac{\rho_g g}{g_c} \quad (20)$$

$$\left(\frac{dP}{dL}\right)_f = \frac{\rho_l g}{g_c} \quad (21)$$

Substituting Equ. (20) and Equ. (21) into Equ. (19), we have

$$(1-\epsilon)\frac{\pi D^2}{4}L\frac{\rho_l g}{g_c} - \epsilon\frac{\pi D^2}{4}L\frac{\rho_g g}{g_c} - 2\tau_i S_i + \tau_{wi} S_l + (1-\epsilon)\frac{\pi D^2}{4}L\frac{\rho_l g}{g_c} - \epsilon\frac{\pi D^2}{4}L\frac{\rho_g g}{g_c} = 0 \quad (22)$$

Collecting like terms,

$$2(1-\epsilon)\frac{\pi D^2}{4}L\frac{\rho_l g}{g_c} - 2\epsilon\frac{\pi D^2}{4}L\frac{\rho_g g}{g_c} - 2\tau_i S_i + \tau_{wi} S_l = 0 \quad (23)$$

$$\frac{2\pi D^2 L g}{4 g_c}\left\{(1-\epsilon)\rho_l - \epsilon\rho_g\right\} - 2\tau_i S_i + \tau_{wi} S_l = 0 \quad (24)$$

Recall, when fluid-film obstructs gas- stream (Pagou and Wu, 2020),

$$\tau_{wi} = 0 \quad (25)$$

Also, gas-core and liquid-film surface areas are,

$$S_i = \frac{\pi D_{cr}^2}{4} \tag{26}$$

$$S_l = \frac{\pi D^2}{4} \tag{27}$$

$$\tau_i = \frac{1}{2} f_i \rho_g \frac{v_{cr}^2}{\epsilon^2} \tag{28}$$

Where
D_{cr} = diameter of gas core/critical diameter (ft)
f_i = interfacial friction factor (-)
v_{cr} = critical velocity (ft/s)

Substituting Equ. (26)-(27) into Equ. (28),

$$\frac{2\pi D^2 Lg}{4g_c}\{(1-\epsilon)\rho_l - \epsilon\rho_g\} - 2\left\{\frac{1}{2} f_i \rho_g \frac{v_{cr}^2}{\epsilon^2}\right\}\frac{\pi D_{cr}^2}{4} = 0 \tag{29}$$

For inclined production tubings, Equ. (29) can equally be expressed as

$$\frac{2\pi D^2 Lg}{4g_c}\{(1-\epsilon)\rho_l - \epsilon\rho_g\}sin\alpha - \left\{f_i \rho_g \frac{v_{cr}^2}{\epsilon^2}\right\}\frac{\pi D_{cr}^2}{4} = 0 \tag{30}$$

$$\frac{\pi D^2 Lg}{2g_c}\{(1-\epsilon)\rho_l - \epsilon\rho_g\}sin\alpha = \left\{f_i \rho_g \frac{v_{cr}^2}{\epsilon^2}\right\}\frac{\pi D_{cr}^2}{4} \tag{31}$$

Making v_{cr}^2 the subject,

$$v_{cr}^2 = \frac{2\epsilon^2 D^2 Lg}{g_c D_{cr}^2 f_i \rho_g}\{(1-\epsilon)\rho_l - \epsilon\rho_g\}sin\alpha \tag{32}$$

However, the volumetric gas-concentration is also expressable as,

$$\epsilon = \frac{R_{cr}}{R} = \frac{D_{cr}}{D} \tag{33}$$

And

$$Z = Lsin\alpha \tag{34}$$

So that,

$$sin\alpha = \frac{Z}{L} \tag{35}$$

Where
Z = true vertical tubing height
Substituting Equ. (33) and Equ. (3.4) into Equ. (32),

$$v_{cr}^2 = \frac{2gZ}{g_c f_i \rho_g}\{(1-\epsilon)\rho_l - \epsilon\rho_g\} \tag{36}$$

Taking square root of both sides,

$$v_{cr} = \sqrt{\frac{2gZ}{g_c f_i \rho_g}\{(1-\epsilon)\rho_l - \epsilon\rho_g\}} \tag{37}$$

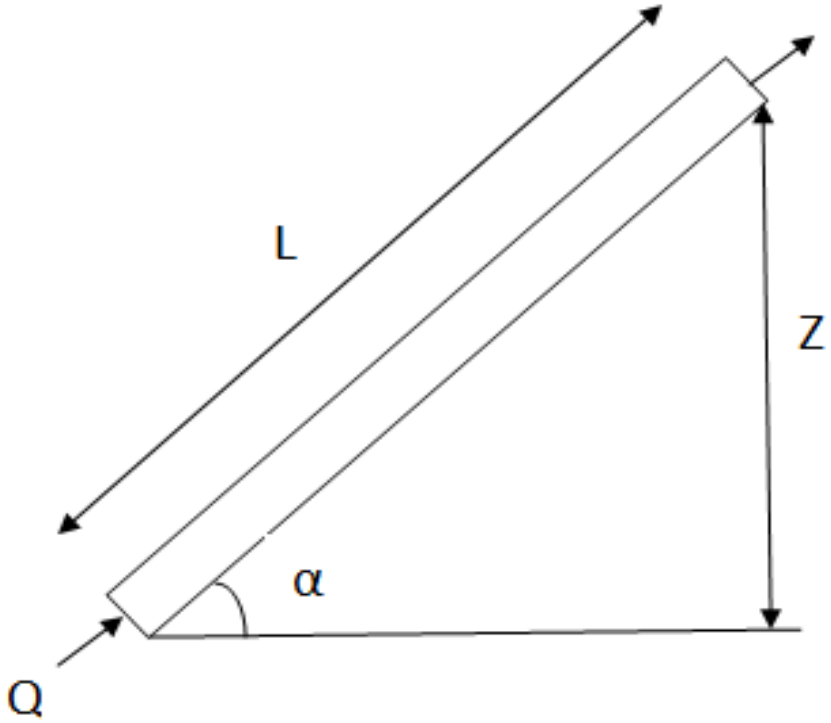

Figure 5 An inclined gas well production tubing showing true vertical tubing height (Ikoku, 1992)

Interfacial Friction Factor

The interfacial friction factor correlated by Fore *et al.* (2000) is ratified for calculation consistency and is:

$$f_i = 0.005\left[1 + 300\left\{1 + \frac{17500}{Re_g}\frac{\delta}{D} - 0.0015\right\}\right] \quad (36)$$

Hewitt and Nicholls (1969) researches on the annular two-phase flow measurement of the liquid film width and found wave heights 4 to 6 times higher than average film-width (δ), and proposed:

$$1 - \epsilon = 4\frac{\delta}{D}\left(1 - \frac{\delta}{D}\right) \quad (37)$$

On rearranging,

$$4\left(\frac{\delta}{D}\right)^2 - 4\left(\frac{\delta}{D}\right) + (1 - \epsilon) = 0 \quad (38)$$

Or

$$4\bar{\delta}^2 - 4\bar{\delta} + (1 - \epsilon) = 0 \quad (39)$$

Where

$$\bar{\delta} = \frac{\delta}{D} \quad (40)$$

Solving above equation using almighty formula,

$$\bar{\delta} = \frac{-4 \pm \sqrt{(-4)^2 - 16(1-\epsilon)}}{8} \quad (41)$$

So that,

$$\bar{\delta} = \frac{1}{2}(-1 \pm \sqrt{\epsilon}) \quad (42)$$

Critical Flow Rate

The volumetric flowrate at critical-velocity is

$$Q_{cr} = v_{cr}A \quad (43)$$

According to Okafor *et al.* (2019), at critical flow, the velocity can be expressed as

$$v_{cr} = \left(\frac{Q_{cr}}{86400}\right).\left(\frac{T}{T_b}\right).\left(\frac{P_b}{P}\right).\left(\frac{z}{1.00}\right).\left(\frac{1}{A}\right) \quad (44)$$

Where

v_{cr} = critical velocity (ft/s)
Q_{cr} = critical volumetric flow rate (scfd)
T = tubing temperature (°R)
T_b = base temperature (°R)
P_b = base pressure (psia)
P = tubing pressure (psia)
z = gas compressibility factor (-)
A = tubing cross sectional area (ft²)

Substituting base temperature and pressure values of $T_b = 520$ °R and $P_b = 14.7$ psia into Equ. (44),

$$v_{cr} = \frac{Q_{cr}}{3.056\times10^9}.\frac{Tz}{PA} \quad (45)$$

Making Q the subject,

$$Q_{cr} = 3.056 \times 10^9 \frac{v_{cr}PA}{Tz} \quad (46)$$

Liquid-loading Evaluation Method

To assess the loading status in those given wells, comparisons are carried out between current-gas flowrate (Q) and the computed critical-gas flow rate (Q_{cr}). Therefore, a gas-well is identified as:

a) Unloading (unloaded) if the difference ΔQ of critical-gas flowrate to actual-gas flowrate is equal or less than zero ($Q_{cr} - Q \leq 0$);
b) Loading-up (loaded) if ΔQ is greater than zero ($\Delta Q > 0$).

From those respective results of ΔQ, the following interpretations are drawn out. The higher the calculated ΔQ, the higher the risks of liquid-loading. While the lower the ΔQ, the lower the risks of liquid-loading occurring.

The graphical representations of loading status are equally represented on graphs where the upright axis represents the computed critical-gas flowrate and the horizontal axis depicts theactual gas flow rate. From the graph, the data points representing the unloading gas-wells are located below the datum line (45° line) for accurate predictions. For the data points representing loading gas-wells, they appear above the 45° line. If any data points fall on datum

line or touches it, the corresponding gas-well will soon experience loading if no solutions are employed to counter or mitigate it.

As for the dots plotted on the graph representing the loading wells, correct predictions should locate them below the datum line. For any dots positioned below the datum line and touching it, loading phenomenon has just begun on those wells, and an immediate action using any Liquid-loading intervention methods on those wells will eliminate the loading phenomenon and the wells will produce again at a high-rate for long.

Liquid-loading Data Set

To authenticate the new model on vertical gas wells, data from 18 vertical gas wells from the Xinjiang North-West gas field was used. Among the data obtained from gas-field, we listed 12 gas-wells as having a low gas-liquid ratio, and 6 gas wells as having high gas-liquid ratio properties. Wellhead pressures and wellbore pressures range, respectively, from 3 MPa to 27.2 MPa, and from 16.1 MPa to 43.6 MPa. The depth of each well varies from 4359 m to 5100 m, and the tubing diameters are same for each well (62 mm). The daily gas production rate varies from 519,337.49 cfd to 5,261,885.34 cfd. From data collected, 10 gas wells are non-loading, 2 are about to load up, and 6 are loading up. Table 3.1 summarizes all the collected data.

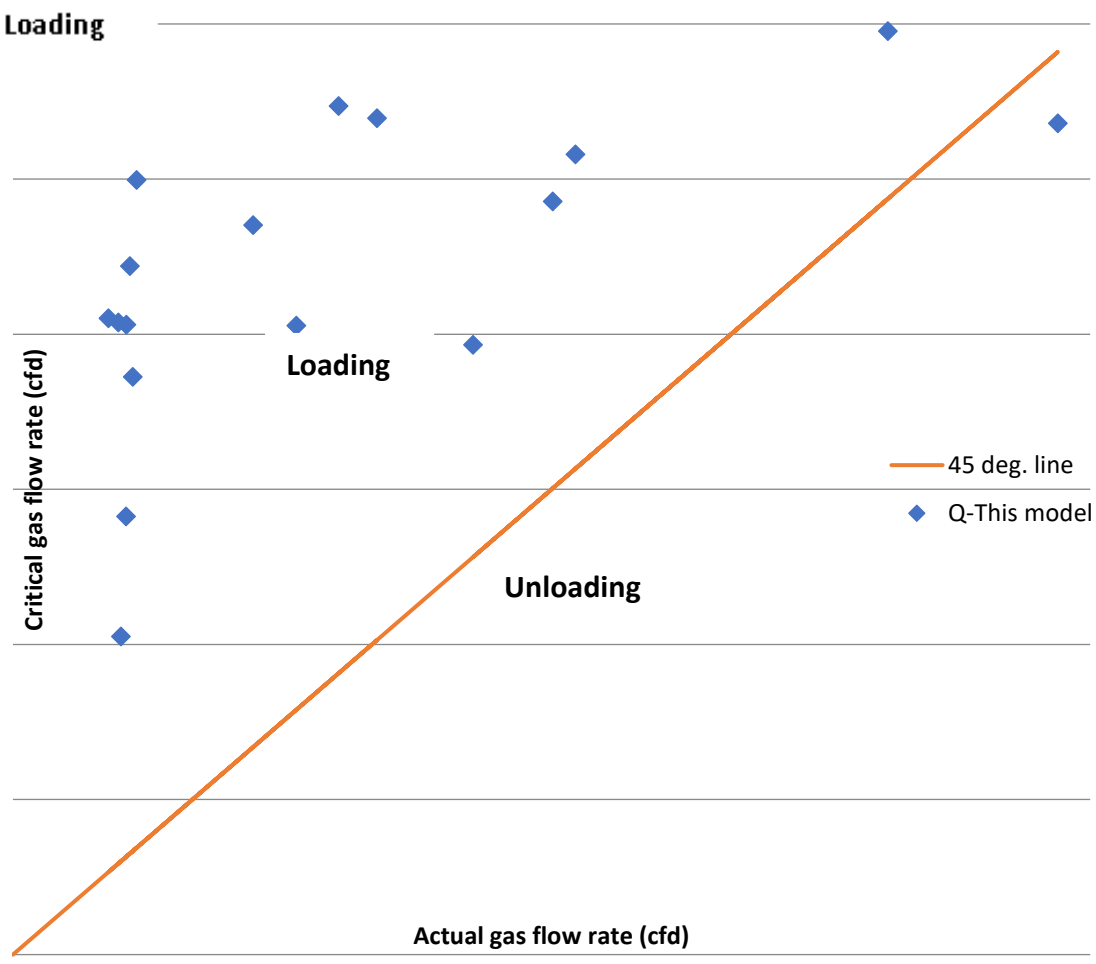

Figure 6 Developed model liquid loading prediction-results

Table 1 Summary of liquid loading predictions

Critical velocity model	Correct prediction	Wrong prediction	Prediction accuracy (%)
Turner *et al.* (1969)	12	6	66.67
Coleman *et al.* (1991)	12	6	66.67
Nossier *et al.* (2000)	16	2	88.89
Li *et al.* (2001)	11	7	61.11
Pagou and Wu (2020)	10	8	55.56
This model	7	11	38.89

Table 2 Effects of model coefficient adjustment on liquid loading prediction accuracy

Percentage reduction (%)	Correct prediction	Wrong prediction	Prediction accuracy (%)
20	8	10	44.44
40	12	8	66.67
60	12	8	66.67
80	14	4	77.78

DISCUSSION

Figure 6 gives liquid-loading prediction-results of developed critical velocity model based on gas flowrate. From the figure, the developed model predicted status of total of seventeen (17) gas wells as loading, while one (1) well was predicted as unloading using the critical gas flowrate as the benchmark. This is different from actual gas well conditions which designated 10 wells as unloading, 6 wells as loading and two wells as about to load. In fact, on well-by-well basis, the developed model predicted correctly the actual conditions of all the loading gas wells, thereby giving it 100% prediction accuracy for the loading gas wells. The model also predicted correctly the actual conditions of one (1) of the unloading gas wells, giving it a prediction accuracy of 10% for the unloading gas wells. But the model could not accurately predict actual condition of two (2) gas wells that are about to load.

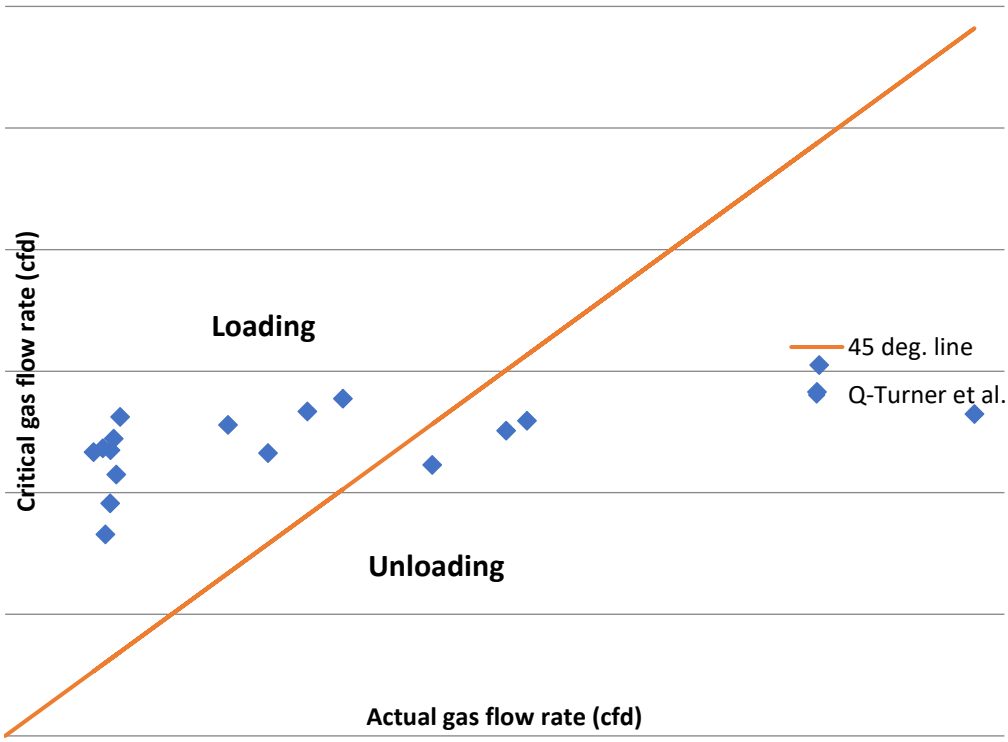

Figure 7 Turner *et al.* (1969) liquid loading prediction-results

Figure 7 gives liquid loading prediction-results of Turner *et al.* critical-velocity model based on gas flow rate. Turner *et al.* model predicted status of total of twelve (12) gas wells as loading, while six (6) wells were predicted as unloading using the critical-gas flow rate as the benchmark. This is however different from the actual gas well conditions which designated 10 wells as unloading, 6 wells as loading and two wells as about to load. In fact, on well-by-well basis, Turner *et al.* model predicted correctly the actual conditions of all the loading gas-wells, thereby giving it 100% prediction accuracy for the loading gas wells. The model also predicted correctly the actual conditions of six (6) of unloading gas wells, giving a prediction accuracy of 60 % for the unloading gas wells. But the model could not accurately predict the actual condition of the two (2) gas wells that are about to load.

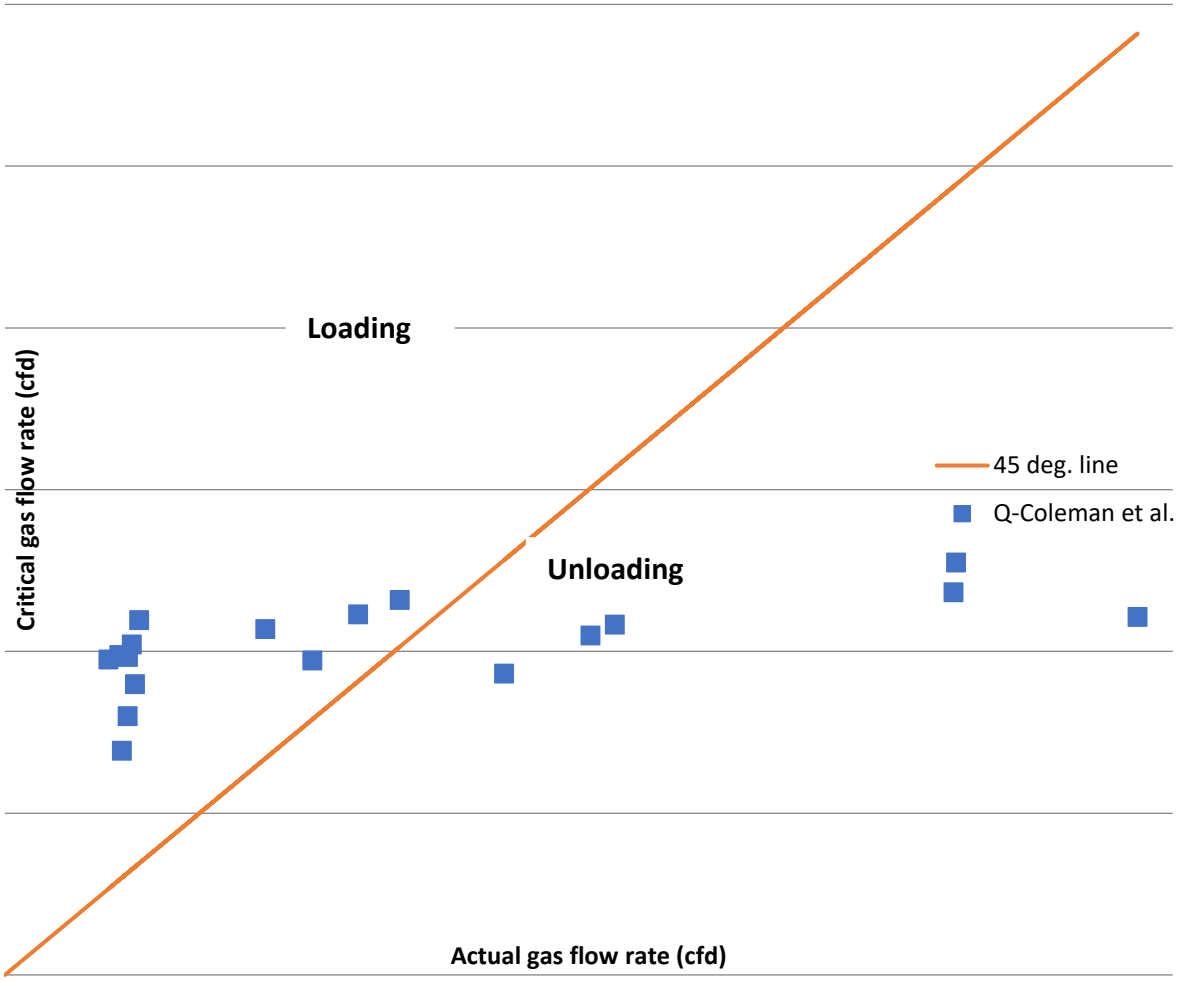

Figure 8 Coleman *et al.* (1991) liquid loading prediction results

Figure 8 gives liquid-loading prediction-results of Coleman *et al.* critical velocity model based on gas flow rate. It is clear that Coleman *et al.* model predicted the status of a total of twelve (12) gas wells as loading, while six (6) wells were predicted as unloading using the critical gas flow rate as the benchmark. This is however different from the actual gas well conditions which designated 10 wells as unloading, 6 wells as loading and two wells as about to load. In fact, on well-by-well basis, Coleman *et al.* model predicted correctly the actual conditions of all the loading gas wells, thereby giving it 100% prediction accuracy for the loading gas wells. The model also predicted correctly the actual conditions of six (6) of the unloading gas wells, giving it a prediction accuracy of 60 % for the unloading gas wells. But the model could not accurately predict the actual condition of the two (2) gas wells that are about to load.

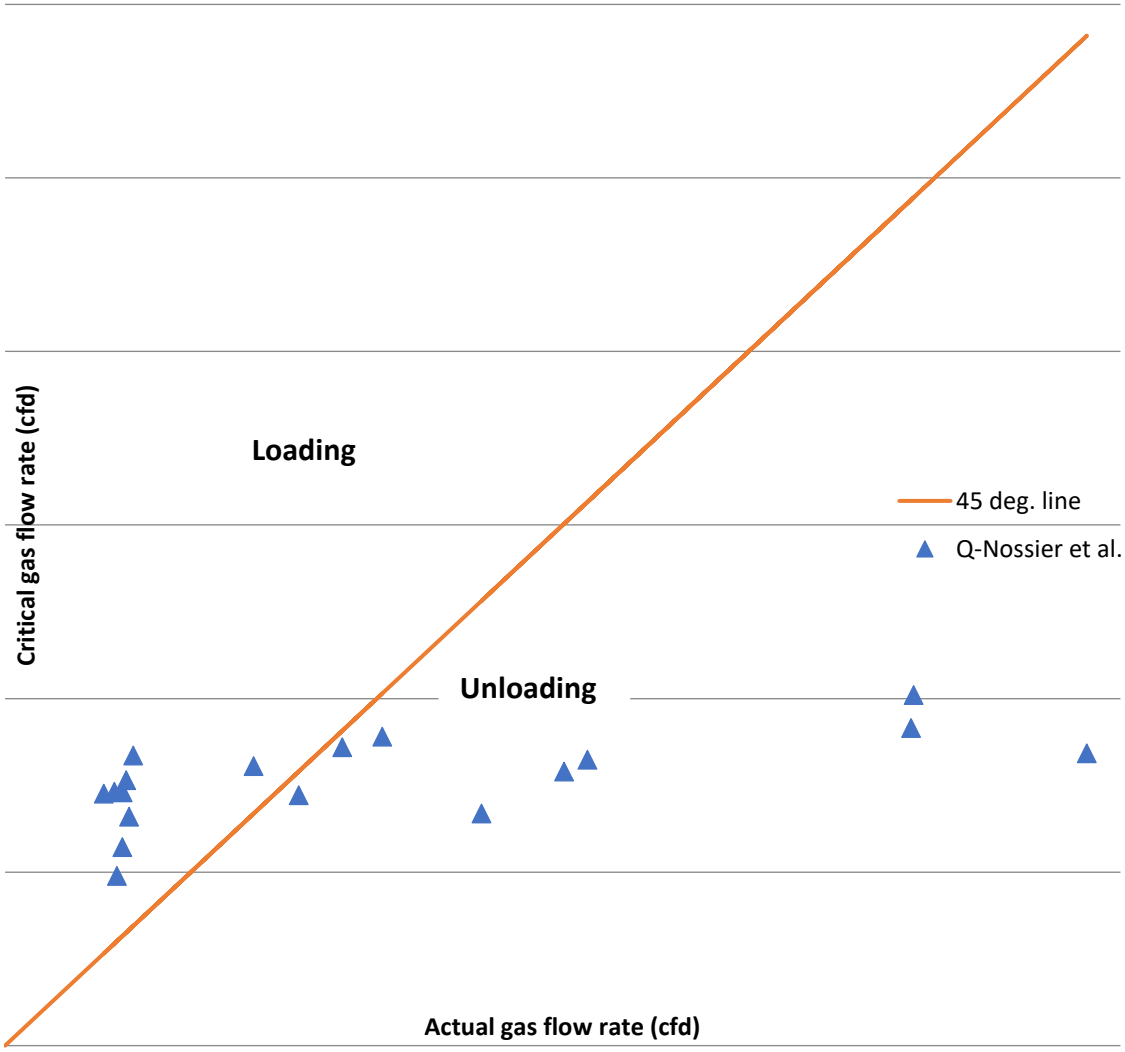

Figure 9 Nossier *et al.* (2000) liquid loading prediction results

Figure 9 gives the Liquid-loading prediction-results of Nossier *et al.* critical velocity model based on gas flow rate. Nossier *et al.* model predicted the status of a total of eight (8) gas-wells as loading, while ten (10) wells were predicted as unloading using critical-gas flowrate as the benchmark. This is however different from actual gas well conditions which designated 10 wells as unloading, 6 wells as loading and two wells as about to load. In fact, on well-by-well basis, Nossier *et al.* model predicted correctly the actual conditions of all loading gas wells, thereby giving it 100% prediction accuracy for the loading gas wells. The model also predicted correctly the actual conditions of ten (10) of the unloading gasses wells, giving a prediction accuracy of 100 % for the unloading gas wells. But the model could not accurately predict the actual condition of two (2) gas wells that are about to load.

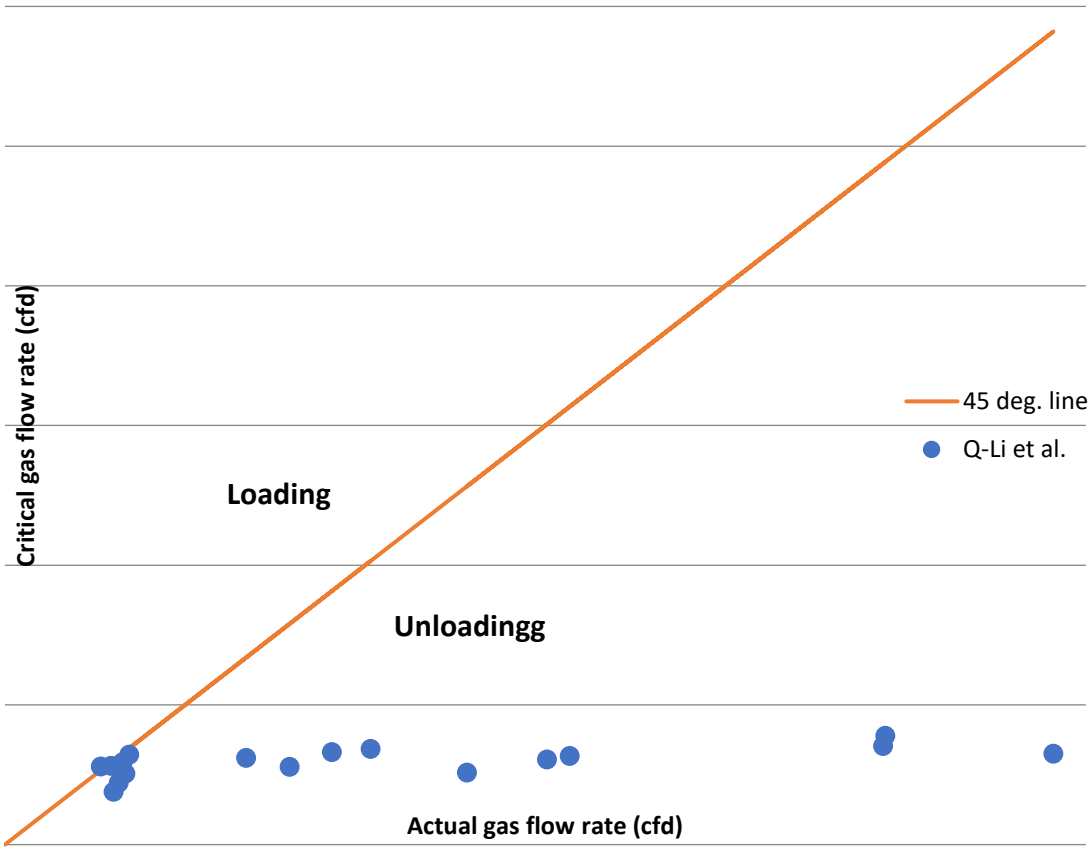

Figure 10: Li *et al.* (2001) liquid loading prediction results

Figure 10 gives liquid-loading prediction-results of Li *et al.* critical-velocity model based on gas flowrate. Li *et al.* model predicted status of one (1) gas-well as loading, while other seventeen (17) wells were all predicted as unloading using the critical gas flow rate as the benchmark. This is however different from the actual gas well conditions which designated 10 wells as unloading, 6 wells as loading and two wells as about to load. In fact, on well-by-well basis, Li *et al.* model predicted correctly the actual conditions of one (1) of loading gas-wells, thereby giving it 20% prediction accuracy for the loading gas wells. The model also did not predict correctly actual conditions of any of the unloading gas wells, giving it a prediction accuracy of 0 % for unloading gas wells. Also, the model could not accurately predict the actual condition of two (2) gas wells that are about to load.

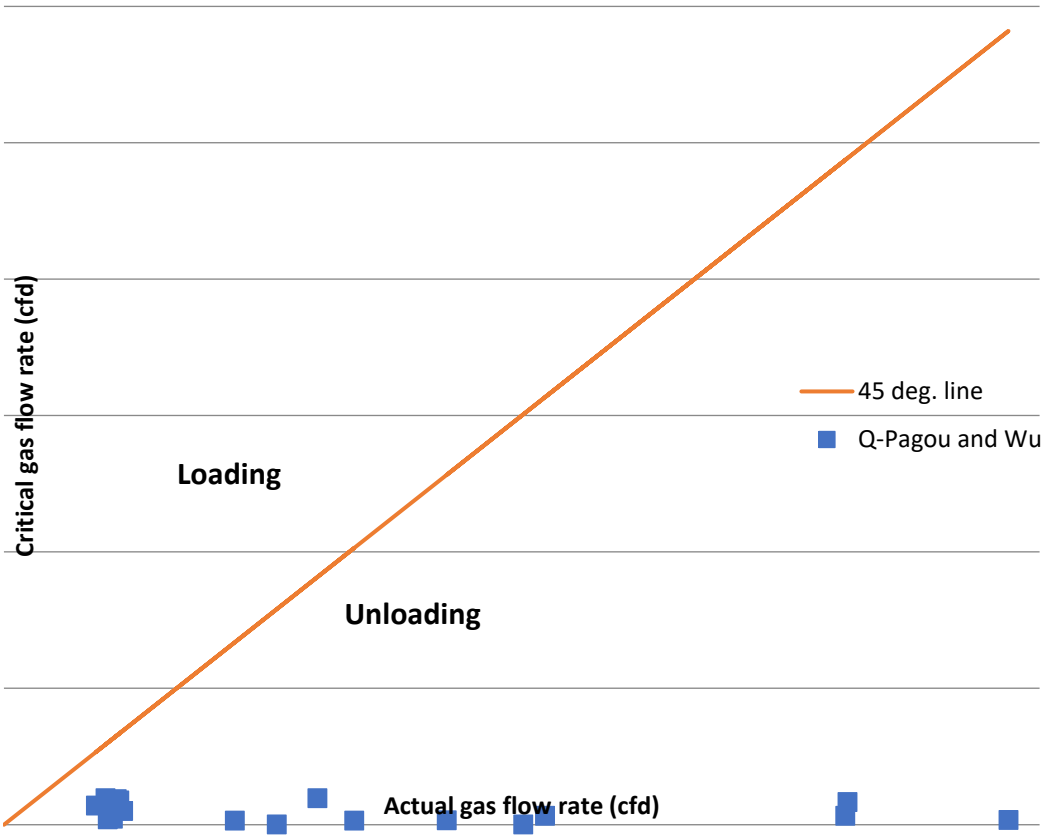

Figure 11: Pagou and Wu (2020) liquid loading prediction-results

Figure 11 gives the Liquid-loading prediction-results of Pagou and Wu *et al.* critical velocity model based on gas flow rate. From the figure, that Pagou and Wu *et al.* model predicted status of all eighteen (18) gas wells as unloading using critical-gas flowrate as the benchmark. This is however different from the actual gas well conditions which designated 10 wells as unloading, 6 wells as loading and two wells as about to load. In fact, on well-by-well basis, Pagou and Wu *et al.* model predicted correctly the actual conditions of all unloading gas wells, thereby giving it 100% prediction accuracy for the unloading gas wells. The model also did not correctly predict the actual conditions of all of the six (6) loading gas-wells, giving it a prediction-accuracy of 0 % for the loading gas wells. Also, the model could not accurately predict the actual condition of two (2) gas wells that are about to load.

Table 1 gives the summary of overall liquid-loading predictions by critical-velocity model's understudy. The table was generated by combining the prediction accuracies for all the categories of well status for each critical velocity model respectively. From the table, Nossier *et al.* critical velocity model gave highest prediction-accuracy of 88.89%. Also, Turner *et al.* and Coleman *et al.* models gave the same overall prediction accuracies of 66.67% respectively. The reason for this is not far from fact that both critical-velocity models were developed based on entrained-droplet model of liquid-loading (Pagou and Wu, 2020).

The next best ranked critical-velocity model was the model by Li *et al.* with an overall prediction accuracy of 61.11%. While the critical velocity model with lowest overall prediction accuracy was the developed model, which had the prediction accuracy of 38.89%. This low prediction accuracy can be explained by fact the data set used were derived from vertical wells and may not be

suitable for a critical velocity model that considers inclination angle like the one developed here (Pagou and Wu, 2020).

Table 2 gives effects of model-coefficient adjustment on liquid-loading prediction-accuracy, which was generated from Tables A13-A16. The model coefficient-adjustment was carried out following usual the work of Wolu *et al.* (2019), in which they considered the effect of model-coefficient adjustment on liquid-loading prediction-accuracies of critical-velocity models.

Model coefficient reduction was chosen because critical-velocity prediction by the developed model was higher than actual gas-velocities. It can also be deduced that model-coefficient reduction is directly proportional to liquid-loading prediction-accuracy.

Hence, by reducing model-coefficient by 20%, model prediction accuracy was increased to 44%. While model coefficient reduction by 40% further increased prediction-accuracy to 66.67%, further reduction by 60% didn't affect prediction-accuracy. But when model-coefficient was reduced further by 80%, prediction-accuracy then increased to 77.78%.

SUMMARY

A new critical velocity model has been developed for predicting onset of liquid-loading in natural gas wells. This was done following the reverse film model, while incorporating separate pressure drops for both liquid and gaseous phases.

Also, influence of production tubing length and liquid film thickness on critical-velocity prediction was equally considered. And the final model showed production tubing length as affecting critical velocities in gas wells that is previously ignored in other critical velocity models. From the model, it was deduced that the critical velocity varies directly as the square root of the tubing height. This means that as the tubing height increases, the critical velocity would equally be expected to increase, although not in a similar way.

A comparative analysis of prediction accuracy of developed-model was also conducted alongside other critical velocity models like Turner *et al.* (1969), Coleman *et al.* (1991), Nossier *et al.* (2000), Li *et al.* (2001), and Pagou and Wu (2020) models using literature data.

The obtained field data was from 18 vertical gas wells from the Xinjiang North-West gas field in China. The prediction accuracies of critical-velocity models followed the order, Nossier *et al.* (2000), Turner *et al.* (1969), Coleman *et al.* (1991), Li *et al.* (2001), Pagou and Wu (2020), and developed-model. This can probably be attributed to dearth of suitable field data sets in literature that includes production tubing height as a parameter.

To increase the prediction accuracy of developed-model, model coefficient adjustments were carried out by percentage reduction of developed model coefficient. This was done following common practice in literature where percentage adjustments are frequently made to critical velocity model coefficients to increase their liquid-loading prediction-accuracies.

In the end, the prediction accuracy of developed-model was tremendously increased by reducing model coefficient.

CONCLUSIONS

From this study, following conclusions are drawn

a) A new critical velocity model was developed for predicting onset of Liquid-loading in natural gas wells, which incorporated tubing height and separate pressure drops for both phases as parameters.
b) The developed critical velocity model was able to correctly predict liquid-loading status of some wells whose field-data were found in literature.
c) Model coefficient adjustments in the form of percentage reduction can substantially increase prediction-accuracy of developed critical-velocity models like percentage increment.

REFERENCES

Aboutaleb, G. J. G. and Vahid, K. (2015). Prediction of gas critical flow rate for continuous lifting of liquids from gas wells using comparative neural fuzzy inference system. *Journal of Applied Environmental and Biological Sciences*, *5*(8S), 196-202.

Adaze, E., Badr, H. M., and Al-Sarkhi, A. (2019). CFD modeling of two-phase annular flow toward the onset of liquid film reversal in a vertical pipe. *Journal of Petroleum Science and Engineering, 176*, 755-774

Ajani, A., Kelkar, M., Sarica, C., and Pereyra, E. (2016). Foam flow in vertical gas wells under liquid loading: Critical velocity and pressure drop prediction. *International Journal of Multiphase Flow, 87*, 124-135

Alamu, M. B. (2012). Gas-well liquid loading probed with advanced instrumentation. *SPE Journal, 17*(01), 251–270. doi: 10.2118/153724-PA.

Ali, A. J, Scott, S. L. and Fehn, B. (2003). Investigation of a New Tool to Unload Liquids from Stripper Gas Wells, SPE 84136, Presented at SPE Annual Technical Conference and Exhibition held at Denver

Alsaadi, Y. (2013). Liquid loading in highly deviated gas wells. Master's Thesis, University of Tulsa.

Arachman, F., Alkouh, A., and Wattenbarger, R. A. (2012). Bias in Rate-Transient Analysis Methods: Shale Gas Wells, SPE 159710, presented at the SPE Annual Technical Conference and Exhibition held at San Antonio, Texas, USA.

Ardhi, H. L. (2016). Modelling two phase pipe flow in liquid loading gas wells using the concept of characteristic velocity, submitted to Texas A & M University, August 2016.

Ayala, L. F. (2001). A unified two-fluid model for multiphase flow in natural gas pipelines. [Masters Dissertation], The Pennsylvania State University.

Baker, O. (1953). Design of pipelines for the simultaneous flow of oil and gas. *Oil and Gas Journal*, *53*, 185.

Barnea, D. (1986). Transition from annular flow and from dispersed bubble flow-unified models for the whole range of pipe inclinations. *International Journal of Multiphase Flow, 12*(5), 553–744. doi: 10.1016/0301-9322(86)90048-0.

Barnea, D. (1987). A unified model for predicting flow-pattern transitions for the whole range of pipe inclinations. *International Journal of Multiphase Flow, 13*(1), 1–12. doi: 10.1016/0301-9322(87)90002-4.

Barnea, D., Shoham, O., and Taitel, Y. (1982). Flow pattern transition for downward inclined two-phase flow; horizontal to vertical. *Chemical Engineering Science, 37*, 735-740.

Beggs, J. P., and Brill, H. D. (1973). A study of two-phase flow in inclined pipelines. *Journal of Petroleum Technology*, 607-617.

Belfroid, S. P. C, Schiferli, W., Alberts, G. J. N., Veeken, C. A. M. and Biezen, E. (2008). Prediction Onset and Dynamic Behaviour of Liquid Loading Gas Wells SPE 115567, presented at the SPE Annual Technical Conference and Exhibition held in Denver, Colorado, USA.

Bello, K. O. and Idigbe, K. I. (2015). Development of a new drag coefficient gas multiphase fluid systems. *Nigerian Journal of Technology*, *34*(2), 280 – 285. http://dx.doi.org/10.4314/njt.v34i2.10

Bolujo, E. O., Fadairo, A. S., Ako, C. T., Orodu, D. O., Omodara, O. J. and Emetere, M. E. (2017). A new model for predicting liquid loading in multiphase gas wells. *International Journal of Applied Engineering Research,* 12, 4578-4586

Brauner, N. (2001). The prediction of dispersed flow boundaries in liquid-liquid and gas-liquid systems. *International Journal of Multiphase Flow*, *27*, 885-910.

Brodkey, R. S. (1967). The phenomena of fluid motions, Addison-Wesley Publishing: Reading, MA.

Chen, X., Cai, X., and Brill, J. P. (1997). Gas-liquid stratified wavy flow in horizontal pipelines, journal of energy resources technology. *Transactions of the ASME*, *119*(4), 209-216.

Chen, D., Ya, Y., Gang F., Hongxia, M., and Shuangxi, X. (2016). A new model for predicting liquid loading indeviated gas wells. *Journal of Natural Gas Science and Engineering,* 34, 178–184. doi: 10.1016/jjngse.2016.06.063.

Cheng, N. (2009). Comparison of formulas for drag coefficient and settling velocity of spherical particles. *Powder Technology*, 189, 395-398

Chongyang, X., Heng, F., Leli, C., and Wenyu, P. (2021). Prediction of critical liquid loading time for water-producing gas wells: Effect of liquid drop rotation. *Journal of Petroleum Exploration and Production Technology.* https://doi.org/10.1007/s13202-021-01417-6

Chupin, G., Hu, B., Haugset, T. and Claudel, M. (2007), Integrated Wellbore/Reservoir Model Predicts Flow Transient in Liquid Loading Gas Wells, paper SPE 110461 presented at the SPE Annual Technical Conference and Exhibition, Anaheim, California,11-14 November 2007.

Cioncolini, A., and Thome, J. R. (2012). Void fraction prediction in annular two-phase flow. *Int. J. Multiphase Flow, 43* (0), 72-84.

Coleman, S. B., Clay, H. B., Mccurday, D.G. and Norris III, L. H. (1991). A new look at predicting gas-well load-up. *Journal of Petroleum Technology, 43*(03), 329–333. doi: 10.2118/20280-PA.

Coskuner, G. and Strocen, T. (2002). Production optimization of liquid loading gas condensate wells: A case study, Paper 2002-107, presented at the Canadian International Petroleum Conference, Calgary, Alberta, Canada.

Daas, M., Golczynski, T., and Harry, J. (2012). Minimum flowrate to unload gas wells: Dynamic multiphase modeling to validate existing correlations. Paper presented at the SPE Latin America and Caribbean Petroleum Engineering Conference, Mexico City, Mexico, April 2012. Paper Number: SPE-152597-MS

Dotson, B. and Nunez-Paclibon, S. (2007). Gas well liquid loading from the power perspective, SPE 110357, presented at the SPE Annual Technical Conference and Exhibition held in Anaheim, California, USA.

Dousi, N., Veeken, C. A. M., and Currie, P. K. (2005). Numerical and analytical modeling of the gas-well liquid-loading process. (English). *SPE Prod & Oper, 21*(4), 475-482. SPE-95282-PA. http://dx.doi.org/10.2118/95282-pa.

Dukler, A. E. (1960). Fluid mechanics and heat transfer in vertical falling-film systems. *Chem. Eng. Prog. Symp. Ser., 56*(30), 1-10.

Duns Jr., H. and Ros, N. C. J. (1963). Vertical flow of gas and liquid mixtures in wells. Paper presented at the 6th World Petroleum Congress, Frankfurt, 19-26 June.

El Fadili, Y., and Shah, S. (2017). A new model for predicting critical gas rate in horizontal and deviated wells. *Journal of Petroleum Science and Engineering, 150*, 154–161. doi: 10.1016/j.petrol.2016.11.038

Fadairo, A., Falode, O., and Nwosu, C. S. (2015). A new model for predicting liquid loading in a gas well. *Journal of Natural Gas Science and Engineering, 26* (2015), 1530-1541

Fan, Y., Eduardo, P., and Cem, S. (2018). Onset of liquid-film reversal in upward-inclined pipes. *SPE Journal, 23*(05), 1630–1647. doi: 10.2118/191120-PA.

Falcone, G. and Barbosa, J.R. (2013). State-of-the-art review of liquid loading in gas wells, DGMK / ÖGEW Spring Conference 2013, Section Exploration and Extraction, Celle.

Fiedler, S., and Auracher, H. (2004). Experimental and theoretical investigation of reflux condensation in an inclinedsmall diameter tube. *International Journal of Heat and Mass Transfer, 47*(19), 4031–4043. doi: 10.1016/j.ijheatmasstransfer.2004.06.005.

Fore, L. B., Beus, S. G., and Bauer, R. C. (2000). Interfacial friction in gas-liquid annular flow. analogies tofull and transition roughness. *International Journal of Multiphase Flow, 26*(11), 1755–1769. doi: 10.1016/S0301-9322(99)00114-7.

Ghadam, A. G. and Kamali, V. (2015): Prediction of gas critical flow rate for continuous lifting of liquids from gas wells using comparative neural fuzzy inference system, *Journal of Applied Environmental and Biological Sciences*, *5*(8S), 196-202

Girija, E. G., Christiansen, R. L, and Miller, M. G. (2007). Experimental study of critical flow rates in the tubing-casing annulus of natural-gas wells. SPE Annual Technical Conference and Exhibition. Society of Petroleum Engineers. SPE-109609-MS.

Govier, G.W. and Aziz, K., (1972). *The flow of complex mixtures in pipes*, 4th ed. Malabar Florida: Robert E. Krieger Publishing Company.

Griffith, P. and Wallis, G. B. (1961). Two-phase slug flow. *J. Heat Transfer, ASME, 83*(3) 307-320
Grolman, E. and Fortuin, J.M.H. (1997). Gas-liquid flow in slightly inclined pipes. *Chemical Engineering Science, 52*(24), 4461-4471.

Guner, M. (2012). Liquid loading of gas wells with deviation from 0° to 45°. Master's Degree Master's Degree, University of Tulsa.

Gunner, M. (2012). An experimental study of low liquid loading in inclined pipes from 90° to 45°. Presented at the SPE Production and Operations Symposium, Oklahoma City, Oklahoma, USA 1-5 March. SPE-173631-MS. http://dx.doi.org/10.2118/173631-MS.

Guo, B., Ghalambor, A. and Xu, C. (2005). A systematic approach to predicting liquid loading in gas wells, SPE 94081, presented at the SPE Production Operations Symposium, Oklahoma City, Oklahoma, USA.

Guo, B., Ghalambor, A., and Xu, C. (2006). A systematic approach to predicting liquid loading in gas wells (English). *SPE Prod & Oper*, *21*(1), 81-88. SPE-94081- PA. http://dx.doi.org/10.2118/94081 -pa.

Hearn, W. (2010). Gas well deliquifaction, SPE 138672, Presented at the Abu Dhabi International Petroleum Exhibition & Conference, held in Abu Dhabi, UAE.

Heng, L., Shenghan, C., Zhanqing, Q., and Qi, Z., (2006). Hydraulic system designing of esp downhole gas water separation system, Paper 2006-54, Presented at the Petroleum Society's 7th Canadian International Petroleum Conference, Calgary, Alberta, Canada.

Hewitt, G. F. (1961). Analysis of annular two-phase flow: Application of the Dukler analysis to vertical upward flow in a tube, *Atomic Energy Research Establishment*, Harwell, Berkshire.

Hewitt, G. F. (2012). Churn and wispy annular flow regimes in vertical gas–liquid flows. *Energy & Fuels, 26*(7), 4067-4077. http://dx.doi.org/10.1021/ef3002422.

Hewitt, G. F., and Nicholls, B. (1969). Film thickness measurements in annular two-phase flow using a fluorescence spectrometer technique. *UICAEA Report AERE* 4506:1969.

Hinze, J. O. (1955). Fundamentals of the hydrodynamic mechanism of splitting in dispersion processes. *AIChE Journal, 1*(3), 289–295. doi: 10.1002/aic.690010303.

Ikoku, C. U. (1992). *Natural gas reservoir engineering*. Malabar, Florida: Krieger Publishing

Jiang, Y. and Rezkallah, K. S. (1993). A study on void fraction in vertical co-current upward and downward two-phase gas-liquid flow—i: Experimental results, *Chemical Engineering Communications*, *126*(1), 221-243, DOI: 10.1080/00986449308936220

Joseph, A. and Ajienka, J. A. (2010). A review of water shut-off treatment strategies in oil fields. SPE 136969, Paper presented at NAICE Tinapa-Calabar Nigeria.

Joseph, A., Ajienka, J. A., and Ukaeju, D. I. (2011). The effect of temperature on the rheology of waxy crude/non-waxy crude oil blends, *International Journal of Engineering Science*, *3* (3), 2011.pp 108-127.

Joseph, A., and Hicks, P. D. (2018). Modelling mist flow for investigating liquid loading in gas wells, *Journal of Petroleum Science and Engineering* doi: 10.1016/j.petrol.2018.06.023.

Ke, W., Hou, L., Wang, L., Niu, J., and Xu, J. (2021). Research on critical liquid-carrying model in wellbore and laboratory experimental verification. *Processes* 2021, *9*, 923. https://doi.org/10.3390/pr9060923

Khor, S. H. (1998). Three-phase liquid-liquid-gas stratified flow in pipelines. [Ph. D. Thesis], Imperial College of Science, Technology and Medicine, London.

Kumar, N. (2005). Improvements for flow correlations for gas wells experiencing liquid loading, SPE 92049, presented at SPE Western Regional Meeting held in Irvin, CA USA

Lea Jr., J. F. and Tighe, R. E. (1983). Gas well operation with liquid production, SPE11583, presented at the Production Operation Symposium held in Oklahoma, USA.

Lea, F. J. and Nickens, V. H (2004). Solving gas-well liquid-loading problems, SPE 72092, Distinguished author's Series.

Lea, J. F., Nickens, H. V. and Wells, M. (2003). *Gas well deliquification - solution to gas well liquid loading problems*. Houston, Texas: Gulf Professional Publishing (Reprint).

Li, H., Yang, D. and Zhang, Q. (2007). A theoretical model for optimizing surfactant usage in a gas well dewatering process, Paper 2007-118 presented at the Petroleum Society's 8th Canadian International Petroleum Conference, Calgary, Alberta, Canada.

Li, J., Almudairis, F., and Zhang, H.Q. (2014). Prediction of critical gas velocity of liquid unloading for entire well deviation. Presented at the International Petroleum Technology Conference, Kuala Lumpur, Malaysia. 10-12 December. IPTC- 17846-MS. http://dx.doi.org/10.2523/IPTC-17846-MS.

Li, M., Sun, L, and Li, S (2001). New view on continuous-removal liquids from gas wells, SPE 70016, presented at the SPE Permian Basin Oil and Gas Recovery Conference held in Midland, Texas, USA.

Liu, L. (2014). The phenomenon of negative frictional pressure drops in vertical two-phase flow. *Int. J. Heat Fluid Flow*, *45*(1), 72-80. http://dx.doi.org/10.1016/j.ijheatfluidflow.2013.12.003.

Liu, Y., Chengcheng, L., Liehui, Z., Zhongbo, L., Chunyu, X., and Pengbo, W. (2018). Experimental and modeling studies on the prediction of liquid loading onset in gas wells. *Journal of Natural Gas Science and Engineering,* 57, 349–358. doi: 10.1016/ijngse.2018.07.023.

Luo, S., Kelkar, M., and Pereyra, E. (2014). A new comprehensive model for predicting liquid loading in gas wells. *SPE Prod & Oper, 29*(4), 337-349. SPE-172501- PA. http://dx.doi.org/10.2118/172501-PA.

Malin, M. (2019). An investigation into the mechanisms of liquid loading in small-diameter vertical pipes. [Masters Dissertation], Montana Tech Graduate School

Mandhane, J.M., Gregory, G.A., and Aziz, K. (1974). A flow pattern map for gas-liquid flow in horizontal pipes. *International Journal of Multiphase Flow, 1*, 537-553.

Meng, W., Chen, X.T., Kouba, G.E., Sarica, C., and Brill, J.P. (1999). Experimental study of low liquid loading gas-liquid flow in near horizontal pipes. SPE Paper 56466 presented at the SPE Annual Technical Conference and Exhibition held in Houston, TX, October.

Ming, R. and He, H. (2017). A new approach for accurate prediction of liquid loading ofdirectional gas wells in transition flow or turbulent flow. *Hindawi Journal of Chemistry*, Volume 2017, Article ID 4969765, 9 pages, https://doi.org/10.1155/2017/4969765

Nennie, E. D., Alberts, G. J. N., Belfroid, S. P. C., Peters, E., and Joosten, G. J. P. (2007). An investigation into the need of a dynamic coupled well-reservoir simulator, paper SPE 110316 presented at the SPE Annual Conference and Exhibition, Anaheim, California,11-14 November 2007.

Neves, T. R. and Brimhall, R. M. (1989). Elimination of liquid loading in low-productivity gas wells, paper SPE 18833 presented at the SPE Production Operations Symposium, Oklahoma City, OK, March 13-14.

Nosseir, M. A., Darwich, T. A., Sayyouh, M. H., and El Sallaly, M. (2000). A new approach for accurate prediction of loading in gas wells under different flowing conditions. *SPE Prod & Oper*, *15*(4), 241 -246. SPE-66540-PA. http://dx.doi.org/10.2118/66540-PA.

Oudeman, P. (1990). Improved prediction of wet-gas-well performance, SPE 19103, 18 SPE 167603 presented at the SPE Gas Technology Symposium held in Dallas.

Okafor, N. A., Aimikhe, V.J., and Kinigoma, B. (2019). Modelling the effect of acceleration term on total pressure drop in horizontal gas pipelines. *Petroleum and Coal, 61*(6), 1314-1320

Okoro, E.E., Bassey, C.I., Sanni, S.E., Ashiq, M.G.B., and Mamudu, A.O. (2019). Application of non-uniform film thickness concept in predicting deviated gas wells liquid loading. *MethodsX , 6*, 2443–2454.

Orkiszewski, J. (1967). Predicting two-. phase pressure drops in vertical pipe. *J. Petroleum*

Applied Sciences Research Periodicals
June 2023, Vol. 1, No. 3, pp. 69-92.

Utilization of Plant Extract for Treatment of Emulsions in Crude Oil Production

Georgewill, Allen and Joseph, Amiebibama

1. Department of Petroleum and Gas Engineering Faculty of Engineering, University of Port Harcourt, Rivers State, Nigeria

Abstract:
Emulsion formation causes enormous challenge in the oil and gas industry. Two types of emulsions are common in the oilfield; water in oil and oil in water emulsions. Water in oil emulsion is the most common and thus considered in this work. Emulsions are formed when two immiscible fluids (oil and water) from the reservoir are agitated in the presence of an emulsifying agent during production. Treatment of water in oil emulsion is a costly process and thus, in this work, environmentally friendly demulsifiers are formulated from orange peels and soya bean husks. The orange peels and soya bean husks were first dried under sunlight and ground into fine particles. Thereafter, Soxhlet Extraction technique was used to extract the demulsifiers; orange peel oil (OPO) and soya bean husk oil (SBHO) respectively. The OPO and SBHO were tested on crude oil sample obtained from Niger Delta and results compared with a commercial demulsifier phase treat (PT). Using bottle test method, the OPO, SBHO and PT were tested on the crude oil sample at different concentrations of 0, 200, 400, 600, 800 and 1000ppm's at 500, 1000 and 1500rpm, respectively. The concentrations and revolutions per minute where SBHO, OPO and PT achieved their best separations of crude oil are thus, at 200ppm and 1500rpm it was observed that OPO had 60% crude oil separation. SBHO had 45% crude oil separation at 400-600ppm's using 500rpm. And PT had its best crude oil separation of 87.5% at 500rpm using a concentration of 1000ppm, respectively. It shows that OPO and SBHO performed below the PT, however, with improvements on OPO, it shows a prospect of becoming a usable commercial demulsifier

Keywords: Emulsion, crude oil, orange peel oil, soya bean husk oil

INTRODUCTION

When two non-miscible fluid, like water and hydrocarbon are mixed together, there is lone dispersion of the liquid in the other instead of dissolving in it, this dispersion typically in a medium that is aqueous or in the company of emulsifying agent is an emulsion. The existence of water in oil causes unwanted issues such as: conductivity raise, corrosion, additives leaching so on (Aske,N. 2002). Techniques presently in use in demulsifying crude oil are thermal, electrical, chemical and gravity settling. Demulsification is the parting away the liquid that was dispersed from the liquid it was suspended. Both chemical and mechanical techniques of demulsification are line with Stokes's law. Reason for demulsifying is to break the boundary and constrain the surfactant to go in the direction of the water/oil region, permitting the oil particles and sediments to come together and rise to the outside. Decrease in water phase-viscosity or increase in the diameter of droplets of the oil and a decrease in the density of oil to water also works. There are numerous approaches used in neutralizing emulsion.

Emulsion decomposing; modification or employing air floatation that are dissolved, oxidation or other processes of oxidation are all expensive. Chemically, the emulsion reacts initiating surfactant modification which cannot acts as an emulsifying agent. neutralization of surfactant s that are ionic is the easiest technique applying acid or base ionizer of the salt comprises of calcium or magnesium, such as $CaCl_2$ or $MgSO_4$ sodium soap adds emulsion stability, whose solubility is the smallest in water consequent upon changes in the interfacial film and the-surfactant solubility increases in the bulk phase. the water -phase solubility could be improved by using acetone or alcohol and can help to heave emulsifier from the oil phase. If brine is the aqueous- phase, addition of water will cause separation. Demulsifiers causes Disruption of the ordered emulsifier interface pact of the with demulsifier. They concentrate at the layers because these materials are not very soluble in either phase, Aske, (2002).

Formation of Emulsion

Emulsion could be seen as liquid-dispersion which is completely immiscible in other liquid. In emulsion, the globule regularly exceeds the usual limits for colloids with respect to sizes. Emulsion generally is not present in the wellbore but their existence occurs as production of oil-water progresses with an immense amount of shakeup in the existence of emulsifying agent. When oil/water enters the well bore from the reservoir to the casing through the perforations, relatively huge differential pressure is produced which viciously blend the oil- water that is produced jointly in the company of emulsifying agent so that emulsion is formed Goldzal, *et al* (2000).

Emulsion consists of three phases: the discontinuous phase of thinly separated drop. The continuous phase is the medium that maintains the droplets in suspension. The inter phase is made up of emulsifiers or stabilizers that maintain the emulsion stability, binding the continuous and discontinuous phase collectively and prevent droplets from coming close to each other to band together Poindexter, *et al* (2004). Generally, emulsifiers are surfactants and soaps present either by themselves or as constituents for formation of detergent. Emulsifiers comprises of molecules with hydrophobic and hydrophilic ends. When immiscible liquids are present, the emulsifier travels to the interphase of the continuous/ discontinuous phases to form a defensive covering around the globules of thin phase at the same time as the molecules of the hydrophobic ends migrate or separates into droplets, while the hydrophilic ends stay in the water Sjoglom (2001). Homogenized milk, shaving cream, mayonnaise are some examples of emulsion etc.

Emulsion Properties

Aske (2002). Highlighted the following properties of emulsion:

1. The two liquids that form an emulsion (oil and water) are immiscible liquids.
2. Density/ viscosity of oils that is high generally contains more emulsifiers than lighter oils.
3. API gravity of crude oil that are low will form emulsion that is more stable and has high percentage volume of emulsion than API gravity of crude oil that is high.
4. Crude oil that has high viscosity will by and large make a more stable emulsion than crude oil low viscosity.
5. The color of emulsion must be dark reddish brown

Stability of Emulsion and Factors Affecting It

Stability is generally seen as emulsion resolution and is recognized as a significant water-in-oil emulsions characteristic. a number of emulsions rapidly separates in oil and water phases once detached from surface of the sea, whereas emulsions that are more stable can continue from

days to years. Current study shows that the emulsion viscosity is associated with its stability (NRT Science & Technology Committee, 1997). It is dependent on several factors; hence stable emulsion is an emulsion that will not break down without treating. These factors include emulsifying agents, viscosity, specific gravity, water percentage and the age of emulsion.

Process of Demulsification

An amount of universal rules assists in the formation of the fundamental viewpoint on the behavior of emulsion surrounded by commercial demulsifiers (Grace, 1992). To start with, emulsions from hydrocarbon comprises principally of immiscible liquids. Their Separation is influenced by the natural processes, by providing the necessary differential density among the liquid. Next, the rate of gravity settling is function of the surface tension of the droplets which are formed in the inner phase of the emulsion. Bigger droplets have poor surface tension which is dependent on the mass rather than tiny droplets.

Thus, separation rate can be increased by increasing the size of the droplets. Again, if a stabilized emulsion exists in an environment, variations in the conditions of the environmental can influence the stability of the emulsion and hence, separation of the phases will occur. Lastly, when emulsifying agents are present, it gives room for emulsion stability. Immiscible liquids will break up when there are changes or removal of emulsifying agents.

From the overview stated above, it becomes obvious that demulfication has several options. Changes in this vicinity may give rise to emulsion resolution. Demulsification is one of the methods or is a chemical method of treating emulsion in the oil industry.
Other methods include

1. Heating
2. Gravity settling
3. Electrical method
4. Filtration
5. Dilution
6. Centrifugation

These demulsifiers tend to focus on the oil-water interface of the emulsion to separate it into oil and water. They are also called stabilizers. Chemically, they are surfactants which are partially soluble in water and oil. This study describes the effect of various demulsifiers on a crude oil sample using practical techniques. Also, demulsifiers will be compared to each other for evaluation of the performance on each of the crude oil. Processing is the act of purifying or removing impurities, fluids produced from an oil and gas wells normally comprises of mixtures of oil, natural gas, and salt water. They are directed through a manifold system and flow lines to a treating facility which are sometimes installed near the production area.

The first stage in processing the produced stream involves the use of mechanical equipment's called separators.In separation, the fluid stream is separated into their respective phases (oil, gas and water). After separation, each separated stream then undergoes extra processing for proper field treatment. The crude oil on leaving the separator does not always meet the requirements expected for use in refining because it still contains a particular percentage of water; (8% to 10%) that exist as emulsified water. As stated earlier, the presence of this water presents corrosion and scaling tendencies to production equipment's and must be removed.

The water present in the oil and produced solids (e.g., silts, sand, etc.) constitute of what is known as the basic sediments and water (BS&W), a maximum of 1% BS&W, and in some cases less than 0.5% is acceptable, and the limit on salt content of the remaining water in oil is usually in the range of 10 to 15 PTB (Pounds of salt per thousand barrels of oil). Current information has recommended that an equivalent amount of water depart through production of a quantity of 60 million barrels of crude oil per day (Ivanov and Kralehevcky, 1996). Under the production conditions, a proportion of this water can become intimately dispersed throughout the crude oil as small droplets. In crude oil handing the method for removing salt includes the inside mixing of the external crude that comes in with a fresh "wash water" to extract the salts that are soluble in water. In a nutshell, the reason for emulsion treatment is to reduce the salt and BS&W content to appreciable limits, so it could be usedfor refining purposes. (Ivanov and Kralehevcky,1996). Demulsifiers are neutralizers of emulsifying agents. Demulsifier molecules tend to occupy the empty space available for absorption in the emulsion.

Types of Emulsion

Oilfield emulsion is of three types namely.

i. Water-in-oil emulsion
ii. Oil-in-water emulsion
iii. Multiple or complex emulsion

The Emulsion Problem

The systems that favour the natural occurrence of emulsion during hydrocarbon exploitation from the well, are described as unstable thermodynamic systems, co-product with water smear, sediments and salt water of dissimilar saline, and comprises of dual liquid phases (Umar *et al.* 2018). Kokal and Aramco (2005) posited that emulsions from crude oil are acknowledged as a dispersed water globules in the hydrocarbon. They are not welcomed in the production and transportation lines since it has better prospect to produce a composition that is stable if the treatment is not properly done, which could lead to a lot of complications, particularly in course of refining. Various problems could arise at some stage in the exploitation of hydrocarbon from the well to be listed (Zolfaghari *et al*. 2016):

a. The buildup of elevated drop in pressure in flow lines.
b. The high pumping and transportation charges of the combined water–oil through the facilities.
c. The damage of facilities
d. The raise in corrosion and scaling rate
e. The separation equipment tripping in the separating plants for gas/oil. (GOSPs) which restricts the exportation value of the hydrocarbon
f. The low API gravity of the hydrocarbon.
g. The destruction of the catalysts of the processing plant for. downstream
h. The difficulty in advancing the crude oil viscosity (owing to dispersed water drops that are tiny in nature).

Crude Oil Emulsions Classification

Hydrocarbon classification is seen in four major categorises which are SARA fractions which are saturates (waxes), aromatics, resins and asphaltene. This classification depends upon its solubility and polarity in a solvent. Precipitating the crude oil in paraffin solvent is a fundamental means to reduce asphaltenes. In the interim, chromatographic fractionation is used to undo the deasphalted oil (saturates, aromatics and resins). Of the four classes, just saturates alone can

simply be differentiated from the other crude-oil in the combination. The deficiency of π-bonds influences them to voluntarily separate the aromatic fractions by using their polarity. The residual oil is including aromatics and hetero-atomic compounds with diverse levels of functionalism, condensation and alkyl substitution (Auflem .2002).

Water in Oil Emulsion Mechanism of Stabilization

The creation of water/oil emulsion was famous in the oil sector oil about 40 years back. (Fingas, 1995). Several works showed that emulsion goes along with several resident solids, surfactants or molecules that function as asphaltenes and resins which adds to the stabilization of emulsion. Amongst the principal research about the water/oil emulsions, according to Goni *et al.* (2015), stability is the main manner in which they are formed. Their studies as well explained that emulsion formation is dependent upon the content of asphaltene and resins as the main fractions. Czarnecki and Moran (2005) and Czarnecki (2009) also posited that asphaltenes and other surfactant material must be present in smaller quantity before an emulsion will stabilize and more studies on the surface interaction were done to find out the molecules that are accountable for high water-in-oil emulsion stability. Surfactant's existences in the interface of the oil–water help to increase small droplets which are important in the formation of emulsion. These surfactants permit the reduction of interfacial tension on the assumption that during demulsification that there are surface free energy changes. Emulsion formation is encouraged by surfactants which produce smaller droplets and assist the stability of the emulsion. Basic information on the emulsifiers will help to proffer pioneering result to make a distinction on stable emulsion formation.

In general, the four major classes (SARA) can be found in hydrocarbon. They differ adequately in adsorptive tendency and solubility, and the applicable techniques are useful in separating them from the hydrocarbon crude oil.

Asphaltenes is usually a fraction of dark brown, black friable substance that sticks, and is a semisolid with no definite melting point, usually foams and swells to deposit residue that is carbonaceous in nature when heated. The subsistence of asphaltenes is recognized to have a significant outcome on both the ability to process and recover hydrocarbon and to solve the issues associated with the stability of emulsion. Certainly, the subsistence of asphaltenes gives raise to low separation rate from the oil medium as a result of solid deposition in the operations for recovery. Formation of coke is caused by separation of phase in processing in addition to asphalt pavement failure by physical structure loss of the asphalt cumulative arrangement (Speight 1992). Therefore, it is important to comprehend the hydrocarbon structure and its stability, by studying the precipitation/flocculation of asphaltene, using solvent/non-solvent mixtures for titration.

Agents which are emulsifiers are accountable for emulsion growth. Griffin (1949) first demonstrated Hydrophilic–lipophilic balances (HLB) and is generally a sufficient and a proficient method to test demulsifier efficiency. The two major dissimilar divisions: hydrophilic head (water liking) and a hydrophobic tail (water disliking) held in the surfactants. (Amphiphilic molecules). The hydrophilic part of the molecules of the surfactant could be positive (cationic), negative (anionic), neutral (non-ionic), or (amphoteric).

However, the hydrophobic part is consisting of one or chains of hydrocarbon, usually carbon atoms ranging from 6 to 22 atoms (Umar *et al.* 2018). Again, Griffin recognized that surfactants that are alkoxylated non-ionic perform better than ionic surfactants.

There was a proposition for the calculation of HLB number from the structure of the chemical that enables the establishment of the surfactants to be employed in water-in-oil or oil-in-water emulsion.

The computation of the HLB number demonstrates that, surfactants with a high HLB number can be exploited for water-in-oil emulsion. On the other hand, surfactants with a smaller HLB number can be exploited for oil-in-water emulsion (Porter 1991).

Table 1: The appearance of water depends on the HLB number (Porter1991)

HLB number	**Appearance of adding surfactant on water**
1–4	Insoluble
4–7	Poor dispersion unstable
7–9	Stable opaque dispersion
10–13	Hazy solution
13–20	Clear solution

Table 1. Shows the HLB number with an appearance on adding surfactant on water.

Appreciably, the emulsions needed for treatment by separating the oil from the water that is dispersed to meet up the market specifications and transport terms and to reduce the troubles of stable emulsion. In addition, the well-ordered handling of the emulsion could decrease corrosion and the poisoning of catalyst in the facilities used for downstream operations (Kokal and Aramco 2005). The emulsion separating method is essential, and several scholars had anticipated an assortment of approach to achieve the desired handling.

Formation and Stability of Water in Oil Emulsions

An agent that acts like an emulsifier must be there to form a stable water-in-crude oil emulsion (Sjöblom *et al.,* 2002). Such agents consist of particles of clay, extra chemicals or the hydrocarbon components like asphaltenes, waxes, resins and naphthenic acids (Sjöblom *et al.,*2002). The means of emulsification was inadequately implicit till the 1990's (Fingas and Fieldhouse,2003). The fundamental physics of water-in-oil emulsification was implicit in the surfactant engineering, but not in the oil sector (Fingas and Fieldhouse, 2003). For a good number of the emulsions, it is seen that the stability of the emulsion reduces as temperature increases, since at high temperatures there is a corresponding decrease in the continuous phase viscosity with the increased rate of collision of dispersed phase droplets (Cormack, 1999). Emulsions that are Stable could have water content of 20 to 80% which emerges as small droplets but an increase in temperature enhances coalescence and concludes with phase separation Cormack (1999), As a result, emulsion formation and stability mainly a function of the temperature, established conditions and the occurrence of natural substances like asphaltenes, waxes, and resins (Lane, 1995).

Demulsification of Water in Crude Oil Emulsions

The emulsions formed at sea subsequent to oil spillage are basically stable. Demulsification is one of the most difficult tasks to perform in the petroleum sector. demulsifying water in crude oil emulsions entails chemical, thermal, electrical, or a blend of these processes depending on the distinctiveness and properties of the emulsion Mohammed *etal.,(1993*). An assortment of techniques of de-emulsification, like use of centrifuge, sedimentation, use of heaters use of dispersants and demulsifiers have been studied Kim *et al (*,2002). Among these methods, use of heaters and the use of centrifuge did not get much acceptance owing to the high cost and energy requirements. The awareness that dispersants cannot deal with higher viscosity emulsions gave confident to the study of the possible use of demulsifiers (Cormack, 1999). The addition of chemical demulsifiers in minute quantities can considerably make oil- water separation easy. Poindexter and Lindemuth, (2004). According to Nordvik *et al.* (1996), the key advantages of using demulsifiers are:

1. Fast and less expensive
2. Reduces the crude oil emulsions viscosity
3. Improvement in pump capability
4. Reduction in oil -waste treatment
5. Reduction in the ultimate disposal rate by a factor of10.

Demulsifying emulsions also entail some quantity of chaotic energy (Lane, 1995). The energy situation is not even and depends on the nature of energy induced and the type of demulsifier utilized (Lane, 1995). The main objective of the emulsion breaker/demulsifier is to displace the naturally occurring emulsifying agents from the oil-water interface (Cormack,1999). Nordvik *et* al. (1996) stated that the efficiency of the demulsifier depends upon:

1. Product efficiency (demulsifier)
2. Characteristics of the crude oil
3. Conditions of the environmental
4. Method of Application
5. Application Time

Demulsification of Crude Oil Emulsion

Demulsification is important in the oil sector, painting, coating and treating waste water in environmental technology (kim, 1995). Demulsification has added extra meaning as the employment of single or combination practice for the recovery of in-situ weighty crude-oil is complex as these processes produces viscous emulsions which is a combination of oil- water and mud. Emulsion demulsification forms a fundamental aspect of oil- production. Emulsion destabilizing could be achieved by mechanical, chemical, thermal, or electrical method. Extra practice like adjustment of pH, use of filters, membrane separation and heat handling techniques, may also be employed (Gafonova, 2000). The awareness regarding emulsion characteristics and the means by which they occur for the phase of coalescence of water globule is essential for speedy separation (Ese et *al.*, 1999).

Quality mechanical tools are utilized in destabilizing emulsion like centrifugal separators and so on. Though, this equipment is considerably huge plus costly to set up on offshore-platforms distinctively for conditions of the North-Sea. Therefore, number of equipment should be at the barest minimum to avoid huge financial involvement (Aufluem, 2002). Thermal process is achieved by adding heat to treat emulsion at the refinery/facilities and the emulsion could be resolved with light oil were the main emulsifier is paraffin. A rise in temperature above the

melting-point of paraffin in the range of 50-60°C could absolutely weaken the emulsion Grace (1992). Consequently, the temperature that produces the desired result at refinery is 70°C.The use of heat alone is barely makes the emulsion to be resolved.

The method of electricity utilizes electrostatic principle to demulsify produced emulsions and desalting in the refineries. The created electric field upset the elastic skin tendency of each of the droplet, perhaps by the re-orientation of polar molecules. These actions deteriorate the layer of the droplets due to non-concentration of the polar molecules at the surface. Besides, a reciprocated magnetism of particles of neighboring emulsion gets induced charges from the electric field applied Grace, (1992). The attractive and repulsive forces bring charge particles that are opposing each other in a close fashion. As a result, the layer is destabilized, and the droplets engrossed electrically and coalescence occurs.

The main familiar technique of breaking emulsion is the utilization of the mixture heat and chemical which could take care of the agents that causes emulsification (Auflern, 2002). The cost incurred by applying a demulsification plan is moderately small and is completed without shutting down. The rate of separation of W/O emulsion is consequent upon the demulsifier that forms stable emulsion, the temperature, the processing vessel, the concentration, the residence time of the process and the energy at which it mixes.The frequently used technique used to determine relative stability of emulsion for laboratory level is the bottle test. it is an experimental investigation in which different quantity of prospective emulsion breakers are administered a succession of bottles holding secondary samples of emulsion to be demulsified. At some definite time, the degree of separation of phase and interface expression of phase separation is taken into cognizance. Apart from demulsifiers, solvent could be introduced to lessen viscosity. Perhaps a number of diverse bottle test method abound as there are persons who use them regularly. Generally, its entails agitating, stirring up to normalize the emulsion or to blend in the demulsifier to be assessed, and a wait and watch time where the degree of separation of phase is observed with interface clarity and water phase turbidity.The optimization of the amount and kind of chemical employed provides to lower the oil content with in the produced water offshore. The improvement and use of environmentally pleasant chemicals are made feasible via gaining fundamental expertise concerning the techniques concerned to stabilize and break the emulsions. Success of chemical demulsifying techniques based on the following:

1. Ample amount of an appropriately chosen chemical must go into the Emulsion.
2. Transparent systematic addition of the chemical in the emulsion.
3. Adequate warmness is necessary to speed up or cause emulsion resolution.
4. Adequate residence time must subsist in vessels that treat the emulsion to allow demulsified water droplets settlement.

Chemical method is the frequent method used to treat water-in-oil and oil-in-water emulsion and it entails applying chemical additives to speed up demulsification. The stable nature of emulsion is typically influenced by the interface/film and method of surfactant adsorption (Kim, 1995). The techniques applied in chemical method of emulsion breaking of a water-in-crude oil emulsion entails the speeding up of the coalescence in addition to the film splitting procedure. Water droplets that are dispersed move toward one another and compress and forming a thin film of oil that is in continuous phase among them, the external drainage flow of the film can - form slopes in interfacial tension which then counter and delay drainage. The coalescence rate will rely on the dynamics that convey the droplets together, e.g., concentration, and then the force balance that makes the interface stable and disarray.

Demulsifier Performance

Demulsifiers and emulsifiers are extremely alike for the reason that they are surfactant in nature. Hence, the exploit of the emulsion breaker is to "disengage" the significance of the presence of the agents that emulsifies. This disengagement is achieved in three basic steps, which are flocculation, coalescence and solid wetting (Leopold, 1992). Diverse categories of chemical emulsion breakers will give dissimilar results in emulsion breaking practice. The awareness of how emulsion forms and becomes stable, emulsion breaking types, mechanisms of emulsion breaking are extremely vital because it could be helpful in the development of emulsion breaker. As a result, it was examined in the study of the parameters that affects the formation of emulsions that are stable. The parameters that are recognized to influence the performance of demulsifiers are: temperature, ph and solvents/diluents

Oilfield Demulsification

The problems related with the processing emulsion presents an incredible effect, and it has become the key concern in the oil and gas sector. Currently, emulsion-breaking method has been the main interest amid the studies that leads. The overcome the problems related to crude oil emulsions, several factors should be considered to break the emulsion without difficulty such as physical and chemical properties of the crude oil, temperature of the crude oil, space connecting topside and the reservoir, level of disturbance felt among reservoir, separator, turbulent flow, presence of solid that improves the emulsion stabilization. Demulsification is a procedure used for separating emulsion into different component ie oil and water. Fundamentally, the means of demulsification: are biological physical and chemical, the efficacy of these techniques can be seen in their ability to reduce the stability of emulsion and cause separation of phases (Zolfaghari *et al.* 2016). In the petrochemical industry, the separation of the emulsion must be in two phases in order to guarantee the smoothness of the refining process (Abdulredha *et al*. 2018).

Demulsifiers

They are seen as a collection of additives that are applied on water/oil and oil/water emulsion typically at concentrations that low to take apart the water from the crude oil. For the duration of exploitation, the hydrocarbon has a substantial quantity of salty water. There should be salty water removal from the hydrocarbon to evade trouble for the duration of refining, so as to minimize corrosion rate. Abdulredha *et al*. (2018) defined additives as organic subdivision that consists of the hydrophilic and hydrophobic part. Usually, demulsifiers could be characterized into four categories: surfactant non-ionic, ionic, and amphoteric and polymer surfactant. The reason for demulsifiers is to plunge the water to a point that is low in the system where it can regularly be removed. Demulsifiers averts oil-water mixing ability and have structures similar to non-ionic emulsifiers. Demulsifiers' are chemicals which are de-salters and de-oilers, and are regarded to be approximately 40% of the chemicals in the global market. Interest has risen amongst researchers in this area.

Chemical Demulsifiers:

The subsistence of surfactants gives room to chemical additive to be mixed with the demulsifier to help in inhibiting the appearance of emulsion (Feitosa *et al*. 2019). A model that describes the potential of an emulsion breaker to disintegrate the emulsion formed by water-in-oil that has redundant lipophilic surfactants known as asphaltenes exists. Grenoble and Trabelsi (2018) did a work on optimal formulation of demulsifiers on the basis of hydrophilic/lipophilic balance. They opined that the key purpose of a demulsification method is to check the emulsification system by voluntarily adsorbing it at the interfacial phase and waning the asphaltenes or resins film

linked with the crude oil to encourage a good interfacial phase destabilization. A number of methods needed to be dealt with. As such, the demulsifier have to aggressive to be adsorbed at the interface to eliminate and disintegrate the asphaltene collection in addition to decreasing the interfacial tension between the crude oil and aqueous phases and thus assist the kinetics of the droplet coalescence (Salager and Forgiarini 2012).

***Demulsification Mechanisms*:**
Various researchers (Biniaz *et al*. 2016.Yang *et al*. 2018; Adewunmi and Kamal 2019;) had established that the emulsion- breaking methods of water/oil emulsion with oil/water emulsions (Martínez-Palou *et al*. 2013; Tao *et al*. 2015). To ably conquer the limitations revealed by the incidence of stabilized emulsion, the chemical, membrane and electrostatic de-emulsifications are the general methods (Behroozi *et al*. 2019). Destabilizing the emulsion formed from crude oil is improved by better temperature, centrifuging, electrical methods, high resonance time and chemical treatment method. Several techniques were formulated for to break emulsion, and many parameters were considered to achieve it, which includes the distribution of droplet size, dosages, and the rate of drainage, the temperature, emulsion viscosity and type of emulsifier/demulsifier (Zolfaghari *et al.* 2016).

Performance Demands on Demulsifiers:
After emulsion-breaking is done, the major thing to look out for is the fundamental demand which is the de-emulsifier performance and its capacity of possessing the characteristics below;

1. Strong interfacial attraction between oil/water with the ability to weaken the layer enclosed by the globules and-or to differ the angle of contact of the solid fraction of the layers interface;
2. Ability to flocculate droplets;
3. Potential to build up coalescence by warm conduit to water's likely attraction to water; and offering reticence of the drainage layer and thinning by induced alterations to the rheology interface (Sjöblom 2001).

The emulsion breaker can influence the interfacial globules layer by dislodgment and owing to its composite nature, changing the continuous-phase solubility and altering interfacial layer viscosity or film drainage supported by adsorption

Chemical Demulsifier as Emulsion Treatment:
Nikkhah et al. (2015) recommended new nanotitania as a tailored demulsifier for emulsion of water-in-oil. A sol–gel technique was made as substitute to synthesis, the nanotitania constituents. They analyzed the nanotitania particles using different techniques. Their outcome demonstrated that the sample that has the highest water separation utilized by the nanotechnology can promote 90% demulsification efficiency and reduced time for water separation.

Feitosa *et al.* (2019) examined additives on the basis of cardanol to evaluate the mechanisms of demulsification. Their results revealed that ethoxylated compounds, at neutral pH, are more appropriate to separate water-in-oil emulsions.

Li *et al*. (2018) examined the dosage and stability analyses, tannic acid phenol amine (TAPA) polyether were used as the demulsifier of water-in-aging- crude-oil (WACO) emulsion They concluded that TAPA could perform as an excellent demulsifier for WACO. Common chemical

Several researchers have used different types of demulsifier formulation to resolve crude oil emulsion. This research attempts to resolve crude oil emulsion using organic based materials for formulation of demulsifiers that are environmentally friendly and economical.

MATERIALS AND METHOD

Materials

Materials used for the research work is summarised in Table 1

Table 1: Materials used as Demulsifiers

Material	Code.	Source	Remark
Soya bean husk oil	SBHO	Soya bean husk	yellowish solvent
Orange peel oil	OPO	Orange peel	brownish solvent
Phase treat	PT	Vendor	colourless solvent

Table 2. IUPAC Name, Molecular Formula and Molecular Weight of Materials Used for experiment

IUPAC NAME	Molecular Formula	Molecular Weight (g/mol)
2-aminoacetic acid	$C_2H_5NO_2$	75.07
(2-methyl(pheyl) diazeny) naphthalen-2-ol	C $_{17}$NH 14N $_2$O	262.3
Phasetreat		

Table 3 Component of Soxhlet extractor and equipment for the experiment

Equipment	Function
Aspirator	contains water that goes into the inlet pipe
Condenser	cooling and condensation of the solvent
Extraction chamber	hold samples for extraction
Round bottom flask	contains solvent and anti-bumping
Inlet pipe	takes water from aspirator to condenser
Outlet pipe	takes water from condenser to containment can
Retort stand	holds the Soxhlet set-up
Measuring cylinder	measuring the solvent (N-Hexane)
Beaker	holds extracted oil
Filter paper	holds grinded samples in the extraction chambers
N-Hexane	solvent used for extraction
Anti- Bumping	make the N-Hexane to boil

Method

Extraction of Orange Peel Oil:

5000 kg of orange peel were sourced from Port Harcourt, Rivers State and was exposed to sunlight for drying. The drying process took seven days to properly dry the samples. After drying, the samples were grinded using a grinding machine.50g of the grinded orange peel was wrapped in a filter paper and put into the extraction chamber of the Soxhlet, for effective extraction of the oil, the n-hexane(400ml) was administered through the top of the condenser with the aid of a funnel, the solvent passed through the condenser to the extraction chamber and finally settles at the round bottom flask mixing up with the anti-bumping. After inspecting the setup, the heating mantle (water bath) was put on and setting the mantle to the boiling point of the n-

hexane. As the n-hexane begins to boil, it evaporates from the round bottom flask through the extraction chamber which contains the sample and finally the condenser containing the water that cools the system traps the n-hexane and condenses it and it drops as liquid back into the extraction chamber and as the liquid n-hexane increases in volume in the extraction chambers it reaches the siphon point and then siphon back into the round bottom flask, this process continues until the n-hexane in the extraction chamber becomes colourless, which indicates that the oil in the sample has been extracted..This process is repeated until the required volume of the essential oil was obtained from the extraction process.

Plate .1: Fresh and dried orange peel and ground orange peel.

Extraction of Soya Bean Husk:

500 kg of soya bean husk were sourced from Port Harcourt, Rivers State and was exposed to sunlight for drying. The drying process took one day to properly dry the samples. After drying, the samples were ground using a grinding machine.50g of the grinded soya bean husk was wrapped in a filter paper and put into the extraction chamber of the Soxhlet, for effective extraction of the oil, the n-hexane(400ml) was administered through the top of the condenser with the aid of a funnel, the solvent passed through the condenser to the extraction chamber and finally settles at the round bottom flask mixing up with the anti-bumping. After inspecting the setup, the heating mantle (water bath) was put on, and setting the mantle to the boiling point of the n-hexane. As the n-hexane begins to boil, it evaporates from the round bottom flask through the extraction chamber which contains the sample and finally the condenser containing the water that cools the system traps the n-hexane and condenses it and it drops as liquid back into the extraction chamber and as the liquid n-hexane increases in volume in the extraction chambers it reaches the siphon point and then siphon back into the round bottom flask, this process continues until the n-hexane in the extraction chamber becomes colourless, which indicates that the oil in the sample has been extracted.

This process is repeated until the required volume of the essential oil was obtained from the extraction process.

Plate 2: Soya bean husk and ground Soya bean husk.

Plate 3: Soya bean husk oil, orange peel oil and Soxhlet and schematic of Soxhlet extractor

Soya Bean Husk Oil and Orange Peel Orange Physio - Chemical Properties

Free Fatty Acid Determination:

0.125g of samples were measured and transferred into conical flask. 25ml of hot ethanol were also included to the blend, which was heated and stirred gently. Three drops of phenolphthalein indicator were also included into the mixture, which was titrated with NaOH standard solution of 0.04M until a pink colour was obtained.

Free acid content was determined using equation.

$$LipidFFA = \frac{\text{VXFXM}}{\text{10XW}} \quad (1)$$

Where:
V = NaOH volume used
F = equivalent weight of FFA expressed in oleic acid (2.83g)
M = molarity of NaOH
W = weight of NaOH

Acid Value Determination:

25ml diethyl ether was mixed with 25ml of alcohol and 1ml of phenolphthalein solution and was carefully neutralised with 0.1ml sodium hydroxide. 10g of the oil was dissolved in the mixed neutralised solvent and was titrated with aqueous 0.1ml sodium hydroxide and agitating the mixture until a pink colour which persisted for 15second was obtained.
Hence:

$$\text{Acid Value} = \frac{\text{Titre value x } 5.61}{\text{weight of oil}}$$

Saponification Value Determination:

Twenty grams of the extract (oil) was weighed into a conical flask and 25ml of alcohol potassium hydroxide solution was added. A reflux condenser was attached, and the flask was heated in boiling water for 1hour, and it was constantly agitated and 1ml of phenolphthalein solution was added and was titrated and a blank was also done at the same time

$$\text{Saponification Value} = \frac{Blank - titre \, x \, 28.05}{weihtofoil}. \quad (2)$$

Where:
Blank and titre value are in ml and weight of oil in grams.

Iodine Value Determination:

Wij's Solution:

Eight grams of iodine trichloride was dissolved in 200ml of glacial acetic acid and 9g of iodine was also dissolved in 300ml carbon tetrachloride. The solutions were mixed and diluted to 1000ml with a glacial acetic acid. The extract (oil) was poured into a small beaker and a suitable quantity the sample was weighed by difference into a dry glass Stoppard bottle at about 250ml capacity. The approximate weight in g of the extract to be taken was calculated by dividing 20 by the highest expected iodine value, then10ml of carbon tetrachloride was added to the oil and dissolved.30ml of wijs

A conical flask was used to weigh 0.4 g of the sample with 20ml of chloroform which was added to dissolve the oil. 25ml Wij's solution and 20 ml of 10% KI were subsequently added to the mixture; the flask was shaken and then kept in the dark for a period of 30 minutes at temperature below 30°C. This mixture was later titrated with a 0.1M of $Na_2S_2O_3$ solution until the yellowish colour nearly disappears. Some droplets of 1% starch indicator was added to the mixture. More drops of $Na_2S_2O_3$ were still added to the titration and shaken vigorously until blue coloration disappears.

$$\text{Value of Iodine} = \frac{12.69C\ (V2 - V1)}{M} \quad (3)$$

Where:
C = $Na_2S_2O_3$concentration used
V_1 =$Na_2S_2O_3$volume used for blank titration
V_2 = $Na_2S_2O_3$volume used for determination
M = Sample mass

Peroxide Value Determination:

1gram of the extract (oil) was measured into a clean dry boiling tube and 1gram of powdered potassium iodide was added. A 20ml of solvent mixture (10ml of glacial acetic acid+ 10ml of chloroform) was added to the initial solvent in the clean dry boiling tube. The tube was placed in boiling water and allowed to boil for 30 seconds and vigorously for another 30 seconds. The content was poured quickly into a flask containing 20ml of potassium iodide solution and 0.002M of sodium thiosulphate was titrated using starch. a blank was prepared at the same time.

The peroxide value is calculated thus

Peroxide value =Titre value x 2 in eq/kgmax. (4)

Density And Specific Gravity Determination:

10ml of refined extract was weighed with a 10ml density bottle and recorded.

$$\text{Density} = \frac{\text{Mass of the oil (g)}}{\text{Volume of the oil (cm3)}} \quad (5)$$

$$\text{Specific gravity} = \frac{\text{Density of oil}}{\text{Density of water}} \quad (6)$$

Characterization of Crude Oil:

Specific Gravity (SG):

Crude oil specific gravity was determined using the hydrometer method.

API Gravity:

API gravity is calculated using the relationship

$$\text{API gravity} = \frac{141.5}{\text{SG}} - 131.5 \quad (7)$$

Demulsification of Crude Oil Emulsion:

10ml of the emulsified crude oil was measured into a test tube and the various demulsifiers for this study was added into the crude oil emulsion at varying concentrations in parts per million (ppm). To test the efficacy of the demulsifier a blank sample was prepared in addition. The samples were centrifuged at various revolutions per minute (rpm) for 5minutes and water separation, emulsion separation and crude oil separation were recorded.

RESULTS AND DISCUSSION

Results obtained from the experimental work are presented in the following tables

Table 4 Crude Oil Emulsion doped with varying concentration of SBHO Demulsifier at 500 (rpm)

Conc (ppm)	Velocity (rpm)	Time (mins)	Emulsion (ml)	Water (ml)	Emulsion separated (ml)	crude oil (ml)	BS$ W%	Crude oil%
0	500	5	10	0.5	90	0.5	5	5
200	500	5	10	0.5	6.3	4.2	5	42
400	500	5	10	1	5.8	4.5	10	45
600	500	5	10	1	6.3	4..5	10	45
800	500	5	10	1	6.2	4	10	40
1000	500	5	10	1.5	5.5	3.8	15	38

Table 5. Crude Oil Emulsion doped with varying concentration of OPO at 500 (rpm)

Conc (ppm)	Velocity (rpm)	Time (mins)	Emulsion (ml)	Water (ml)	Emulsion separated (ml)	crude oil (ml)	BS$W %	Crude oil%
0	500	5	10	0.5	9	0.5	5	5
200	500	5	10	1	3.5	5.5	10	55
400	500	5	10	1	3.7	5.3	10	53
600	500	5	10	1.5	3.5	5	15	50
800	500	5	10	1.5	3.7	4.8	15	48
1000	500	5	10	1.5	3.7	4.8	15	48

Table 6 Crude Oil Emulsion doped with varying concentration of Phasetreat Demulsifier at 500 (rpm)

Conc (ppm)	Velocity (rpm)	Time (mins)	Emulsion (ml)	Water (ml)	Emulsion separated (ml)	crude oil (ml)	BS$W %	Crude oil%
0	500	5	10	0.5	90	0.5	5	5
200	500	5	10	1.5	1	7.5	15	75
400	500	5	10	1	0.5	8.5	10	85
600	500	5	10	1	0.5	8.5	10	85
800	500	5	10	1	1	8	10	85
1000	500	5	10	1	0.25	8.75	10	87.5

Table 7. Crude oil separated (%) at 500 rpm

Conc (ppm)	Crude oil PT	crude oil OPO	Crude oil SBHO
0	5	5	5
200	75	55	42
400	85	53	45
600	85	50	45
800	80	48	40
1000	87.5	48	38

Table 8. BS&W (%) And Demulsifiers at 500 rpm

Conc	BS$W% PT	BS$W% OPO	BS$W% SBHO
0	5	5	5
200	15	10	5
400	10	10	10
600	10	15	10
800	10	15	10
1000	10	15	15

From figure 1: the Phasetreat demulsifier performed well, followed by orange peel oil. Soya bean husk oil performed least which were 87.5% of Phasetreat at 1000 ppm, 55% of orange peel oil (OPO) at 200ppm and 45% of Soya bean husk oil (SBHO) at 400 and 600 ppm.

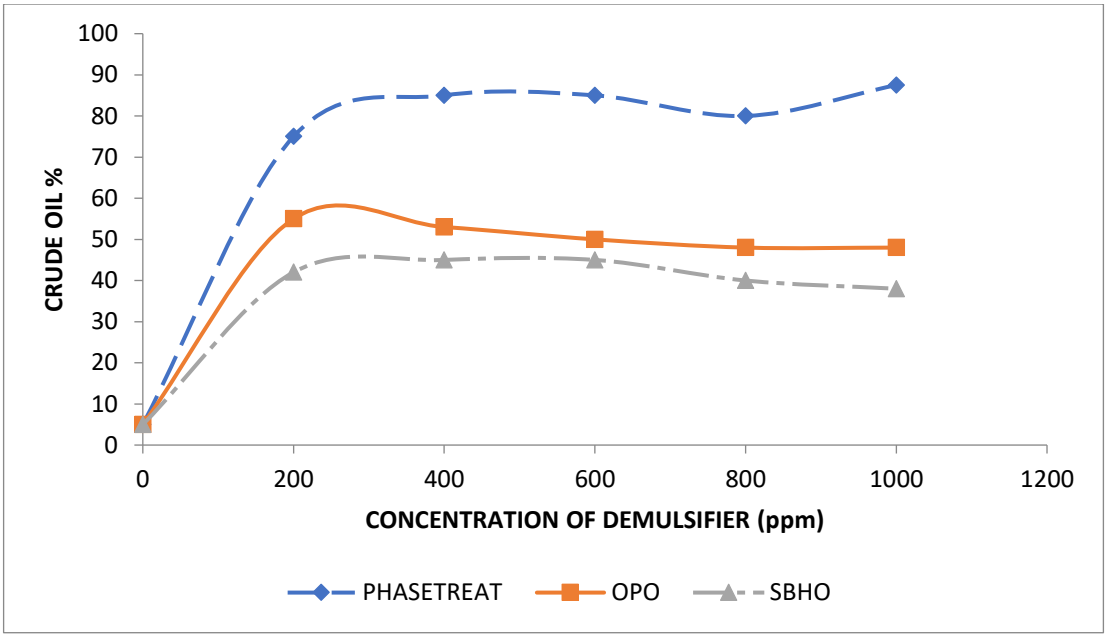

Figure 1 Crude oil (%) VS Concentration of demulsifier at 500 rpm

From Figure 2: the crude oil sample with Soya bean husk oil (SBHO) had the highest BS&W (%) followed by orange peel oil (OPO) It was observed that phase treat had the best separation of basic sediment and water which implied that the sample with the Phasetreat had the best oil separation and SHBO with the least crude oil separation which were 45%, at 1000 ppm 85% at 200 to 1000 ppm and 100% at 1000 ppm respectively

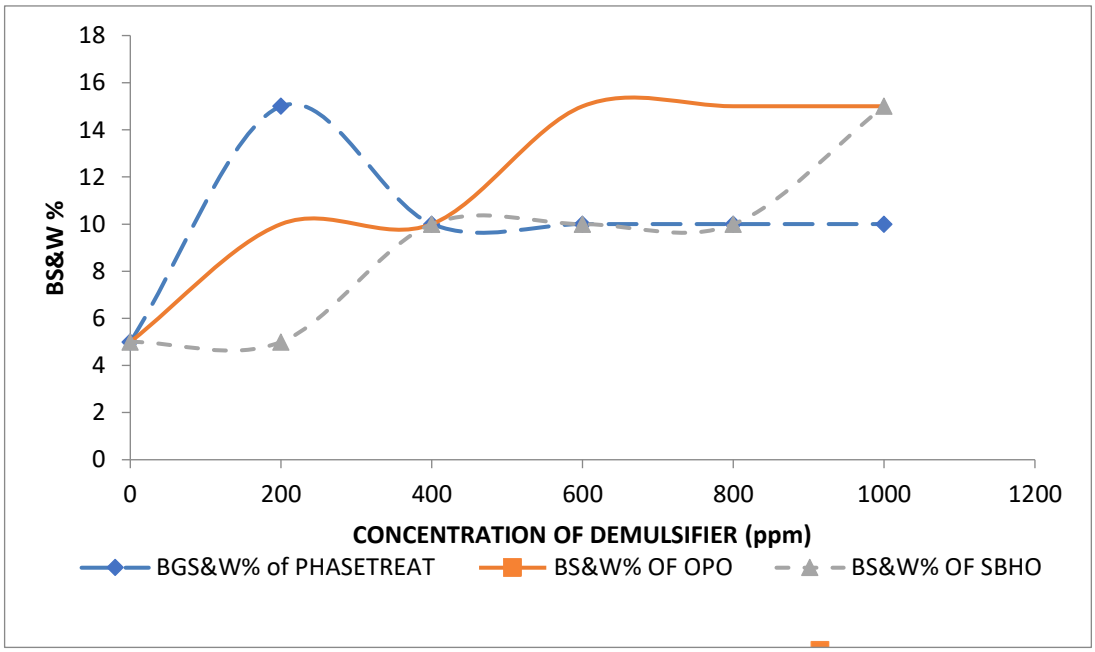

Figure 2: Plot of BS&W (%) VS Concentration of demulsifiers (ppm) at 500 rpm

Table 9: Crude Oil Emulsion doped with varying concentration of SBHO Demulsifier at 1000 (rpm)

Conc (ppm)	Velocity (rpm)	Time (mins)	Emulsion (ml)	Water (ml)	Emulsion separated (ml)	crude oil (ml)	BS$W%	Crude oil%
0	1000	5	10	0.5	9	0.5	5	5
200	1000	5	10	1	5	4	10	40
400	1000	5	10	1	4.8	4..2	10	42
600	1000	5	10	1.5	4.3	4.2	15	42
800	1000	5	10	1.5	4.7	3.8	15	38
1000	1000	5	10	1	5.4	3.6	10	36

Table 10: Crude Oil Emulsion doped with varying concentration of OPO Demulsifier at 1000 (rpm)

Conc (ppm)	Velocity (rpm)	Time (mins)	Emulsion (ml)	Water (ml)	Emulsion separated (ml)	crude oil (ml)	BS$W%	Crude oil%
0	1000	5	10	0.5	90	0.5	5	5
200	1000	5	10	1	3.2	5.8	10	58
400	1000	5	10	1.5	3.2	5.3	15	53
600	1000	5	10	1.5	3.5	5	15	50
800	1000	5	10	2	3	5	20	50
1000	1000	5	10	1.5	3.5	5.,0	15	50

Table 11: Crude Oil Emulsion doped with varying concentration of Phasetreat Demulsifier at 1000 (rpm)

Conc (ppm)	Velocity (rpm)	Time (mins)	Emulsion (ml)	Water (ml)	Emulsion separated (ml)	crude oil (ml)	BS$W%	Crude oil%
0	1000	5	10	0.5	9	0.5	5	5
200	1000	5	10	1.5	1.5	7.5	15	75
400	1000	5	10	1	1	8	10	80
600	1000	5	10	1	1	8	10	80
800	1000	5	10	1	1	8	10	80
1000	1000	5	10	1	1	8	10	80

Table 12: Crude oil (%) of demulsifiers (ppm) at 1000 rpm

Conc	Crude oil (%) SBHO	Crude oil (%) OPO	Crude oil (%) Phase treat
0	5	5	5
200	40	58	75
400	42	53	80
600	42	50	80
800	38	50	80
1000	36	50	80

Table 13: BS&W (% of demulsifiers(ppm) at 1000 (rpm)

Conc	BS$W%SBHO	BS$W% OPO	BS$W% PHASETREAT
0	5	5	5
200	10	10	15
400	10	15	10
600	15	15	10
800	15	20	10
1000	10	15	10

From figure 3. it was observed that Phasetreat performed best in terms of crude oil separation followed by orange peel oil (OPO)and lastly soya bean husk oil (SBHO) was 85% of Phasetreat at 200 ppm, 58% of OPO at 200 ppm and 42% of SBHO at 400ppm to 600 ppm

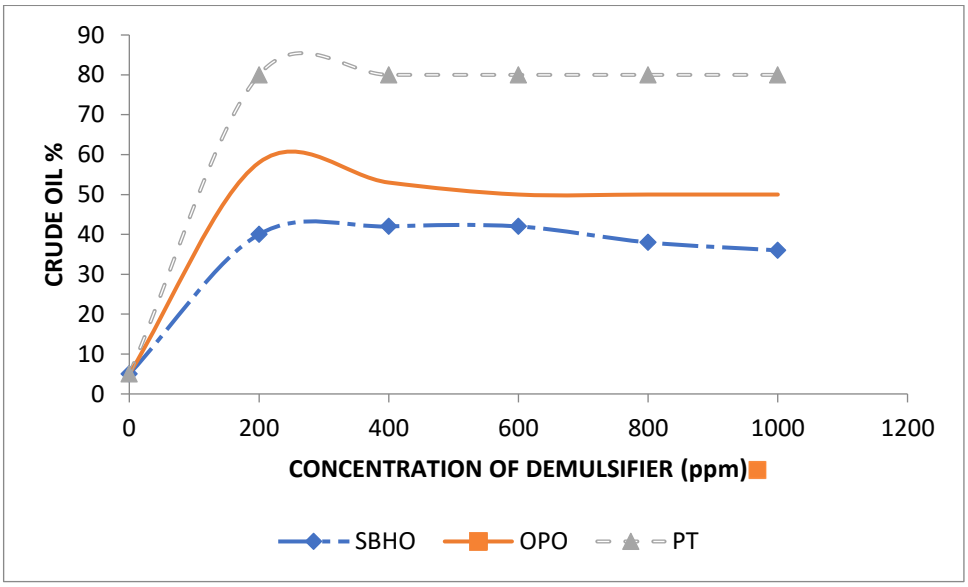

Figure 3: Crude oil separated (%) VS Concentration of demulsifiers (ppm) 1000 RPM

From Figure 4: Phasetreat had a better BS&W (%), followed by orange peel oil (OPO) and then soya bean husk oil (SBHO)

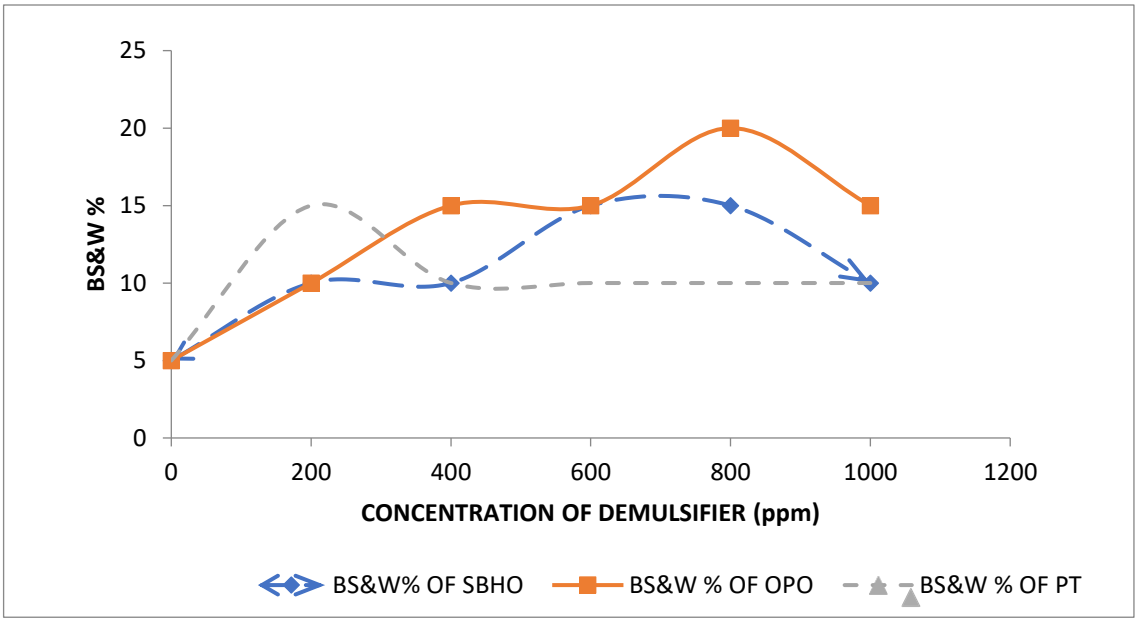

Figure 4 BS&W (%) VS Concentration of demulsifiers (ppm) at 1000 rpm

Table 14: Crude Oil Emulsion doped with varying concentration of soya bean husk oil (SBHO) Demulsifier at 1500 (rpm)

Conc (ppm)	Velocity (rpm)	Time (mins)	Emulsion (ml)	Water (ml)	Emulsion separated (ml)	crude oil (ml)	BS$W%	Crude oil%
0	1500	5	10	0.5	9	0.5	5	5
200	1500	5	10	1.5	5-Apr	4	15	40
400	1500	5	10	1.5	4.5	4	15	40
600	1500	5	10	1.5	4.5	4	15	40
800	1500	5	10	2	4.25	3.75	20	37.5
1000	1500	5	10	1.5	5	3.5	15	35

Table 15 Crude Oil Emulsion doped with varying concentration of OPO at 1500 (rpm)

Conc (ppm)	Velocity (rpm)	Time (mins)	Emulsion (ml)	Water (ml)	Emulsion separated (ml)	crude oil (ml)	BS$W%	Crude oil%
0	1500	5	10	0.5	90	0.5	5	5
200	1500	5	10	1.5	2.5	6	15	60
400	1500	5	10	1.5	3	5..5	15	55
600	1500	5	10	2	3	5	20	50
800	1500	5	10	2	3	5	20	50
1000	1500	5	10	1.5	3.5	5	15	50

Table 16 Crude Oil Emulsion doped with varying concentration of Phasetreat Demulsifier at 1500 (rpm)

Conc (ppm)	Velocity (rpm)	Time (mins)	Emulsion (ml)	Water (ml)	Emulsion separated (ml)	crude oil (ml)	BS$ W%	Crude oil%
0	1500	5	10	0.5	9.0	0.5	5	5
200	1500	5	10	1.5	1	7.5	15	75
400	1500	5	10	1	1	8	10	80
600	1500	5	10	1	1	8	10	80
800	1500	5	10	1.5	1.5	7	15	70
1000	1500	5	10	1.5	1.5	7	15	70

Table 17: Crude oil separated (%) at demulsifier concentration (ppm) at 1500 (rpm

Conc	**Crude SBHO**	**Crude OPO**	**Crude Phase treat**
0	5	5	5
200	40	60	75
400	40	55	80
600	40	50	80
800	37.5	50	70
1000	35	50	70

Table 18: BS&W (%) of demulsifies (ppm) at 1500 rpm

Conc	BS$W% SBHO	BS$W% OPO	BS$W% Phase treat
0	5	5	5
200	15	15	15
400	15	15	10
600	15	20	10
800	20	20	15
1000	15	15	15

From Figure 5: it was observed that Phasetreat performed best in terms of crude oil separation followed by orange peel oil (OPO) and lastly soya bean husk oil (SBHO) which were 80% at 400-600 ppm, 60% at 200ppm and 40% at 200-600 ppm respectively. However, all the plots are in line with the result obtained by Sulaiman, *et al* (2015) and Udonne (2012).

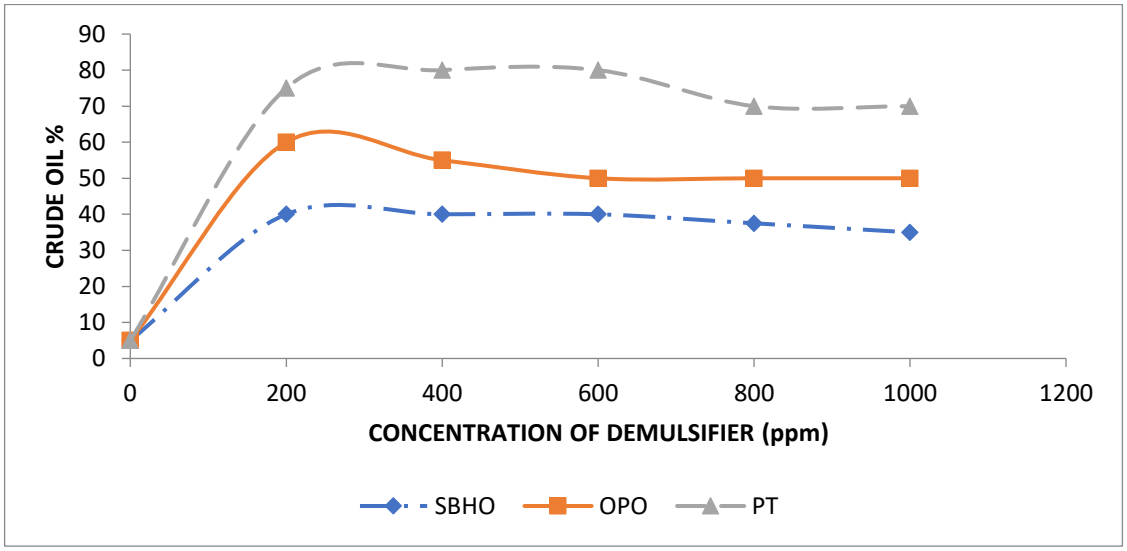

Figure 5 Crude oil separated (%) VS Concentration of demulsifiers (ppm) at 1500 rpm

From Figure 6: Phasetreat had a better BS&W (%) 50% at 400-600ppm followed by orange peel oil (OPO) with 70% at 200 ppm and then soya bean husk oil (SBHO) had 80% at 200-600 pp respectively,

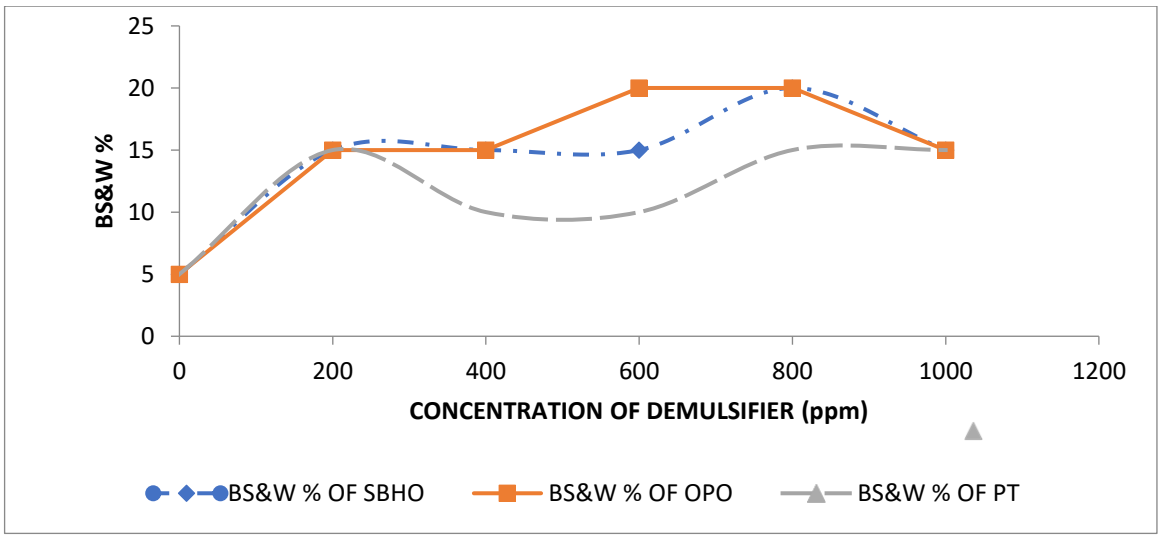

Figure 6:BS&W (%) VS Concentration of demulsifiers (ppm) at 1500 rpm.

CONCLUSION

In this research, utilization of plant extract for treatment of emulsions in crude oil production was successfully investigated by experimental method.

Demulsifiers was formulated from plant extracts (Orange peel and soya bean husk). Treatment of the crude oil emulsion was carried out using the demulsifiers formulated from these plant extracts and the demulsifier obtained from a vendor to resolve the emulsion using the bottle test

method. The percentages of crude oil, basic sediment and water and the emulsion separated was obtained at varying concentration in ppm and at various rotation per minutes(rpm). From the results of the test carried out OPO had a better water separation and crude oil separation ability in all the rotation per minute followed soya bean husk oil respectively. For comparative purpose, Phasetreat a conventional demulsifier was used to compare with the formulated demulsifier from plant extracts. At the various rotation per minute (rpm) that is, 500rpm, 1000 rpm and 1500rpm for the various demulsifiers used to resolve the crude oil emulsion, OPO had 60% of crude oil separation from the emulsion at 200 ppm, SBHO had 42% at 400ppm and 600ppm and Phasetreat had 87.5% crude oil separation at 1000 ppm.Finally,Phasetreat performed well at 500 and 1000 rpm and dropped it value at 15000 rpm conversely orange-peel oil and soya bean husk oil showed improvement in their performance from 40 percent and 53 percent at 500-1000 ppm to 60 percent and 42 percent at 1500 rpm. These results were in line with the results obtained by Udonne (2012).

REFERENCES

Abdulredha, M.M, Siti, A. H. and Luqman, C.A (2018) Overview on petroleum emulsions, formation, influence and demulsification treatment techniques. *Arabian Journal Chemistry* 13:1–26

Adewunmi, A.A and Kamal, M.S (2019) Demulsification of water-in-oil emulsions using ionic liquids: effects of counterion and water type. *Journal of Molecular Liquid* 279:411–419. Https: //doi.org/10.1016/j.molli q.2019.02.008

Aske,N. (2002).Ph.D thesis, "Characterization of crude oil components, and water in crude Emulsion stability by means of near infrared spectroscopy" Norwegian University of Science and Technology, 2002.

Auflem IH (2002) Influence of asphaltene aggregation and pressure on crude oil emulsion stability by Department of Chemical Engineering.Norwegian University of Science and Technology. Doktor Ingeniør Thesis, June, p 58.

Behroozi AH, Kasiri N.,Mohammadi, T (2019) Multi-phenomenal macroscopic investigation of cross-flow membrane flux in microfiltration of oil-in-water emulsion, experimental & computational. J Water Process Engineering 32:100962. https ://doi.org/10.1016/j. jwpe.2019.10096 2

Biniaz, P., Farsi, M. and Rahimpour, M.R (2016) Demulsification of water in oil emulsion using ionic liquids: statistical modeling and optimization. *Fuel* 184:325–333. https ://doi.org/10.1016/j. fuel.2016.06.093.

Czarnecki, J (2009) Stabilization of water in crude oil emulsions. Part2. *Energy Fuels 23(3):1253–1257*. https ://doi.org/10.1021/ef800607u.

Czarnecki, J and Moran, K (2005) On the stabilization mechanism of water -in- oil emulsions in petroleum systems. *Energy Fuels 19(5):2074–2079*. https ://doi.org/10.1021/efo50 1400.

Ese, M.H., Galet, L., Clausse, D and Sjöblom J (1999) Properties of Langmuir surface and interfacial films built up by asphaltenes and resins: influence of chemical demulsifiers. *Journal of Colloidal Interface Science 220(2):293–301.* https ://doi.org/10.1006/jcis.1999.6549.

Feitosa, F.X., Alves, R.S and de Sant'Ana, H.B (2019) Synthesis and application of additives based on cardanol as demulsifier for water-in-oil emulsions. *Fuel 245(February):21–28.* https ://doi.org/10.1016/j. fuel.2019.02.081.

Fingas, M (1995) Water-in-oil emulsion formation: a review of physics and mathematical modelling. *Spill Science and Technology Bulletin 2(1):55–59.* https ://doi.org/10.1016/1353-2561(95)94483 -Z.

Fingas M, Fieldhouse B (2004) Formation of water-in-oil emulsions and application to oil spill modelling. J Hazard Mater 107(1–2):37–50. https ://doi.org/10.1016/j.jhazm at.2003.11.008.

Fingas, M and Fieldhouse, B (2009) Studies on crude oil and petroleum product emulsions: water resolution and rheology. Colloids Surface A: Physicochemical and Engineering Aspect 333(1–3):67–81. https ://doi. org/10.1016/j.colsu rfa.2008.09.029.

Feitosa, F.X., Alves, R.S and de Sant'Ana, H.B (2019) Synthesis and application of additives based on cardanol as demulsifier for water-in-oil emulsions. *Fuel 245(February):21–28.* https ://doi.org/10.1016/j. fuel.2019.02.081

Fridjonsson, E.O., Graham, B.F., Akhfash, M., May, E.F and Johns, M.L (2014) Optimized droplet sizing of water-in-crude oil emulsions using nuclear magnetic resonance. *Energy Fuels 28(3):1756–1764.* https://doi.org/10.1021/ef402 117k.

Goodarzi, F,and Zendehboudi, S (2019) A comprehensive review on emulsions and emulsion stability in chemical and energy industries .*Canadian Journal of Chemical Engineers 97(1):281–309*. https ://doi.org/10.1002/ cjce.23336.

Gafonova, O.V. (2000). *Role of Asphaltenes and Resins in stabilization of water in Hydrocarbon Emulsions.* The University of Calgary:Msc.Thesis.

Goni, G.J., Trinanes, J.A., MacFadyen, A., Streett D., Olascoaga, M.J and, Imhoff, M.L (2015) Variability of the deepwater horizon surface oil spill extent and its relationship to varying ocean currents and extreme weather conditions. https ://doi.org/10.1007/978-3-319-16459 -5_1.

Grace, R. (1992). *Commercial emulsion breaking* in.: Schrumm. L.L. Emulsions Fundamental and Applications in the Petroleum Industry American Chemical Society Washington Dc. 313-338.

Grenoble, Z and Trabelsi, S (2018) Mechanisms, performance optimization and new developments in demulsification processes for oil and gas applications. *Advance Colloidal Interface Science 260:32–45.* https ://doi.org/10.1016/j.cis.2018.08.003.

Griffin, W.C (1949) Classification of surface-active agents by "HLB." Chicago chapter, pp 311 326. http://www.hinda wi.com/journals/jam/2012/18742 1/. Accessed 17 July 2019.

Goldzal, A., Bourrel, M., (2000). Demulsification of crude oil emulsions: Correlation to microemulsion phase behavior. Ind.Eng.Chem. Res. 39 (8), 2746-2751.

Ivanov I.B., and Ktalchevcky, P.A. (1996). Stability of emulsion under equilibrium and dynamic Conditions. *Coll. Surf. A.Physcochemical and Engineering Aspects.* 128: 155-175.

Kim, Young. Ho. (1995). *A study of Dynamic interfacial mechanisms for demulsification* of *water in oil emulsion. Illinois institute of technology:* PhD thesis.

Kokal, S and, Aramco S (2005) Crude oil emulsions: a state-of-the-art review. *Society of Petroleum Engineering Production Facilities 20(December 2004):5–13.* https ://doi.org/10.2118/77497 –PA

Lane, P., (1995). The use of chemicals in oil spill response. Philadelphia, Pennsylvania.

Leopold, G. (1992). *Breaking produced fluid and process stream emulsion.* In schramm, L.L emulsions fundamental and application in the petroleum industry. American chemical society. Washington. DC 341-383.

Li,Z., Geng, H., Wang, X., Jing, B., Liu, Y and Tan, Y (2018) Noval tannic acid-based polyether as an effective demulsifier for water-inaging crude oil emulsions. *Chemical Engineering Journal 354(May):1110–1119*. https ://doi.org/10.1016/j.cej.2018.08.117

López-Chávez, E., Pacheco-Sánchez, J.H., Martínez-Magadán. J.M, Castillo-Alvarado, F.D.L, Soto-Figueroa, C and García-Cruz, I (2007) Methodology for predicting the phase envelope of a heavy crude oil and its asphaltene deposition onset. *Petroleum Science Technology 25(1–2):19–39.* https ://doi.org/10.1080/10916 46060 10541 80.

Martínez-Palou, R., Cerón-Camacho, R., Chávez, B., Vallejo, A.A., Villanueva-Negrete, D., Castellanos, J and Aburto, J (2013) Demulsification of heavy crude oil-in-water emulsions: a comparative study between microwave and thermal heating. Fuel 113:407–414.https ://doi.org/10.1016/j.fuel.2013.05.094.

Mohammed, R.A., Bailey, A.I., Luckham, P.F and Taylor, S.E (1994) Dewatering of crude oil emulsions 3. Emulsion resolution by chemical means. *Colloids Surface Advances: Physicochemical and Engineering Aspect 83(3):261–271.* https ://doi.org/10.1016/0927-7757(93)02706 –K.

Nakama, Y (2017) Surfactants. In: Cosmetic science and technology, pp231–244. https ://doi.org/10.1016/B978-0-12-80200 5-0.00015 -X.

Nikkhah, M., Tohidian, T., Rahimpour, M.R and Jahanmiri, A (2015) Efficient demulsification of water-in-oil emulsion by a novel nano-titania modified chemical demulsifier. *ChemicalEngineeringResearch and Design 94:164–*172.https ://doi.org/10.1016/j.cherd .2014.07.021.

Nordvik, A. B., Simmons, J. L., Bitting, K. R., Levis, A., & Kristiansen, T. S. (1996). Oil and water separation in marine oil spill clean-up operations. Spill science & Technology 3 (3), 107-122.

NRT Science and Technology Committee (1997). Emulsion breaks and inhibitors fortreating oil spills. Fail sheet

Poindexter, M. K., Lindemuth, P. M, (2004). Applied statistics: Crude oil emulsions and demulsifiers. Journal of Dispersion Science Technology 25 (3), 311-320

Porter, M.R (1991) Handbook of surfactants. Springer, BostonSalager JL (2002) Surfactants types and uses. FIRP Booklet(E300A), p 2

Salager, J.L and Forgiarini, A.M (2012) Emulsion stabilization, breaking, and inversion depend upon formulation: advantage or inconvenience in flow assurance. Journal of *Energy Fuels 26(7):4027–4033.* https ://doi.org/10.1021/ef300 1604

Schramm, L.L., Stasiuk, E.N and Marangoni, D.G (2003) Surfactants and their applications. Annual Report on the Progress of Chemistry Section C 99(August):3–48. https://doi.org/10.1039/B2084 99F

Sjöblom, J (2001) Encyclopedic handbook of emulsion technology.CRC Press, Hoboken

Speight, J.G (1992) Proceeding of the 4th international conference on stability and handling of liquid fuels. U.S. Department of Energy (DOE/CONF-911102), p 166

Speight, J.G (2014) The chemistry and technology of petroleum, 5th edition. *Fuel Processing Technology. C*RC Press, p 953

Tao, J., Shi, P., Fang, S., Li, K., Zhang, H and Duan, M (2015) Effect of rheology properties of oil/water interface on demulsification of crude oil emulsions. *Industrial & Engineering Chemistry Research 54(17):4851–4860.* https ://doi.org/10.1021/acs.iecr.5b006 39

Udonne, J. D (2012) Chemical treatment of emulsion problem in crude oil production. *Journal of petroleum and Gas Engineering vol.3(7). Pp. 135-141,*

Umar, A.A., Saaid, I.B.M., Sulaimon, A.A., and Pilus, R.B.M (2018) A review of petroleum emulsions and recent progress on water-in-crude oil emulsions stabilized by natural surfactants and solids. *Journal of Petroleum Science and Engineering 165(September 2017):673–690.* https ://doi.org/10.1016/j.petro l.2018.03.014

Zolfaghari, R., Fakhru'l-Razi, A., Abdullah, L.C., Elnashaie, S.E and Pendashteh, A (2016) Demulsification techniques of water-in-oil and oil-in-water emulsions in *petroleum industry. Separation and Purification Technol10gy70:377–407*. https ://doi.org/10.1016/j.seppu r.2016.06.026 Publisher's Note Springer Nature remains neutral with regard to jurisdictional claims in published maps and institutional affiliatio*n*

Applied Sciences Research Periodicals
June 2023, Vol. 1, No. 3, pp. 93-97.

First Time Record of Canadian Toad Anaxyrus hemiophrys (Cope,1886), (Amphibia; Anura; Bufonidae) from Idukki District, Kerala State, India

Selvaraj Selvamurugan

1. Translational Health Science and Technology Institute Building (THSTI), Faridabad-121001

Abstract:
The Canadian toad frog, Anaxyrus hemiophrys (Cope,1886) is reported first time from Idukki district, Kerala. It is an anuran Amphibia under the family Bufonidae. The species is listed as "Least Concern" under IUCN Red List. In this paper discuss about the Canadian toad descriptions, habitat, biology and threats.

Key words; Amphibia, Anura, Idukki, Canadian toad, Least Concern, south India.

INTRODUCTION

Amphibians are the primary tetra pods arose between quite a while back, which interfaces between land environment and water biological system. these creatures of land and water are the primary connection among fishes and the reptiles assuming a significant part as both prey and hunter in pecking order. The creatures of land and water are serving us by diminishing irritations in the harvest fields or by checking the number of inhabitants in bugs which go about as vector for some sicknesses. Creatures of land and water, a novel gathering of vertebrates containing north of 7,000 known species, are the extensions among land and water biological system which are presently compromised overall because of different reasons.

Amphibians are important predator and prey species in both aquatic and terrestrial habitats, especially in the tropics where the diversity and abundance of taxa are high. According to Whiles *et al.* (2006) loss of one species is akin to loss of two species in the case of amphibians. Baillie *et al.* (2004) stated that among the vertebrates of the world, amphibians are the most threatened taxa and have the highest proportion of species on the verge of extinction. The most pervasive threats to amphibians are habitat loss and habitat degradation.

For the amphibians of the Western Ghats the species accumulation curve has not yet reached a plateau (Aravind *et al.* 2004). According to Nameer *et al.* (2015) & Das (2015) 90% of amphibians in Kerala are endemic to the Western Ghats and 33% belong to various threatened categories. Generally, protected area networks are considered as the corner stone of biodiversity conservation efforts.

Hence, for a realistic conservation strategy one should evaluate the conservation value of these multiple land use systems such as agroecosystems. The present study is expected to shed light on the amphibian diversity and richness in Forest area and ecosystems of Kerala.

STUDY AREA

Materials and Methods

On 6th April 2023 evening around 04.30 hours, an uncommon anuran Amphibia was caught under a, near forest area of Kanthalloor is a village in Devikulam taluk of Idukki district in the Indian state of Kerala. It is a village nestled in the Western Ghats of India. The salubrious climate and the picturesque landscapes and wide variety of tropical crops coupled with the close proximity of Munnar, has transformed this village into a tourist destination. In this (Canadian toad, *Anaxyrus hemimorphy's)* toad species was first time record in Idukki district, Kerala state in India.

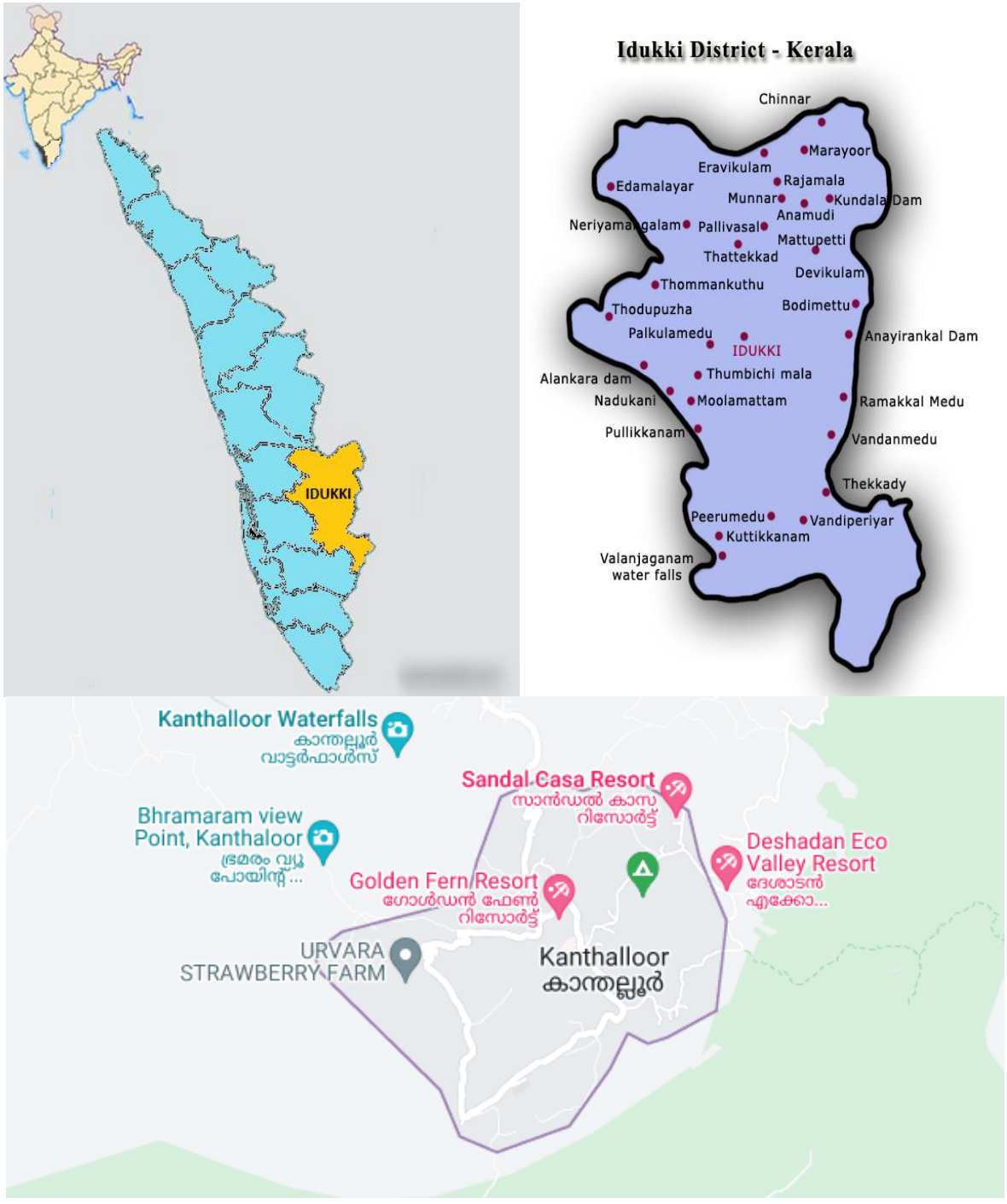

Figure 1. study area in Kanthalloor, Devikulam taluk, Idukki district, Kerala, India

Figure 2. Canadian toad *Anaxyrus hemiophrys* (Cope,1886).

DESCRIPTION

The Canadian Frog is a medium-sized amphibian and can develop to 9 cm in body length, with guys being somewhat more modest than females. People are tan, light brown, dim, caramel green or rosy brown with more obscure blotches. There is generally a white or cream-hued vertebral stripe that runs down the back, however it tends to be blurred on certain people. The stomach is white to tan with dim spotting. Canadian Frogs have granular skin with huge mole like knocks, an enormous, kidney-molded parotoid organ behind each eye, and articulated cranial peaks (raised edges between the eyes). The legs are short and there are two noticeable tubercles on the rear feet that are utilized for tunneling. Hatchlings (fledglings) have long tails with an enormous balance and need front legs (recently incubated fledglings are legless). The hatchlings are dark with a bi-shaded tail and clear tail balances. The hatchlings can grow up to 3 cm in complete length before transformation. The rearing call is a piercing quaver.

We found that edge habitat between upland and wetland landscapes is important for breeding Canadian Toads based on the quadratic relationship between toad occurrence and the proportion upland covariate. Models consistently showed toad occurrence in wetlands directly adjacent to uplands. Toads are known to typically leave wet areas to forage in uplands following breeding, so proximity of breeding sites to upland habitat seems to be important (Roberts and Lewin 1979; Hamilton *et al.* 1998; Hannon *et al.* 2002; Bull 2006; Long and Prepas 2012).

Browne and Paszkowski (2010) found that Western Toads travelled nearly 2 km to reach hibernation sites in the Boreal Forest. Canadian Toads have been recorded to move up to 1.5 km from the breeding wetland and use upland habitats for overwintering (Constible *et al*. 2010; Patrick Garcia *et al*., unpubl. report). While not physically observed, it can be inferred that neigh boring upland habitats are used by Canadian Toads in our study area for post-breeding foraging and for access to overwintering habitat. Historically, many viewed the Canadian Toad as the least terrestrial of the bufonids found in western North America (Breckenridge and Tester 1961;

Roberts and Lewin 1979). Early reports on this species did not associate this toad with forest habitats (Breckenridge and Tester 1961; Roberts and Lewin 1979). Here, we found the first-time record of the Canadian toad (*Anaxyrus hemiophrys*) from kanthaloor, (near forest area) Idukki district, Kerala state, India.

SIMILAR SPECIES

The Canadian Amphibian can be mistaken for the American Frog, Incredible Fields Frog, Western Frog and Fields Spadefoot. In any case, the Canadian frog is the main species with cranial peaks that associate at the rear of the head to from a conspicuous knock (chief). The Western Frog needs cranial peaks, and the cranial peaks of the American Frog and Extraordinary Fields Amphibian separate at the rear of the head and structure a "V" shape. The scope of the American Amphibian covers with the Canadian Frog in south eastern Manitoba and the species interbreed around here, making ID of certain people troublesome. The Fields Spadefoot needs cranial peaks and parotoid organs and has vertical understudies (CHS,2019).

HABITAT

Canadian Frogs breed in different shallow amphibian territories, like the edges of lakes, lakes, wetlands, slow-streaming segments of streams and waterways, and trenches. Reproducing locales are situated in open natural surroundings, like grassland and aspen parkland, as opposed to in forested regions. Throughout the mid-year, Canadian Amphibians scatter into earthbound environments, like grassland and meadow, aspen parkland, forest, and willow or lush swamps, yet they by and large stay near water. People rest underground underneath the ice line in tunnels that they exhume (CHS,2019).

BIOLOGY

Canadian Amphibians rest for a significant part of the year and are just dynamic from May until early September. Guys call to draw in females during the reproducing season, which happens in May to early July, contingent upon scope. During rearing, the male handles the female (amplexus) and treatment happens remotely in oceanic territories as the female lay's eggs. The female lays 3,000-6,000 eggs in two long strings. The eggs grow quickly and hatch in 2-7 days and the fledglings change into adolescent frogs following 6 two months, contingent upon water temperature. Guys arrive at sexual development 1-3 years after transformation, while females mature at 3-4 years old. Canadian Frogs can live to as long as 12 years old, yet most just carry on with a couple of years. People search for different bugs, fundamentally insects and scarabs, as well as insects and different spineless creatures. Poisons that dissuade hunters are created by organs in the amphibian's skin, especially in the parotoid organs and the mole like knocks. Canadian Frogs are less lenient toward dry circumstances than different amphibians and they are commonly found near water or in clammy conditions (CHS,2019).

THREATS

Canadian Amphibians happen all through enormous scopes of Canada that are generally lacking, and dangers to this species are negligible all through the majority of its reach. Natural surroundings annihilation, especially the deficiency of rearing lakes, can bring about populace declines or nearby extirpation. Pesticides/herbicides, street salt and other natural poisons can be inconvenient to frog and amphibian populaces by causing direct mortality as well as formative disfigurements. Street mortality can be a critical danger when streets divide the species' territory. Microorganisms, for example, chytrid organism and Rana infection, can cause mass mortality of frog and amphibian populaces. Environmental change likewise represents a danger

to this animal groups, especially by expanding the recurrence and seriousness of dry spells (CHS,2019).

REFERENCES

1. Aravind, N.A., R.U. Shaanker & K.N. Ganeshaiah (2004). Croak, croak, croak: are there more frogs to be discovered in the Western Ghats?Â Current ScienceÂ 86(11): 1471â€"1472.

2. Browne, C.L., and C.A. Paszkowski. 2010. Hibernation sites of Western Toads (Anaxyrus boreas): characterization and management implications. Herpetological Conservation and Biology 5:49–63.

3. Baillie, Jonathan & Hilton-Taylor, Craig & Stuart, Simon. (2004). 2004 Red List of Threatened Species. A Global Species Assessment. 10.2305/IUCN.CH.2005.3.en.

4. Bull, E.L. 2006. Sexual differences in the ecology and habitat selection of Western Toads (Bufo boreas) in northeastern Oregon. Herpetological Conservation and Biology 1:27–38.

5. Breckenridge, W.J., and J.R. Tester. 1961. Growth, local movements and hibernation of the Manitoba Toad, Bufo hemiophrys. Ecology 42:637–646.

6. Constible, J.M., P.T. Gregory, and K.W. Larsen. 2010. The pitfalls of extrapolation in conservation: movements and habitat use of a threatened toad are different in the Boreal Forest. Animal Conservation 13:43–52.

7. Canadian herpetology society, Canada 2019.

8. Hamilton, I.M., J.L. Skilnick, H. Troughton, A.P. Russell, and G.L. Powell. 1998. Status of the Canadian Toad (Bufo hemiophrys) in Alberta. Alberta Wildlife Status Report No. 12, Alberta Environmental Protection, Wildlife Management Division, and the Alberta Conservation Association, Edmonton, Alberta, Canada. 37 p.

9. Hannon, S.J., C.A. Paszkowski, S. Boutin, J. DeGroot, S.E. Macdonald, M. Wheatley, and B.R. Eaton. 2002. Abundance and species composition of amphibians, small mammals, and songbirds in riparian forest buffer strips of varying widths in the boreal mixed wood of Alberta. Canadian Journal of Forest Research 32:1784–1800.

10. Long, Z.L., and E.E. Prepas. 2012. Scale and landscape perception: The case of refuge use by Boreal Toads (Anaxyrus boreas boreas). Canadian Journal of Zoology 90:1015–1022.

11. Nameer, P.O., J. Praveen, A. Bijukumar, M.J. Palot, S. Das & R. Raghavan (2015). A checklist of vertebrates of the Kerala State. Journal of Threatened Taxa 7(13): 7961â€ "7970.

12. Matt R Whiles, Karen R Lips, Cathy M Pringle, Susan S Killham, Rebecca J Bixby, Roberto Brenes, Scott Connelly, Jose Checo Colon-Gaud, Meshagae Hunte-Brown, Alexander D Huryn, Chad Montgomery, and Scot Peterson (2006). The effects of amphibian population decline on the structure and function of Neotropical stream ecosystems. Front Ecol Enviro 4(1): 27–34.

13. Roberts, W., and V. Lewin. 1979. Habitat utilization and population densities of the amphibians of north eastern Alberta. Canadian Field-Naturalist 93:144–154.